The structural and functional characterization of the extracellular domain of vascular endothelial growth factor receptors: Their role in receptor activation and use as therapeutic targets

Inauguraldissertation

zur

Erlangung der Würde eines Doktors der Philosophie

vorgelegt der

Philosophisch-Naturwissenschaftlichen Fakultät

der Universität Basel

von Edward Stuttfeld

aus Baden-Baden, Deutschland

Zürich, 2012

Genehmigt von der Philosophisch-Naturwissenschaftlichen Fakultät
auf Antrag von:

Prof. Dr. Kurt Ballmer-Hofer

(Fakultätsverantwortlicher & Dissertationsleiter)

Dr. Nicolas Thomä

(Koreferent)

Basel, den 21.06.2011

Prof. Dr. Martin Spiess

(Dekan)

1   Table of content

2   Abbreviations

AMD	age-related macular degeneration
Ang	angiopoietin
C-terminus	carboxy-terminus or COOH-terminus
Da, kDa	Dalton, kilo-Dalton
DARPin	designed ankyrin repeat protein
DNA	deoxyribonucleic acid
E. coli	*Escherichia coli*
ECD	extracellular domain
EM	electron microscopy
Eph	ephrin receptor
FGF	fibroblast growth factor
Flt-3	Fms-like tyrosine kinase-3
HIF-1	hypoxia-inducible factor 1
HSPG	heparan sulfate proteoglycan
Ig	immunoglobulin
ITC	isothermal titration calorimetry
MALS	multi-angle light scattering
Nrp	neuropilin
N-terminus	amino-terminus or NH_2-terminus
PDGF	platelet-derived growth factor
PDGFR	platelet-derived growth factor receptor
PI3K	phosphatidylinositol-3 kinase
PLCγ1	phospholipase C-γ1
PIGF	placenta growth factor
PKC	protein kinase C
PNGaseF	peptide N-glycosidase F
PTB	phospho-tyrosine binding
RTK	receptor tyrosine kinase
SAXS	small-angle X-ray scattering
scFv	single-chain variable fragment

Sck	Src-like protein
SEC	size exclusion chromatography
SH	Src-homology
Shb	SH2 in β-cells
SHP	Src-homology phosphatase
TGF	transforming growth factor
TSAd	T-cell-specific adaptor
VE-cadherin	vascular endothelial cadherin
VEGF	vascular endothelial growth factor
VEGFR	vascular endothelial growth factor receptor

3   Summary

The vascular endothelial growth factor (VEGF) family plays key roles in the development of the blood and lymphatic vasculature. Five members, VEGF-A, -B, -C, -D, and PlGF can be found in the human body. They bind in an overlapping pattern to three receptor tyrosine kinases (RTKs), which constitute the type V family of RTKs: VEGF-receptor (VEGFR)-1 (also known as Flt1), VEGFR-2 (KDR/Flk1), and VEGFR-3 (Flt4). While VEGFR-1 and VEGFR-2 are mainly involved in angiogenesis, VEGFR-3 is the key player in lymphangiogenesis. VEGFRs consist of seven immunoglobulin-homology domains constituting the extracellular domain (ECD), a single transmembrane helix, and a split tyrosine kinase domain. Ligand binding to the VEGFR ectodomain initiates receptor dimerization, followed by kinase activation and autophosphorylation. Phosphorylated tyrosine residues in the intracellular domain of VEGFRs act as docking sites for a number of different signaling molecules.

In addition to physiological angiogenesis, aberrant VEGFR signaling is associated with a variety of pathological conditions such as in cancer, in ischemic, and in inflammatory disorders. Several inhibitors of VEGF-signaling have been developed most of which are at different stages in clinical trials. However, anti-angiogenic treatment of cancer is often accompanied by severe side-effects and tumor patients tend to develop resistance to the treatment. Hence, structural studies of the VEGF receptor system may further elucidate the molecular mechanism underlying receptor activation and thereby help to develop new more specific drugs complementing existing therapies.

During this project, I showed that binding of individual VEGFR-1 ligands resulted in conformationally similar ligand/VEGFR-1 ECD complexes. Besides showing ligand induced dimerization, the complexes reveal homotypic receptor/receptor interactions in the membrane proximal Ig-homology domains. Our study is also the first addressing the thermodynamic contributions of individual Ig-homology domains of VEGFR-1 to ligand binding. I showed that VEGFR-1 D4-7 positively contribute to ligand binding as shown by the higher

affinities of the ligands for VEGFR-1 D1-7 compared to binding to the minimal ligand binding domain D1-3. Surprisingly, I discovered that Ig-homology domain 1 blocks PlGF-1 binding to VEGFR-1 D1-3 but not to D1-7. The exact mechanism explaining this phenomenon remains unclear.

In a second project, we showed that Ig-homology domains 4 and 7 are indispensable for VEGFR-2 activation. The loop connecting β-strand E and F in Ig-homology domain 7 represents the element that are required for receptor activation by mediating contacts with Ig-homology domain 7 of the second receptor chain in the dimerized complex. We generated Designed Ankyrin Repeat Proteins (DARPins) that specifically target the low affinity receptor/receptor interactions formed upon ligand binding and identified a DARPin binding to Ig-homology domain 4 that blocks VEGFR-2 activation and phosphorylation without preventing the formation of the VEGF-A/VEGFR-2 complex. This inhibitor also affected downstream signaling and inhibited sprout formation of endothelial cell spheroids. This type of inhibition displays a new inhibition mechanism for VEGFR-2 that might be applied complementarily to other therapeutic approaches to improve the efficiency of anti-angiogenic therapy.

4   Zusammenfassung

Die Familie der VEGFs spielt eine wichtige Rolle in der Entwicklung des Blut- und Lymphgefässsystems. Im menschlichen Körper sind fünf Mitglieder, VEGF-A, -B, -C, -D, und PlGF anzutreffen. Sie binden in einem überlappendem Muster zu drei Rezeptor Tyrosin Kinasen, die die Typ V Familie der RTKs bilden: VEGFR-1 (auch bekannt als Flt1), VEGFR-2 (Flk1), und VEGFR-3 (Flt4). Während VEGFR-1 und VEGFR-2 hauptsächlich in der Angiogenese involviert sind, stellt VEGFR-3 eine Schlüsselfigur in der Lymphangiogenese dar. VEGFRen bestehen aus 7 Immunoglobulin-ähnlichen Dömanen in der extrazellulären Domäne, einer einzelnen membrandurchziehenden Helix, und eine geteilten intrazellulären Kinasedomäne. Ligandenbindung an die extrazelluläre Domäne initiiert Rezeptordimerisierung, gefolgt von Kinasenaktivierung und Autophosphorylierung. Phosphorylierte Tyrosinseitenketten in der intrazellulären Domäne von VEGFRen agieren als Bindestellen für eine Vielzahl von Signalmolekülen.

Neben der physiologischen Angiogenese sind VEGFR-Signalwege auch in einer Vielzahl von pathologischen Konditionen involviert, z.B. Krebs, ischämischen und Entzündungskrankheiten. Eine Reihe an Inhibitoren wurde entwickelt, von denen die meisten sich in verschiedenen Stadien von klinischen Studien befinden. Allerdings wird die Anti-Angiogenese Behandlung von Krebs oft von starken Nebenwirkungen begleitet und Krebspatienten neigen dazu eine Resistenz gegen die Behandlung zu entwickeln. Daher könnten strukturelle Studien dieses Rezeptorsystems weiter dazu beitragen den molekularen Mechanismus, der der Rezeptoraktivierung unterliegt, aufzuklären, als auch helfen neue Medikamente zu entwickeln die benötigt werden um bestehende Therapien zu erweitern.

Während dieses Projektes, habe ich gezeigt, dass die Bindung der einzelnen VEGFR-1 Liganden in ähnlichen Liganden/VEGFR-1 ECD Konformationen resultierte. Die Komplexe sind neben der Dimerisierung durch den Liganden durch weitere homotypische Rezeptor/Rezeptor Interaktionen in den membrannahen Ig-homologen Domänen geprägt. Ausserdem, ist dies die erste

Studie, die die thermodynamische Beteiligung individueller Ig-homologie Domänen zum Prozess der Ligandenbindung behandelt. Dabei habe ich gezeigt, dass VEGFR-1 Domäne 4-7 eine positive Beteiligung am Prozess der Ligandenbindung besitzt, was durch niedrigere Affinitäten der Liganden für VEGFR-1 D1-7 im Vergleich zur minimalen Ligandenbinde Domäne gezeigt wurde. Überraschenderweise, habe ich entdeckt dass Ig-homologie Domäne 1 die PlGF-1 Bindung an VEGFR-1 D1-3 aber nicht die Bindung an D1-7 behindert. Der genaue Mechanismus, der dieses Verhalten erklären würde, ist jedoch unklar.

In einem zweiten Projekt, zeigen wir dass Ig-homologie Domäne 4 und 7 unersetzlich für die VEGFR-2 Aktivierung sind. Innerhalb der Ig-homologie Domäne 7 ist es der Loop, der β-Strang E und F verbindet, der die wichtigen Elemente für die Rezeptoraktivierung beinhaltet. Dieser Loop interagiert mit demselben Loop in der Ig-homologie Domäne 7 der zweiten Rezeptorkette im dimerisierten Komplex. Daher haben wir DARPins generiert die spezifisch die niedrigaffinen Rezeptor/Rezeptor-Interaktionen anzielen, die sich durch die Ligandenbindung bilden. Wir beschreiben einen DARPin, der Ig-homologie Domäne 4 bindet und der zu einer verringerten VEGFR-2 Phosphorylierung führt ohne dabei die Ligandenbindung zu stören. Dieser Inhibitor wirkt sich auch auf Abwärtssignalwege zu PLCγ1 aus und inhibiert die Bildung von neuen Trieben von Endothelzellen. Diese Art von Inhibition stellt einen neuen Inhibitionsmechanismus für VEGFR-2 dar, der komplementär zu anderen Behandlungen benutzt werden kann um die Effizienz der Anti-Angiogenese Therapie zu verbessern.

5   Introduction

5.1   The vascular system

5.1.1 Vasculogenesis & angiogenesis

In humans, the cardiovascular system serves as an internal communication network. Molecules, nutrients, but also waste products are delivered to or removed from distant organs and tissues. Thus, the cardiovascular system is one of the first organs that develops during embryonic growth of vertebrates. Two major processes are responsible for the development of the vasculature, vasculogenesis and angiogenesis. While vasculogenesis mainly occurs during early embryonic development, angiogenesis plays also an important role in adults. Wound healing and the formation of the corpus luteum during the female reproductive cycle are just two exemplary events, where angiogenesis is involved.

Vasculogenesis represents the process of the *de novo* formation of an immature vasculature in an avascular environment. In the embryo, premature vessels are built by angioblasts, which are differentiated endothelial cells from the mesoderm. Angioblasts coalesce at or close by their site of origin to construct a first network of vascular tubes, the primary capillary plexus (Risau and Flamme, 1995). This network already contains vessels in the developing embryo, for instance the aorta and major veins. In order to further mature the vasculature, a process called angiogenic remodeling occurs. Smooth muscle cells and pericytes are recruited to the existing vessels. They pack tightly with the endothelial cells and the extracellular matrix to form compact vessel walls.

Angiogenesis, the second step of vasculature maturation, signifies vessel growth from a preexisting vascular system into an avascular tissue region. There two major types of angiogenesis, which refer to sprouting angiogenesis and non-sprouting angiogenesis are observed. During sprouting angiogenesis endothelial cells proliferate and migrate into the proteolytically degraded extracellular matrix to form a new branch derived from an existing vessel. In

9

non-sprouting angiogenesis or intussusception, endothelial cells, which proliferated inside an existing vessel, form a lumen that can be divided by fusion or splitting of capillaries. Both angiogenic processes occur during the development of the cardiovascular system giving rise to the mature vasculature, but only angiogenesis is implicated to take place also in adults.

5.1.2 Molecular mechanisms of vessel formation

The formation of the vasculature is regulated by a plethora of molecules (Fig. 1). Early in embryonic development members of the fibroblast growth factor (FGF)-family induce the differentiation of hematopoietic precursor cells, the hemangioblasts which give rise to endothelial cells (Krah et al., 1994). Subsequently, the vascular endothelial growth factor (VEGF)-family plays an essential role in determining the fate of endothelial cells (Risau and Flamme, 1995; Risau, 1997). Mice that do not express VEGF-A show severe defects in the vascular development and die at embryonic day 9.5-10.5 (Carmeliet et al., 1996). The mutation of one single VEGF-A allele is enough to promote vascular abnormalities that lead to lethality at embryonic day 11-12 (Carmeliet et al., 1996; Ferrara et al., 1996). Most likely, VEGF exerts its differentiation inducing function through the receptor tyrosine kinase (RTK) VEGF-receptor (VEGFR)-2. This is supported by a VEGFR-2 knockout mouse that lacks both angioblasts and hematopoietic cells (Shalaby et al., 1995; Yamashita et al., 2000). Another VEGF-receptor, VEGFR-1, plays a crucial role in vasculogenesis. In mice deficient for VEGFR-1 angioblasts are present but they lack the primary vascular network, leading to lethality at embryonic day 8.5-9 (Fong et al., 1995). At the cellular level, overproliferation of hemangioblasts in *VEGFR-1$^{-/-}$* -mice has been shown to cause the malformation of the immature vasculature (Fong et al., 1999).

Fig. 1: Schematic representation of vascular development and the involved molecules and cells
The individual stages of vascular development are presented and below the molecules that are implicated in these steps are shown in boxes (a). Nascent vessels are composed of a single layer of endothelial cells forming a tube (b). As the nascent blood vessels mature into capillaries, they are surrounded by a basement membrane and pericytes (c). Mature arterioles and veins are additionally covered by smooth muscle cells, which contain their own basement membrane (d). (adapted from (Tallquist et al., 1999) & (Jain, 2003))

Further vessel maturation and remodeling of the initial vascular network are induced by angiopoietins (Ang), their receptors Tie1/2, and the ephrin-family of growth factors. In mice lacking Ang1 or its receptor Tie2 initially an immature vasculature is formed (Dumont et al., 1994; Sato et al., 1995). However, the endothelial cells forming the primary vasculature seem to be unable to associate with the supporting cells (Suri et al., 1996). Another member of the Ang-family, called Ang2, is important for further angiogenic and vasculogenic

remodeling. Ang2, an antagonist of Ang1 for Tie2, induces uncoupling of smooth muscle cells from endothelial cells and loosening of the extracellular matrix at the sites where angiogenic sprouting is supposed to occur (Maisonpierre et al., 1997). This enables endothelial cells to migrate and to form a new branch of the vessel.

Another important step in the maturation of blood vessels is the recruitment of periendothelial cells, such as vascular smooth muscle cells and pericytes. The platelet-derived growth factor (PDGF)-family plays an important role in this process. This family comprises four ligands, PDGF-A, -B, -C, and -D, and two receptors, PDGFR-α and PDGFR-β. The vascular endothelial cells building the immature network express PDGF-B, thereby recruiting mesenchymal progenitor cells expressing PDGFR-β (Hellstrom et al., 1999). Mice that are homozygous null for PDGF-B lack pericytes associated to vascular endothelial cells and show an impaired microvasculature (Hellstrom et al., 2001; Lindahl et al., 1997; Leveen et al., 1994). In addition to the recruitment of mural cells, PDGF-B expression leads to the migration of existing vascular smooth muscle cells and pericytes along the growing tip of a sprouting vessel.

In one of the final steps of the formation of the vasculature, vessels need to be defined as arterial or venous. Here the ephrin signaling system comes into play. The ephrin receptors (Eph) represent the largest known family of RTKs and in contrast to other ligand/receptor families ephrins need to be membrane anchored to bind to their receptors. Inactivation of either ephrinB2 or EphB4 in mice leads to similar effects as observed in Ang1/Tie2-deficient mice, such as the development of a normal primary vasculature with impaired association of supporting and endothelial cells (Wang et al., 1998). EphrinB2 is preferentially expressed in arterial endothelial cells, while its receptor EphB4 is mainly found in venous endothelial cells (Wang et al., 1998; Gerety et al., 1999). This expression pattern and the results of the knockout mice suggest that ephrinB2 and EphB4 determine the identity of venous and arterial vessels and they might be involved in the process of fusing them. Another role of ephrinB2 in the regulation of angiogenic sprouting and branching has been discovered recently (Sawamiphak et al., 2010; Wang et al., 2010). In these studies, the authors showed that ephrinB2-signaling through its PDZ interacting domain controls

VEGFR-2 and VEGFR-3 internalization and thus signaling by these two receptors. Mice expressing ephrinB2 that lacks its PDZ binding motif showed a decreased number of tip cells with a lower amount of filipodia in the mouse retina, suggesting that ephrinB2 regulates VEGF/VEGFR-2 induced filipodia extension of endothelial tip cells (Sawamiphak et al., 2010).

Other factors involved in the development of the vasculature are members of the transforming growth factor (TGF)-β superfamily, vascular endothelial (VE)-cadherin, and members of the Notch family of receptors. TGF-β1 is involved in vascular remodeling by initiating extracellular matrix deposition and the differentiation of mural cells from mesenchymal precursor cells (Pepper, 1997). Experiments performed with mice that are deficient for VE-cadherin or its β-catenin binding motif showed vascular plexus formation, but impaired vessel maturation, and increased endothelial apoptosis implicating a role of VE-cadherin/β-catenin signaling in controlling endothelial cell survival (Carmeliet et al., 1999a; Carmeliet and Collen, 2000). The Notch signaling pathway with its ligands Delta-like-4, Jagged-1, and Jagged-2 and its receptors Notch-1, Notch-3, and Notch-4 is implicated in the determination of endothelial cell fate as well as in the control of tip cell selection (Hellstrom et al., 2007). Notch signaling represses venous cell differentiation while favoring arterial cell differentiation in zebrafish (Lawson et al., 2001). In the event of blood vessel sprouting, Notch signaling acts as a repressor system in the cells adjacent to tip-cells, the so called mural cells (Hellstrom et al., 2007; Siekmann and Lawson, 2007).

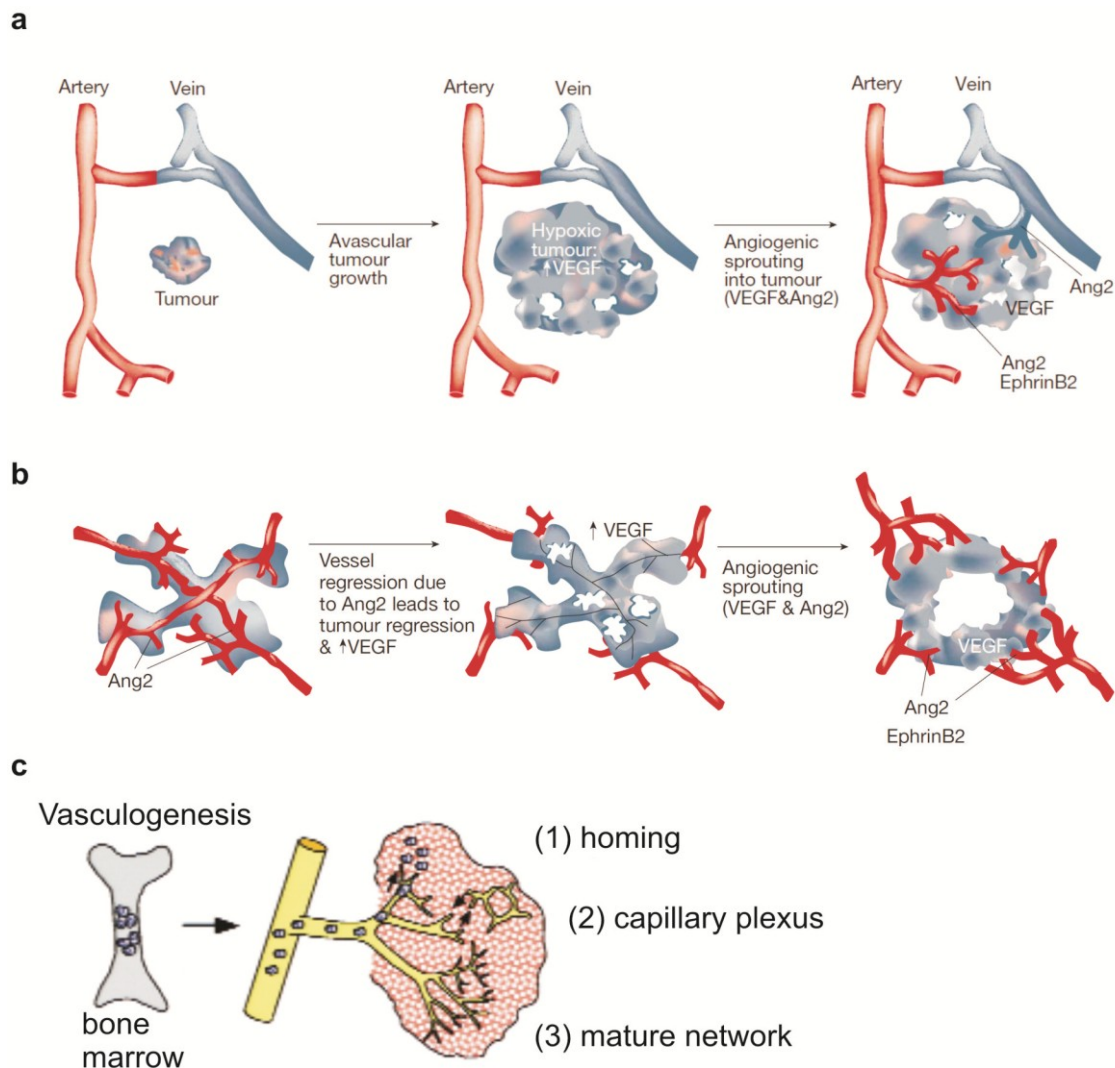### 5.1.3 Pathological angiogenesis in cancer

There are numerous human diseases involving excessive angiogenesis, abnormal vascular remodeling, insufficient vessel growth, or impaired vessel regression. The most prominent pathology hallmarked by excessive angiogenesis is cancer. Others include arthritis, psoriasis, artherosclerosis, obesity, and several retinopathies, for instance due to age-related macular degeneration (AMD) or diabetes. Insufficient vessel growth or abnormal blood vessel regression are characteristics of neurodegeneration, osteoporosis, heart

ischemia, and brain ischemia (Ferrara and Davis-Smyth, 1997; Ferrara and Kerbel, 2005).

Angiogenesis in cancer involves several different types of blood vessel formation in tumors: (1) avascular tumor growth initiates angiogenic sprouting towards the tumor of surrounding blood vessels, (2) tumor cells grow on and along existing host-vessels, and (3) endothelial precursor cells recruited from the bone-marrow further contribute to tumor angiogenesis (Fig. 2) (Yancopoulos et al., 2000; Carmeliet, 2000). Tumors can survive quiescent by quite a while, mainly regulated by a well balanced expression of pro-angiogenic and anti-angiogenic factors (Folkman, 1995). This balanced regulation of pro- and anti-angiogenic molecules is often referred to as the 'angiogenic switch'. There are a number of inducers of the 'angiogenic switch', including metabolic stress, mechanical stress, immune/inflammatory response, and mutations of oncogenes or tumor suppressor genes (Carmeliet and Jain, 2000).

The diffusion limit of oxygen in tissues is 100-200 μm. Hence, blood vessels need to be close to surrounding cells for the proper distribution of oxygen and nutrients. If tumors reach a size bigger than the oxygen diffusion limit, they become hypoxic and need to be vascularized. A hallmark of hypoxia is the upregulation of the transcription factor hypoxia-inducible factor 1 (HIF-1). Activation of HIF-1 in hypoxic tumors induces transcription of pro-angiogenic factors, such as VEGF, VEGFR, FGF, and TGF-β1 (Tang et al., 2004; Carmeliet et al., 1998). The expression of these molecules causes angiogenesis characterized by sprouting, branching, or intussusception of nearby vessels, followed by ingrowth of blood vessels into the tumor. Although the process of tumor angiogenesis and physiological angiogenesis are very similar, the newly formed blood vessels show quite distinct features. Tumor blood vessels often lack proper association with perivascular cells, such as smooth muscle cells or pericytes, or they do not even form a surrounding cell layer (Hashizume et al., 2000). This phenomenon leads to instability of the vessels, rendering them often leaky. Other features of tumor blood vessels include disorganization, uneven sizes, non-uniform layering by endothelial cells, and excessive branching and sprouting, aggravating the difficulties that anti-cancer treatments face (Morikawa et al., 2002; Chang et al., 2000; Baish

and Jain, 2000).

Fig. 2: Mechanisms of pathological angiogenesis associated with tumor growth
The tumor grows avascular leading to hypoxia induced expression of pro-angiogenic factors, which in turn initate blood vessl sprouting (a).The tumor co-opts existing blood vessels and grows along them, followed by vessel regression. The tumor becomes secondarily avascular causing angiogenic sprouting (b). Endothelial progenitor cells are recruited from the bone marrow by factors released by tumor cells leading to angiogenesis of adjacent blood vessels (c). (adapted from (Yancopoulos et al., 2000) & (Carmeliet, 2000))

In the case of tumors growing on and along existing blood vessels by co-option, vessels recognize the tumor cells and start to regress (Holash et al., 1999). This leads to a secondarily avascular and hypoxic tumor, which is accompanied by a significant tumor cell loss. At the margin of the tumor, angiogenesis is initiated, rescuing remaining tumor cells. Ang2 and VEGF seem to be key players of this

process, since Ang2 shows increased expression in the co-opted blood vessels, while VEGF is detectable in neighbouring tumor cells (Holash et al., 1999).

5.1.4 Pathological angiogenesis in age-related macular degeneration

Age-related macular degeneration describes a leading cause of blindness of elderly people and is the third major cause of blindness worldwide. There are two forms of AMD: dry (nonexudative) and wet (exudative) AMD. While in the dry form visual loss only slowly progresses over several years, patients suffering from the wet form can lose vision over a very short time frame, if the disease stays untreated. In the wet form of AMD, abnormal vessels grow from the choroidal vascular network which lies directly underneath the retina. This process is described as choroidal neovascularization and thought to be triggered by the permeability inducing function of VEGF. Blood, coming from the newly formed and excessively leaky vessels, leads to a swelling of the retina and edema formation, which subsequently results in impaired vision. Hence, a lot of therapeutic applications for wet AMD aim at inhibiting VEGF.

VEGF plays important roles in a number of pathological angiogenesis associated diseases, especially in the eye. One example in which VEGF induces pathological neovascularization in the eye is proliferative diabetic retinopathy.

5.1.5 Therapeutic approaches

Since the VEGF/VEGFR-signaling system is the major network involved in physiological and pathological angiogenesis, many therapeutic treatments focus on the members of the VEGF/VEGFR-family, no matter if promoting or inhibiting their function. Two types of anti-angiogenic therapies targeting the VEGF/VEGFR-system are used. The first aims at preventing ligand binding to the receptor by either blocking the ligand binding site at the receptor or vice-versa blocking the binding site of VEGF for the receptor. The second approach uses small molecule inhibitors that bind the intracellular kinase domain and block kinase activity.

The first drug targeting VEGF got the approval for treating colorectal cancer in

combination with chemotherapy by the US Food and Drug Administration in 2004 (Ferrara et al., 2004). It was a humanized monoclonal antibody neutralizing VEGF, known as bevacizumab or Avastin (Genentech). In the meantime it got also approved for treating breast and lung cancer. Ranibizumab, commercially available as Lucentis (Genentech), is an optimized Fab fragment of bevacizumab, which is successfully used to treat wet AMD (Ferrara et al., 2006). Patients suffering from wet AMD are able to regain sight, when treated with Lucentis at a monthly basis. In 2004, the US Food and Drug Administration approved pegaptanib (Macugen), an anti-VEGF aptamer, for the treatment of wet AMD (Willis et al., 1998; Gragoudas et al., 2004). Another concept to block ligand/receptor complex formation was to create a VEGF trap. Hence, Holash and colleagues engineered a recombinant protein consisting of Immunoglobulin (Ig)-like domain 2 of VEGFR-1 and Ig-homology domain 3 of VEGFR-2 predimerized by the constant region (Fc-region) of human IgG1 (Holash et al., 2002). The VEGF-trap (Regeneron) showed significantly higher affinity for VEGF than the native receptors. The researchers at ImClone Systems Incorporated also used antibodies against VEGFR-1 and/or VEGFR-2 to suppress tumor growth in mouse cancer models (Dias et al., 2000; Wu et al., 2006).

In a second approach to block pathological angiogenesis, small molecule inhibitors blocking the kinase domain have been developed. Among these types of inhibitors are Sutent (SU11248, Pfizer), Sorafenib (BAY 43-9006, Bayer), Vatalanib (PTK787/ZK222584, Novartis), and Recentin (AZD2171, AstraZeneca). Two types of small molecule inhibitors exist. One type targets the active conformation of the ATP-binding pocket of the kinases (type I inhibitors) and the other type prevents the kinase domain from undergoing structural and conformational changes that are needed to exploit its full function (type II inhibitors). Since the kinase domains of RTKs are highly conserved and thus structurally very homologous, small molecular weight inhibitors targeting the kinase domain are not very specific. Sutent, for instance, binds and inhibits VEGFR, PDGFR, Fms-like tyrosine kinase-3 (Flt-3), and c-Kit.

Another very promising approach for blocking VEGFR signaling emerged very recently. Alitalo and colleagues generated an antibody against VEGFR-3 that

binds the extracellular domain (ECD), but does not block ligand binding (Tvorogov et al., 2010). They showed that this antibody leads to decreased signal transduction, migration, and sprouting of microvascular endothelial cells *in vitro* and *in vivo*. A similar approach was successfully applied to VEGFR-2 (Kendrew et al., 2011).

One major problem in anti-angiogenic therapies targeting cancer lies in the development of resistance to the treatment (Fig. 3). The expression of other angiogenic factors than VEGF that take over as the disease progresses is a possible reason. Other explanations could be the recruitment of bone-marrow derived endothelial progenitor cells expressing angiogenic factors, pericytes protecting tumor blood vessels from anti-angiogenic treatment, increased tumor cell invasiveness, the co-opted growth of tumor cells along existing vessels making angiogenesis as a survival promoting process obsolete, and the existence of tumor cells that are hypoxia resistent (Fig. 3) (Bergers and Hanahan, 2008). Therefore, it is likely that anti-angiogenic treatment of tumors is not a standalone therapy. Targeting several angiogenic factors in combination with other treatments of tumor cells might be a successful option in treating cancer.

In addition, extensive efforts have been laid into developing therapeutic angiogenesis to treat ischemic disorders. Despite several preclinical and clinical trials using several angiogenesis inducing factors, such as application of VEGF and FGF isoforms, researchers are still waiting to achieve a major breakthrough.
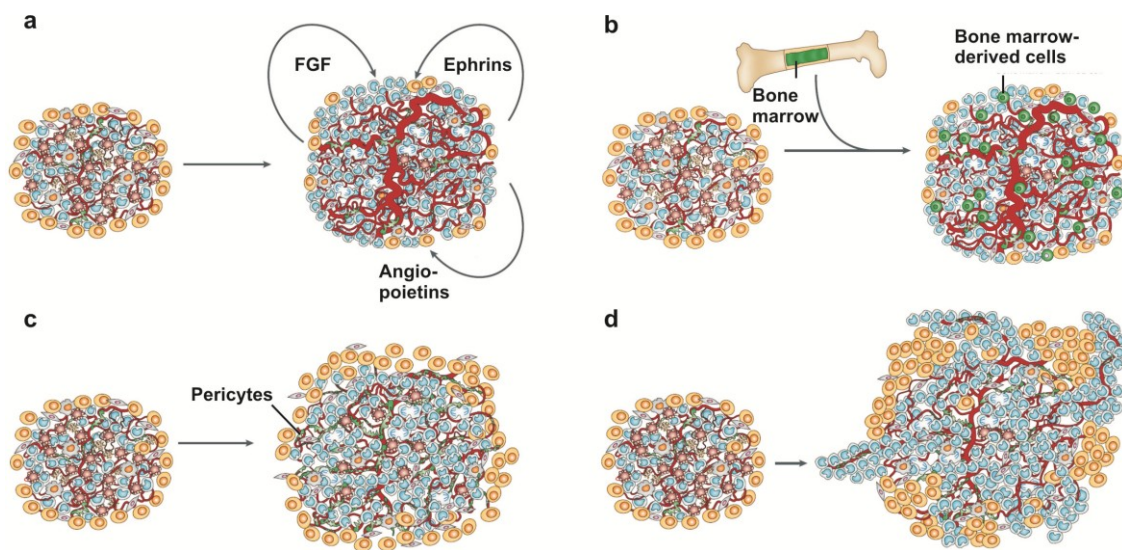
Fig. 3: Development of resistance to anti-angiogenic treatment of tumors; mechanisms
Upregulation of other pro-angiogenic factors, such as FGFs, ephrins, or angiopoietins circumvents anti-angiogenic therapy (a). Recruitment of bone marrow-derived endothelial progenitor cells expressing angiogenic factors can lead to new vascularization of tumor tissue (b). Development of a good perivascular cell layer including pericytes can render tumor blood vessels resistant to anti-angiogenic treatment (c). Increased invasiveness and growth of tumor cells along existing vasculature allows tumor cells to escape from oxygen and nutrient deprivation (d). (adapted from (Bergers and Hanahan, 2008))

5.2   The VEGF/VEGFR-signaling system

In humans, the VEGF family of growth factors consists of five members, namely VEGF-A, VEGF-B, VEGF-C, VEGF-D, and placenta growth factor (PlGF). Structurally related proteins that also belong to this family and do not exist in mammals, are VEGF-E, VEGF variants produced by some parapox viruses, and VEGF-F, VEGFs that were found in some snake venoms (Shibuya, 2003; Yamazaki et al., 2009). The VEGFs bind in an overlapping pattern to three different RTKs, which are called VEGFR-1, VEGFR-2, and VEGFR-3 (Fig. 4).
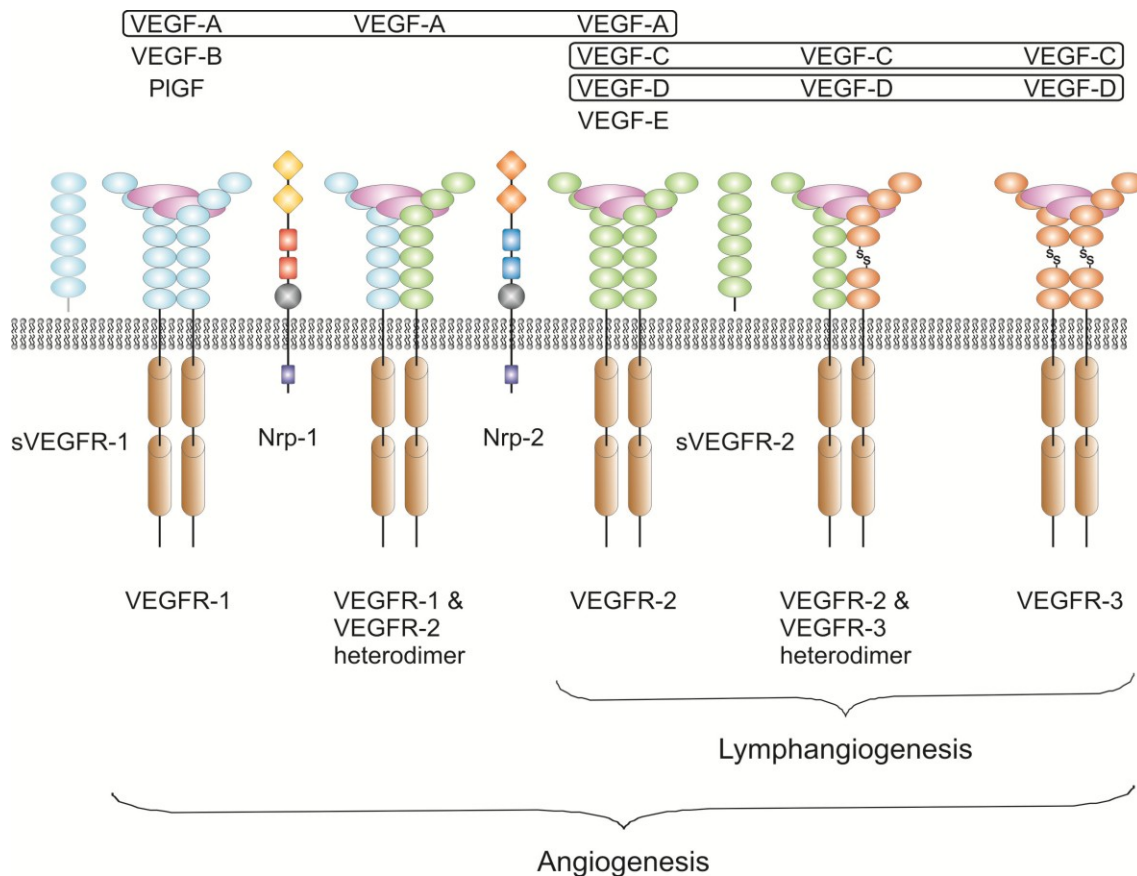
Fig. 4: Overview of the VEGF/VEGFR-signaling system
VEGFs bind three different RTKs, called VEGFR-1, -2, and -3. Ligand binding causes homo- and heterodimerization of the VEGFRs and subsequent activation. In addition, soluble VEGFR-1 (sVEGFR-1) and VEGFR-2 (sVEGFR-2) act as decoy receptors by capturing soluble VEGF. The signaling output is further modulated by co-receptors such as Neuropilin-1 and -2.

Alternative splicing and proteolytic processing give rise to several isoforms of every VEGF family member leading to different signaling functions (Fig. 5) (Takahashi and Shibuya, 2005). Ligand binding leads to dimerization of the receptor, followed by activation and tyrosine phosphorylation of the intracellular domain of the receptor. The phosphorylated tyrosines act as docking sites for signaling molecules such as phospholipase C-γ1 (PLCγ1), T-cell-specific adaptor (TSAd), and Shb (Src-homology-2 protein in β-cells) (Olsson et al., 2006). The binding of downstream signaling molecules of VEGFRs depends on which tyrosine residue gets phosphorylated leading to combinatorial signal output. The signaling output can be further modified by binding of co-receptors, such as neuropilin-1 (Nrp-1), neuropilin-2 (Nrp-2), clotho, or heparan sulfate proteoglycans (HSPG) (Grünewald et al., 2010).
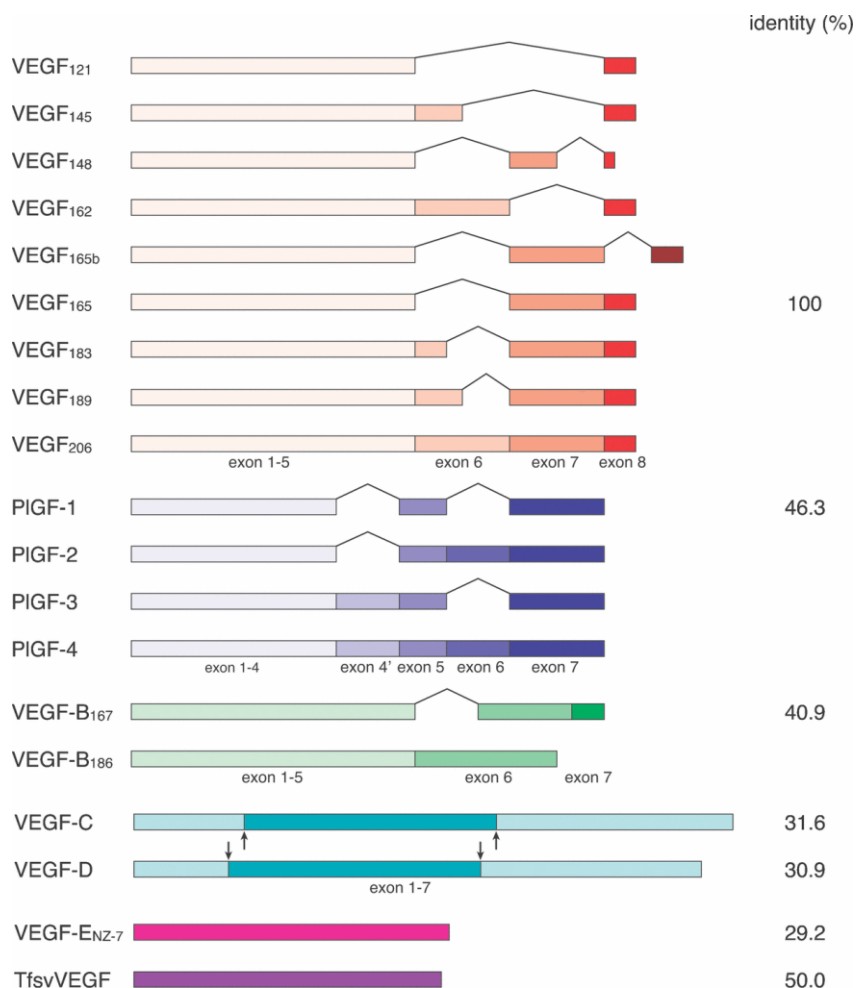
Fig. 5: Splice variants of the VEGF family and their mRNA structure
Alternative splicing and proteolytic processing give rise to a number of isoforms of VEGF-A, VEGF-B, and PlGF. The numbers on the right indicate the sequence identity to VEGF-A$_{165}$ at the amino acid level. Arrows indicate the sites of proteolytic digestion to generate VEGFR-2 binding variants of VEGF-C and VEGF-D. (Takahashi and Shibuya, 2005)

The VEGFRs belong to type V RTKs. They consist of seven Ig-homology domains in the extracellular region, a single transmembrane helix, a juxtamembrane domain, a split tyrosine-kinase domain, and a long tail at the C-terminus. VEGFR-3 is a special case, since it is proteolytically processed in the region of Ig-homology domain 5. Nevertheless, VEGFR-3 maintains its overall topology by crosslinking the proteolytic products through a disulfide-bridge. Ig-homology domain 2 and 3 compose the minimal ligand binding site (Keyt et al., 1996b), while the other Ig-homology domains are implicated in stabilizing the dimeric receptor or in preventing receptor dimerization in the absence of ligand (Ruch et al., 2007; Tao et al., 2001).

5.2.1 The ligands

<u>VEGF-A</u>

VEGF-A is the best characterized member of the VEGF family. Due to alternative splicing up to nine isoforms of VEGF-A can be found in the human body: VEGF-A$_{121}$, VEGF-A$_{145}$, VEGF-A$_{148}$, VEGF-A$_{162}$, VEGF-A$_{165}$, VEGF-A$_{165B}$, VEGF-A$_{183}$, VEGF-A$_{189}$, and VEGF-A$_{206}$ (Fig. 5). The subscript digits indicate the number of amino acids each isoform is composed of. All VEGF-A variants bind VEGFR-1 and VEGFR-2 with high affinity. The VEGF-A gene is located on human chromosome 6p21.3 (Vincenti et al., 1996) and is composed of eight exons and seven introns, giving rise to the aforementioned isoforms (Tischer et al., 1991; Houck et al., 1991). VEGF-A is expressed in endothelial cells, macrophages, T-cells and a number of other cells (Ferrara and Davis-Smyth, 1997; Freeman et al., 1995). The most abundant isoforms of VEGF-A are VEGF-A$_{121}$, VEGF-A$_{165}$, and VEGF-A$_{189}$.

VEGF-A$_{121}$ lacks the amino acid sequences of exon 6 and 7, rendering it incapable of binding HSPG. Thus, VEGF-A$_{121}$ is freely diffusible upon secretion by cells. Knockout of VEGF-A$_{164}$ or VEGF-A$_{188}$ in mice (in mice the VEGF-variants are all one amino acid shorter) results in lethality shortly after birth due to excessive organ bleeding in 50% of the cases and the remaining mice die within 14 days post-natally due to cardiac failure (Carmeliet et al., 1999b). In addition, mice exclusively expressing VEGF-A$_{120}$ show severe defects in skeletal development, vascularization of the retina, and in myocardial angiogenesis (Maes et al., 2002; Zelzer et al., 2002). These findings indicate that the heparin binding domain of VEGFs is essential to initiate vascular branching and sprouting in a spatially very restricted way.

VEGF-A$_{165}$, often only referred to as VEGF, contains the amino acid sequence encoded by exon 7 and thus shows a reasonable affinity for heparin (Ferrara and Henzel, 1989). Mice engineered to express only VEGF-A$_{164}$ show normal development of the vasculature (Stalmans et al., 2002). On the other hand, mice expressing no VEGF-A die before embryonic day 9.5-10.5 (Carmeliet et al., 1996). Even the mutation of one single VEGF-A allele is sufficient to severely impair the development of the vasculature leading to lethality at

embryonic day 11-12 (Ferrara et al., 1996). These results underscore the central role that VEGF-A$_{165}$ plays in the development of the vasculature. Interestingly, the VEGF-A$_{165B}$ splice variant that differs from VEGF-A$_{165}$ only in the last 6 amino acids has an inhibitory effect on angiogenesis when added together with VEGF-A$_{165}$ (Bates et al., 2002). This is explained by the fact that VEGF-A$_{165B}$ lacks the ability to bind Nrp-1 (Cébe-Suarez et al., 2006).

Whereas VEGF-A$_{121}$ is freely diffusible and VEGF-A$_{165}$ has an intermediate affinity for HSPG or other extracellular matrix components, VEGF-A$_{189}$ shows a very high affinity for HSPG, which results from the additional amino acids encoded by exon 6 (Park et al., 1993). However, proteolytic digestion can render extracellular matrix or cell bound VEGFs diffusible. Plasmin cleavage at the carboxy-terminus (C-terminus) produces a VEGF-variant consisting only of amino acids 1-110 (Keyt et al., 1996a). The mitogenic function of VEGF-A$_{1-110}$, similar to VEGF-A$_{121}$, is significantly decreased compared to VEGF-A$_{165}$. VEGF-A$_{189}$ can be converted to an endothelial cell differentiation factor by urokinase controlled proteolysis (Plouet et al., 1997). This shows that the different VEGF isoforms have distinct functions in the vascular development, with VEGF-A$_{165}$ as the central player.

VEGF-B

As is the case with VEGF-A, the VEGF-B gene gives rise to more than one isoform by alternative splicing: VEGF-B$_{167}$ and VEGF-B$_{186}$ (Fig. 5). Both VEGF-B proteins contain the same 116 amino-terminal (N-terminal) amino acids, but differ significantly in their C-terminus. VEGF-B$_{167}$ is able to bind to HSPGs with its carboxy-terminal tail and is thus associated with the extracellular matrix or cell-surface bound HSPGs (Olofsson et al., 1996a). VEGF-B$_{189}$ on the other hand is not capable to bind to HSPGs with its C-terminal domain and is thus a freely diffusable protein once it is secreted by cells (Olofsson et al., 1996b). Both isoforms exert their functions exclusively through binding to VEGFR-1, but they are also able to bind Nrp-1 (Makinen et al., 1999).

The functional role of VEGF-B was and still is under debate. Since VEGFs are

major players in the vascular development, researchers mainly focused on the angiogenic potential of VEGF-B. The knockout of VEGF-B in mice was not lethal and led to healthy and fertile animals as opposed to VEGF-A knockout mice. However, they showed a reduced heart size, dysfunctional coronary vasculature, and an impaired recovery from cardiac ischemia (Aase et al., 2001; Bellomo et al., 2000). These findings correlated with the expression pattern of VEGF-B, which is mainly found in the heart, but also in other tissues such as brown fat, skin, and the brain (Aase et al., 1999; Lagercrantz et al., 1996). Nevertheless, VEGF-B has not been proven so far to be a pro-angiogenic factor, although it has been detected in a number of different cancer types (Salven et al., 1998; Niki et al., 2000), where it is believed to supplement the angiogenic potential of other VEGF family members.

A new role of VEGF-B has been proposed very recently by the lab of Ulf Eriksson (Hagberg et al., 2010). They report that VEGF-B regulates the fatty acid uptake of endothelial cells and thereby the transport of fatty acids to peripheral organs. Mice that are deficient for VEGF-B show a decreased level of lipids in heart, muscle, and brown adipose tissue. Hence, the function of the VEGF family is not restricted to the development and regulation of the vasculature; instead it is also involved in the regulation of metabolic pathways.

PlGF

PlGF was initially described in 1991 as a growth factor that was isolated from a placental cDNA-library (Maglione et al., 1991). Its transcript is detectable in the placenta at all stages of human gestation and has been also observed in the heart, lung, thyroid gland, and skeletal muscle (Persico et al., 1999). Alternative splicing generates four different isoforms (Fig. 5), which display different binding properties: PlGF-1 ($PlGF_{131}$), PlGF-2 ($PlGF_{152}$), PlGF-3 ($PlGF_{203}$), and PlGF-4 ($PlGF_{224}$). While PlGF-2 and -4 are able to bind heparin, PlGF-1 and -3 do not contain a heparin binding motif (Maglione et al., 1993; Yang et al., 2003). PlGF binds to VEGFR-1, but not to VEGFR-2 or -3 (Park et al., 1994). PlGF-2 is also known to bind Nrp-1 and -2.

The deletion of PlGF in mice did not affect the development of the vasculature

in the embryo. However, it affected angiogenesis in pathological conditions, such as in ischemia, inflammation, and cancer (Carmeliet et al., 2001). Further implications that PIGF is involved in pathological angiogenesis come from Peter Carmeliet's research group. They showed that treatment of ischemic tissue with PIGF led to a revascularization and that angiogenesis was inhibited in tumors, atherosclerosis, and arthritis when treated with anti-VEGFR-1 antibodies (Luttun et al., 2002). Moreover, PIGF signaling through VEGFR-1 leads to transphosphorylation or activation of VEGFR-2 by VEGFR-1, indicating that PIGF enhances VEGF-A signaling (Autiero et al., 2003). In 2007 a monoclonal antibody raised against PIGF has been shown to inhibit tumor angiogenesis, growth, and metastasis, even in tumors that were resistant to other VEGFR-inhibitors (Fischer et al., 2007). The anti-PIGF antibody displayed no side effects on normal, physiological angiogenesis, raising the hopes for a new anti-cancer treatment, also in combination with already existing therapies. However, a recent study where researchers analyzed several new anti-PIGF antibodies in 15 different models, showed no effect on tumor angiogenesis either as a standalone treatment or in combination with anti-VEGF-A treatment (Bais et al., 2010). This report has been promptly answered by testing additional anti-PIGF antibodies as well as by reagents blocking PIGF using genetic tools in animal tumor models, showing that anti-PIGF treatment can be an option in specific types of tumors (Van, V et al., 2010). Hence, more studies are needed to explore the exact functions as well as the therapeutical potential of PIGF.

5.2.2 The receptors

<u>VEGFR-1</u>

VEGFR-1 was reported for the first time in 1990, when it was cloned from a placental cDNA-library (Shibuya et al., 1990). In addition to vascular endothelial cells, VEGFR-1 is also expressed in non-endothelial cells such as macrophages, monocytes, and hematopoietic stem cells (Sawano et al., 2001; Hattori et al., 2002). It is a high-affinity receptor for VEGF-A, VEGF-B, PIGF, and some VEGFs that are found in snake venoms. The affinity of VEGF-A

binding to VEGFR-1 is at least 10-fold higher than for VEGFR-2. However, the kinase domain of VEGFR-1 shows only weak tyrosine phosphorylation activity compared to VEGFR-2 (Waltenberger et al., 1994; Seetharam et al., 1995). Work with chimeric VEGFR-1/VEGFR-2 proteins suggests that the juxtamembrane domain of VEGFR-1 contains an inhibitory element causing attenuation of kinase activity (Gille et al., 2000). In addition, mutation of the amino acid N1050 to D in the activation loop of the VEGFR-1 kinase domain changed the characteristics of the kinase domain and increased its activity (Meyer et al., 2006). The modest activity of the VEGFR-1 kinase domain made it very challenging to study the function of this receptor.

In total, there exist six tyrosine residues in the kinase domain and one in the juxtamembrane domain of VEGFR-1 that have been reported to get phosphorylated leading to interactions with downstream signaling molecules (Fig. 6) (Cunningham et al., 1995; Sawano et al., 1997; Ito et al., 2001). Tyrosine phosphorylation depends on the ligand binding to VEGFR-1. For instance, Autiero et al. reported that Y1213 gets phosphorylated upon VEGF-A binding, whereas PlGF leads to phosphorylation of Y1309 (Autiero et al., 2003). Several interacting downstream molecules binding to phosphorylated tyrosine residues have been identified, such as p85/phosphatidylinositol-3 kinase (PI3K), PLCγ1, Src-homology phosphatase-2 (SHP2), growth-factor-receptor-bound-2 (Grb2) protein and Nck (Matsumoto and Claesson-Welsh, 2001). However, the individual signaling pathways and their functional output are still not well characterized.

The knockout of VEGFR-1 in mice caused prenatal lethality at embryonic day 8.5-9 (Fong et al., 1995). Later it was revealed that the lack of the VEGFR-1 protein leads to overproliferation of endothelial progenitor cells (Fong et al., 1999). These data suggest, that VEGFR-1 may act as a decoy receptor during embryonic development of the vasculature, sequestering excessive VEGF-A and thereby spatially controlling the VEGF-A concentration. Further support for this hypothesis came from experiments with mice that express a truncated VEGFR-1 lacking the intracellular tyrosine-kinase domain. These animals survived and developed a normal vasculature (Hiratsuka et al., 1998). The localization of the VEGFR-1 ECD seems to be important, since 50% of the mice

expressing only soluble VEGFR-1 ECD suffer from embryonic lethality due to impaired vasculogenesis, whereas the other half survives (Hiratsuka et al., 2005). Another function of VEGFR-1 is its ability to induce macrophage and monocyte migration upon VEGF-A or PlGF-stimulation (Barleon et al., 1996; Clauss et al., 1996). This biological function of VEGFR-1 was supported by the decreased migration rate of macrophages that was observed in mice expressing VEGFR-1 lacking the tyrosine kinase domain (Hiratsuka et al., 1998).

Next to its involvement in physiological processes, VEGFR-1 seems also to be part of pathological angiogenesis. VEGFR-1 transcripts were observed in ischemic and inflammatory diseases (Luttun et al., 2002), but also in a number of tumors, such as in non-small cell lung cancer, prostate, breast and colon cancer, pulmonary adenocarcinoma, hepatocellular carcinoma, glioblastoma, and multiple myeloma (Andre et al., 2000; Plate et al., 1994). This raised the interest of researchers to target VEGFR-1 as a therapeutic strategy (Fischer et al., 2008). However, further insight into the signaling properties of VEGFR-1 and clinical data are still missing.
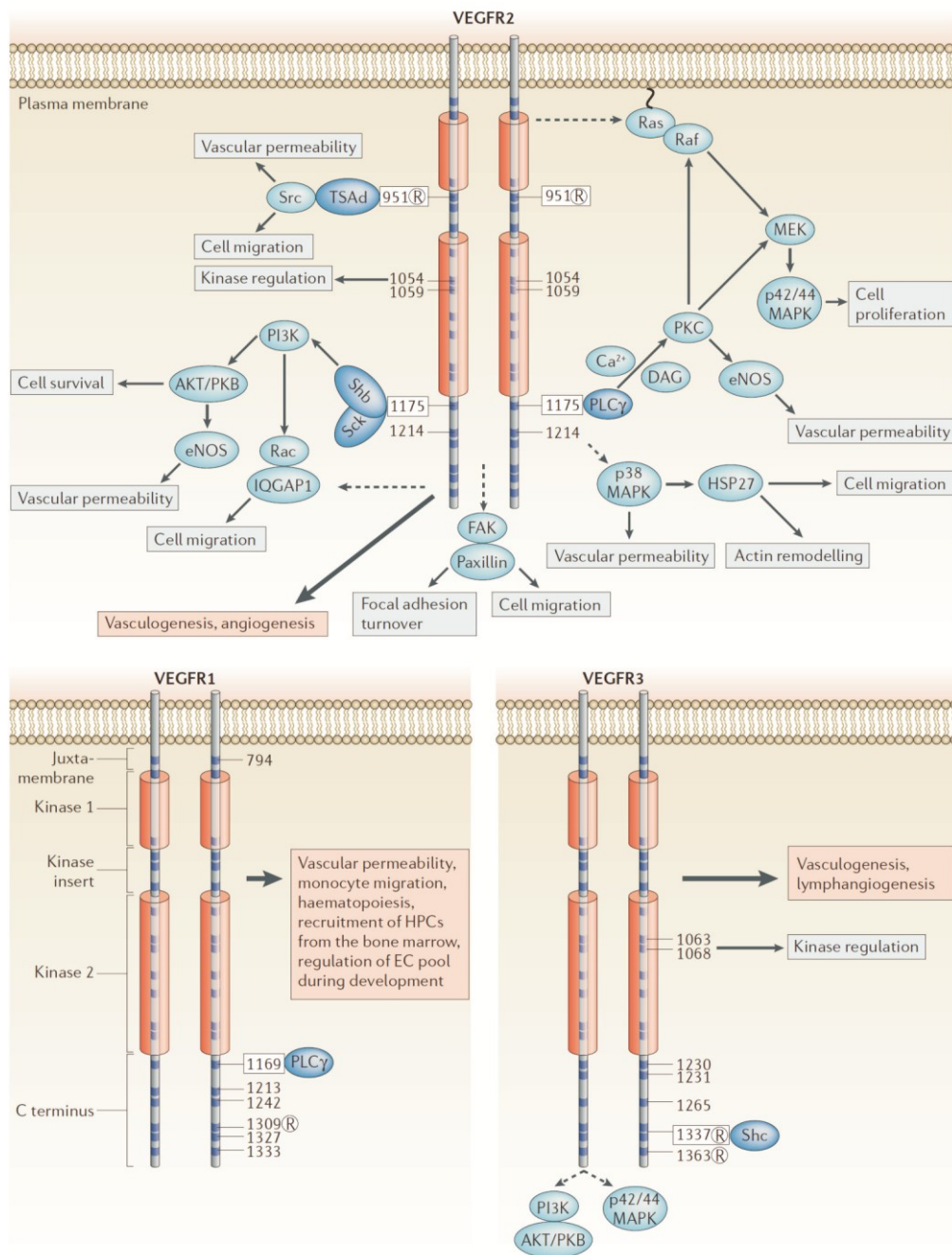
Fig. 6: Schematic representation of the intracellular VEGFR-tyrosine residues that are phosphorylated and upon activation recruit downstream signaling proteins
Schematic representation of the intracellular domains of VEGFR-1 (bottom left), VEGFR-2 (top), and VEGFR-3 (bottom right). Dark blue boxes indicate tyrosine residues. Signaling proteins that are known to interact with phosphorylated tyrosines are displayed in dark blue ovals. Subsequent signaling-cascades (light blue ovals) activate specific biological responses (pale boxes). (adapted from (Olsson et al., 2006)

In addition to the full length receptor, a soluble variant of VEGFR-1 (sVEGFR-1), which is composed of the first six Ig-homology domains of the

VEGFR-1 ECD, has been identified (Kendall and Thomas, 1993). The soluble variant of VEGFR-1 acts as a ligand trap by binding with high affinity to VEGF-A, VEGF-B, and PIGF. Therefore, its biological function appears to be inhibition of angiogenesis by sequestering VEGF-A preventing it thereby from binding to VEGFR-2. This leads to inhibition of oedema formation by interfering with VEGF-A mediated vascular permeability, and an anti-inflammatory function, by preventing VEGFR-1 induced monocyte/macrophage migration. Pathologically, sVEGFR-1 is upregulated in preeclampsia, a syndrome affecting 5% of all pregnancies, leading to decreased levels of VEGF-A and PIGF and ultimately to endothelial dysfunction (Maynard et al., 2003). Administration of exogenous VEGF-A and PIGF rescued this phenotype.

VEGFR-2

VEGFR-2 is the key receptor in embryogenic vascular development and probably the best characterized VEGFR, due to the fact that it shows a higher tyrosine kinase activity than VEGFR-1. It can be activated by binding to VEGF-A, VEGF-E, VEGF-C, and VEGF-D once the latter two are proteolytically processed. Terman and colleagues were the first researchers to be able to isolate the gene encoding VEGFR-2 (Terman et al., 1991).

As with the other VEGFRs, ligand binding induces receptor dimerization followed by intracellular autophosphorylation. The phosphorylated tyrosine residues serve as docking sites for downstream signaling molecules, containing either Src-homology (SH) domains or phospho-tyrosine binding (PTB) domains. Several intracellular tyrosine residues that get phosphorylated and recruit proteins have been mapped (Fig. 6). The most important tyrosines that play a functional role are Y951 in the kinase-insert domain, Y1054, and Y1059 in the kinase activation loop, and Y1175, and Y1214 in the C-terminal tail. The phosphorylation of amino acid Y951 has been shown to mediate the binding of TSAd regulating the induction of vascular permeability and cell migration (Matsumoto et al., 2005; Wu et al., 2000). Phosphorylation of Y1054 and Y1059 is a prerequisite for the kinase to gain full activity (Kendall et al., 1999; Takahashi et al., 2001). PLCγ1 signaling to protein kinase C (PKC) and

subsequent activation of the mitogen-activated protein kinases p42/44 is mediated through the phoshorylation of Y1175, which is the binding site for PLCγ1 (Cunningham et al., 1997). The adaptor proteins Shb and Shc-like protein (Sck) also bind to phosphorylated Y1175 (Holmqvist et al., 2004; Warner et al., 2000).

The fact that VEGFR-2 is a major mediator of angiogenesis is supported by its early presence in endothelial cells during murine embryogenesis. VEGFR-2 protein is first observed in mesodermal blood island progenitors at embryonic day 7 and later detected in vascular endothelial precursor cells and developing endothelial cells (Millauer et al., 1993; Yamaguchi et al., 1993). As mentioned earlier, mice that are deficient for VEGFR-2 die at the embryonic stage owing to malformation of the vasculature (Shalaby et al., 1995). VEGFR-2 mediates several physiological functions in endothelial cells such as migration, proliferation, survival, and permeability. The PLCγ1 activating signaling pathway appears to be a key regulator of cell proliferation and vascular permeability. PLCγ1 binding to VEGFR-2 leads to the generation of diacylglycerol and inositol-1,4,5-triphosphate, which causes PKC activation and an increase in the intracellular calcium concentration, respectively. This in turn activates the mitogen-activated protein kinases p42/44 resulting in endothelial cell proliferation (Takahashi et al., 2001). Mice that carry a mutation at position Y1173 (murine VEGFR-2 is two amino acids shorter) are embryonically lethal due to defective endothelial and hematopoietic cells, highlighting the importance of PLCγ1 signaling in vasculogenesis and angiogenesis (Sakurai et al., 2005). Although it still needs to be determined whether or not the observed effects are really mediated through PLCγ1 and not through Shb and Sck, which also bind VEGFR-2 at this site. Endothelial cell migration is an important function that is needed in angiogenesis. Several signaling cascades activated by VEGFR-2 are implicated in cell migration. Binding of TSAd to Y951 followed by complex formation between TSAd and Src leads to cell migration, which was indicated by point mutagenesis of Y951 (Matsumoto et al., 2005). Other adaptor proteins that lead to an initiation of cell migration are Nck that signals through the p38-kinase pathway (Lamalice et al., 2006) and focal adhesion kinase which is activated by Shb (Holmqvist et al., 2003). Cell survival is mainly mediated

through Y1175 which recruits Shb, followed by activation of PI3K and protein kinase B/Akt (Fujio and Walsh, 1999). The induction of vascular permeability through VEGFR-2 requires the activation of eNOS. Two signaling pathways can result in eNOS activation: PLCγ induced influx of calcium and the activation of protein kinase B/Akt (Fulton et al., 1999; Dimmeler et al., 1999).

Interestingly, as in VEGFR-1, alternative splicing and/or proteolytic processing give rise to a soluble VEGFR-2 consisting only of the first six Ig-homology domains (Ebos et al., 2004). Its function is not quite clear yet, but a recent study suggested that sVEGFR-2 acts as a negative regulator of lymphangiogenesis by capturing VEGF-C (Albuquerque et al., 2009).

<u>VEGFR-3</u>

VEGFR-3 is a RTK important in lymhangiogenesis. This effect is mainly mediated by VEGF-C, since knockout of VEGF-C in mice causes embryonic lethality due to impaired lymph vessel development (Karkkainen et al., 2004), whereas VEGF-D deficient mice develop with only minor defects (Baldwin et al., 2005). During embryogenesis VEGFR-3 is present in all endothelial cells, whereas in adults its expression is limited to lymphatic endothelial cells (Kaipainen et al., 1995). Mice that do not express VEGFR-3 die during embryogenesis before lymphatics start to develop owing to vascular remodeling defects (Dumont et al., 1998). This indicates an additional role of VEGFR-3 in angiogenesis. Indeed, blocking of VEGFR-3, which is also highly expressed in sprouting endothelial cells, by monoclonal antibodies caused impaired angiogenesis and defects in vascular network formation (Tammela et al., 2008). It was also shown that VEGFR-3 can form VEGF-C mediated heterodimers with VEGFR-2, for instance to positively regulate angiogenic sprouting (Nilsson et al., 2010; Dixelius et al., 2003).

5.3   The structure of VEGFs and VEGFRs

To date there are a number of structures of VEGF or VEGFR molecules (Table 1) available in the Protein Data Bank (www.pdb.org) (Berman et al.,

2000). These include the receptor binding core of all ligands either alone or in complex with minimal ligand-binding domains of VEGFR-1 and -2, and the kinase domain of VEGFR-1 and -2 either alone or in complex with inhibitors (reviewed in (Grünewald et al., 2010)). However, several features are still not structurally characterized. For instance a structure of the complete ECD is still missing, as it is the case with the transmembrane domain. The structure of the kinase domain lacks the juxtamembrane domain, the kinase insert domain, and the C-terminal tail, all which are of high interest and act as adaptor sites for downstream molecules.

Table 1: Crystal structures found in the protein data bank (PDB), when searched for VEGF
The names of the molecules that are present in the crystal structure are listed together with their PDB-entry codes (PDB-ID), their resolution in Å, and the references.

PDB ID	Molecules	Resolution [Å]	Reference
1FZV	PlGF-1	2.00	(Iyer et al., 2001)
1RV6	PlGF-1/VEGFR-1 D2	2.45	(Christinger et al., 2004)
1WQ8	Vammin	1.90	(Suto et al., 2005)
1VPF	VEGF-A	2.50	(Muller et al., 1997b)
2VPF	VEGF-A	1.93	(Muller et al., 1997a)
1MJV	VEGF-A (C51A and C60A)	2.10	(Muller et al., 2002)
1MKG	VEGF-A (C57A and C102A)	2.50	(Muller et al., 2002)
1MKK	VEGF-A (C61A and C104A)	1.32	(Muller et al., 2002)
1BJ1	VEGF-A/antibody-complex	2.40	(Muller et al., 1998)
1CZ8	VEGF-A/antibody-complex	2.40	(Chen et al., 1999)
2FJH	VEGF-A/B20-4 Fab-complex	3.10	(Fuh et al., 2006)
3BDY	VEGF-A/bH1-Fab-complex	2.60	(Bostrom et al., 2009)
2QR0	VEGF-A/Fab-complex	3.50	(Fellouse et al., 2007)
2FJF	VEGF-A/G6 Fab-complex	2.65	(Fuh et al., 2006)
2FJG	VEGF-A/G6 Fab-complex	2.80	(Fuh et al., 2006)
1VPP	VEGF-A/Receptor Blocking Peptide-complex	1.90	(Wiesmann et al., 1998)
1FLT	VEGF-A/VEGFR-1 D2	1.70	(Wiesmann et al., 1997)
1QTY	VEGF-A/VEGFR-1 D2	2.70	(Starovasnik et al., 1999)
1TZH	VEGF-A/YADS1 Fab-complex	2.60	(Fellouse et al., 2004)
1TZI	VEGF-A/YADS2 Fab-complex	2.80	(Fellouse et al., 2004)
2C7W	VEGF-B	2.48	(Iyer et al., 2006)
2VWE	VEGF-B/Fab-complex	3.40	(Leonard et al., 2008)
2XAC	VEGF-B/VEGFR-1 D2	2.71	(Iyer et al., 2010)
2X1W	VEGF-C/VEGFR-2 D2-3	2.70	(Leppanen et al., 2010b)
2X1X	VEGF-C/VEGFR-2 D2-3	3.10	(Leppanen et al., 2010b)
2XV7	VEGF-D	2.90	(Leppanen et al., 2010a)
2GNN	VEGF-E NZ2	2.30	(Pieren et al., 2006)
3HNG	VEGFR-1 Kinase Domain / inhibitor-complex	2.70	
1VR2	VEGFR-2 Kinase Domain	2.40	(McTigue et al., 1999)
2XIR	VEGFR-2 Kinase Domain / PF-00337210-complex	1.50	
3KVQ	VEGFR-2 D7	2.70	(Yang et al., 2010)
1WQ9	VR-1	2.00	(Suto et al., 2005)

5.3.1 The ligands

The first structure of a VEGF family member that has been solved was the crystal structure of VEGF-A (Muller et al., 1997b). It shows an anti-parallel dimeric organization of the protein, where the monomers are crosslinked by two disulfide bridges composed of C51 and C60 (Fig. 7a). The structure contains a cystine-knot motif, a feature that is characteristic for all VEGFs and the related growth factors PDGF and TGFβ (Oefner et al., 1992; Schlunegger and Grutter, 1992). The knot is formed by a disulfide bond between C26-C68 passing through a ring like structure that is built by two intramolecular disulfide bonds between C57-C102 and C61-C104. A twisted β-sheet formed by four β-strands, called β1, β3, β5, and β6, extends from the cystine-knot motif. The individual β-strands are connected by three solvent exposed loops that form receptor binding sites. In addition, each monomer contains an N-terminal helix.
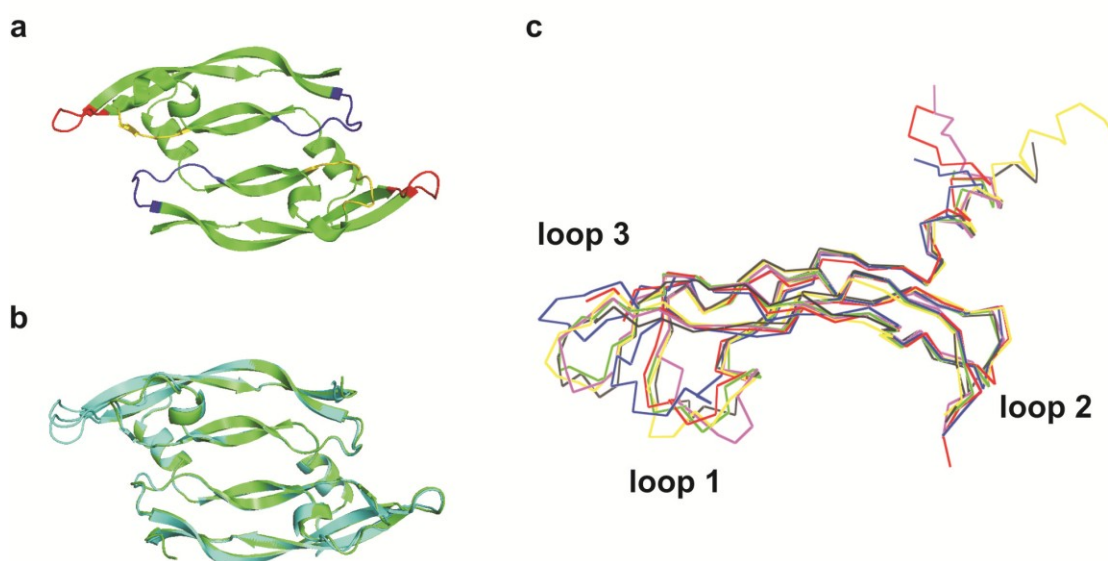
Fig. 7: Crystal structures of the VEGF family of growth factors
Bottom view of VEGF-A (PDB-entry 1VPF) is shown in the cartoon representation (a). The loops that are involved in VEGFR binding are highlighted: loop 1 (yellow), loop 2 (blue), and loop 3 (red). In the superimposition of the free VEGF-A (green; PDB-entry 2VPF) and the receptor-bound VEGF-A (cyan; PDB-entry 1FLT) only minor conformational changes are observed (b). Superimposition of the VEGF-A (green; PDB-entry 1VPF), VEGF-B (blue; PDB-entry 2C7W), VEGF-C (gray; PDB-entry 2X1W), PlGF (magenta; PDB-entry 1FZV), VEGF-E (red; PDB-entry 2GNN) with VEGF-D (yellow; PDB-entry 2XV7) (c). The Cα-traces are shown in the ribbon representation.

Later on, the structures of VEGF-B (Iyer et al., 2006; Leonard et al., 2008), PlGF (Iyer et al., 2001), VEGF-C (Leppanen et al., 2010b), VEGF-D (Leppanen et al., 2010a), VEGF-E (Pieren et al., 2006), and VEGF-F (Suto et al., 2005) have been solved. All VEGFs share the commonly found structural features typical for this protein family, such as the cystine-knot motif, the irregular β-sheet composed of four β-strands, and the N-terminal helix, which folds back on top of the other monomer, thereby stabilizing the dimer. The cores of all these ligands show high similarities, indicated by root mean square deviations of ~1.0 Å, when superimposing VEGF-E with its homologs VEGF-A, VEGF-B, PlGF, and Vammin and VR-1, two snake venom VEGFs (Pieren et al., 2006). The most significant differences can be found in the loops connecting the β-strands, and in the N-terminal helix, which appears to be much more extended in VEGF-C and -D (Fig. 7c). Interestingly, prolonged N-terminal helices of VEGF-C and -D provide additional interaction sites for VEGFR-2 and -3 (Leppanen et al., 2010a; Leppanen et al., 2010b). Major conformational changes in loop 1 and 3 of VEGF-E account for the binding selectivity of VEGF-E, which binds only to VEGFR-2 but not to VEGFR-1 (Pieren et al., 2006). Similar observations have been made with the VEGF-B and PlGF structures.

To date, structural data for ligands in complex with receptor domains are only available for VEGF-A (Wiesmann et al., 1997), VEGF-B (Iyer et al., 2010), VEGF-C (Leppanen et al., 2010b), and PlGF (Christinger et al., 2004). The structure of VEGF-A in complex with Ig-homology domain 2 of VEGFR-1 revealed that loop 1 and loop 3 of one VEGF-A monomer interact with the receptor, and loop 2, located at the other pole of the monomer, interacts with the second molecule of VEGFR-1 thereby inducing receptor dimerization (Wiesmann et al., 1997). This also explains the conformational differences found in these loops within the VEGF family. Nonetheless, when comparing the structures of the free ligands with the receptor-bound ligands, no major structural changes are observed (Fig. 7b).

5.3.2 The extracellular domain of VEGFRs

In addition to the VEGF/VEGFR-complex structures mentioned above, only one additional crystal structure of a VEGFR ECD domain has been solved, which is the structure of VEGFR-2 Ig-homology domain 7 (Fig. 8) (Yang et al., 2010). All structures combined show that the Ig-homology domains of VEGFRs belong to the I-set of the immunoglobulin superfamily, although the VEGFR-2 D2 and D3 do not show all the characteristic features (Harpaz and Chothia, 1994). In VEGFR-1 D2, the β-strands βa', βc, βc', βf, βg, and the β-strands βb, βd, βe form two β-sheets that are organized in a sandwich-like conformation and that are connected by a disulfide bond between C158 and C207 (Wiesmann et al., 1997). In VEGFR-2 D7, the two β-sheets are each formed by four β-strands and are also covalently linked through a disulfide bond between C688 and C737 (Yang et al., 2010).
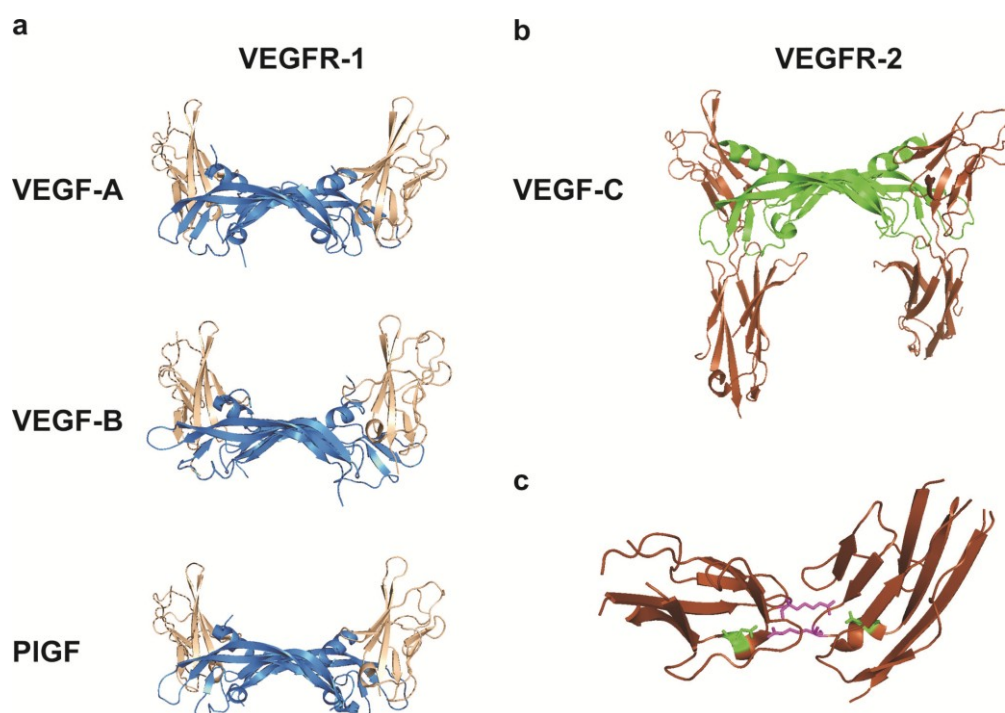
Fig. 8: Crystal structures of VEGFR ECD domains
Cartoon representation of the VEGFR-1 D2 (wheat) in complex with VEGF-A, VEGF-B, and PlGF (blue) (a).Structure of VEGF-C (green) in complex with Ig-homology domain 2-3 of VEGFR-2 (brown) (b). Top view on the structure of VEGFR-2 D7 (c). The amino acids R726 and D731 that form salt bridges are highlighted in magenta and green, respectively.

The binding interfaces of all ligand/receptor complexes seem to be rather flat and mainly be mediated by hydrophobic interactions. The analysis of the electrostatic surface potential of the ligand-binding regions on the receptor domains revealed that VEGFR-1 contains a positively charged binding interface, whereas VEGFR-2 displays a negatively charged surface at the binding interface (Iyer et al., 2010). Complementary to these findings ligands with binding specificities for VEGFR-1, such as VEGF-B and PlGF, display negatively charged patches at the binding interface. In agreement with this, mutation of the basic amino acids H223 and R224 located in VEGFR-1 D2 abolishes PlGF binding and decreases the affinity of VEGF-A for VEGFR-1 D2 (Davis-Smyth et al., 1998). VEGF-A, which binds VEGFR-1 and -2, shows a more neutral charge distribution at these binding sites and VEGF-C, which does not bind VEGFR-1, contains mainly positively charged patches (Iyer et al., 2010). This suggests that charge distributions at the binding interfaces contribute to receptor specificity. Interestingly, a comparison of the VEGF-C/VEGFR-2 D2-3 complex with the complex of VEGF-A/VEGFR-1 D2 showed that VEGF-C bound to VEGFR-2 is tilted by 15° and twisted by 9° from the D2 interface when superimposing the complexes based on the orientation of D2 (Leppanen et al., 2010b).

A NMR-structure of the free VEGFR-1 D2 domain showed, that no structural changes are induced by the binding of VEGF-A (Starovasnik et al., 1999). Unfortunately, no free ligand-binding receptor domains of VEGFR-2 have been crystallized to date, making it difficult to judge whether or not ligand-binding induces conformational changes in the receptor. However, electron microscopy (EM) images of the VEGFR-2 ECD in complex with its ligand VEGF-A showed a rigid structure, where Ig-homology domains 4 and 7 of the two receptor molecules seem to interact with each other (Ruch et al., 2007). Later the crystal structure of the c-Kit ectodomain, a related RTK comprised of five extracellular Ig-homology domains, in complex with its ligand stem cell factor showed that ligand binding induces a conformational rearrangement of the C-terminal Ig-homology domains (Yuzawa et al., 2007). This conformational change enables homotypic interactions between a conserved pair of basic and acidic amino acids. Sequence alignment revealed that this motif is conserved among

several RTKs and can be found in Ig-homology domain 7 of all VEGFRs. Indeed, the crystal structure of VEGFR-2 shows D7 dimers held together by these conserved residues (Yang et al., 2010).

5.3.3 The kinase domain

The intracellular kinase domain has been of special interest for the development of drugs to inhibit VEGFR signaling. To date, the crystal structure of the VEGFR-1 and VEGFR-2 kinase domain have been solved (McTigue et al., 1999). Additional crystal structures of the VEGFR-2 kinase domain in complex with different inhibitors are also available (Table 1). Already the very high sequence homology between RTK kinase domains pointed to the structural homology that most kinases of RTKs share. The kinase is composed of two major folds, the N-lobe and the C-lobe (Fig. 9). The catalysis of the phosphotransfer from ATP to the hydroxyl group of a tyrosine side chain takes place in the cleft between the two lobes.
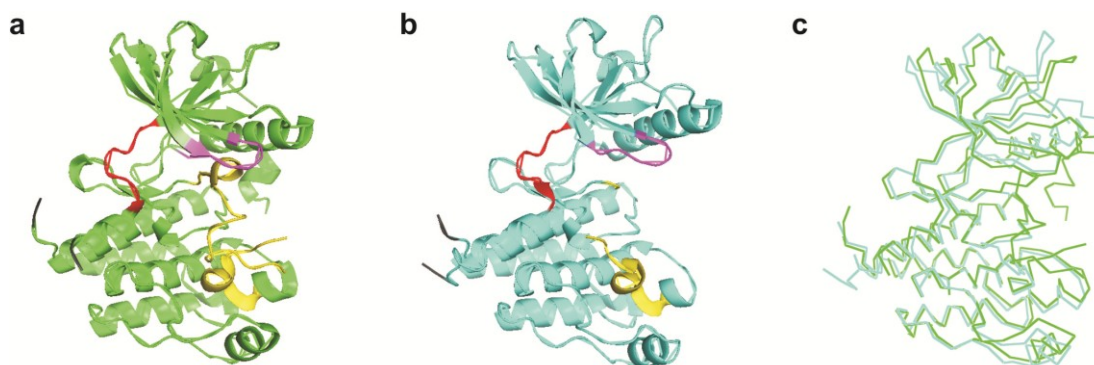
Fig. 9: Structures of the VEGFR-1 and VEGFR-2 kinase domain
The VEGFR-1 (a) and the VEGFR-2 kinase domain (b) are shown in a cartoon representation. The glycine rich nucleotide binding motif (magenta), the catalytic site (red), the ends of the kinase insert domain (gray), and the activation loop (yellow) are highlighted. Superimposition of the VEGFR-1 (green) and the VEGFR-2 (cyan) kinase domains show the same overall topology with minor differences in the positioning of the N-lobe (c). (adapted from PDB-entries 3HNG and 1VR2)

Although several features are missing in the VEGFR-2 kinase domain structures, important motifs such as the glycine rich nucleotide binding loop, the catalytic site, and the DFG motif, also known as the activation segment, can be

observed. As the name implies the glycine rich nucleotide binding loop, consisting of a conserved GXGXXG motif (C-lobe), interacts with the adenosine-5'-triphosphate (ATP) and brings it close to the catalytic site. In VEGFR-2 the activation segment contains two major phosphorylation sites, Y1054 and Y1059, which need to be phoshorylated for full activity of the kinase. Although the protein has been phosphorylated at Y1059 prior to crystallization, the activation loop adopts an inhibitory conformation, which is obvious when superimposing it with the structure of the VEGFR-1 kinase domain that has been cocrystallized with an inhibitor (Fig. 9). As already mentioned, key features such as the kinase insert domain and the juxtamembrane domain are missing in the VEGFR-2 kinase and in part also in the VEGFR-1 kinase structure. Hence, further structures including these domains and the C-terminal tail would be of great benefit.

5.4   Mechanism of receptor tyrosine kinase activation

Although RTK activation always involves receptor oligomerization and RTKs contain similar overall architectures, such as a ligand binding ECD, a single transmembrane spanning helix, and an intracellular kinase domain, the mechanisms of activation can differ remarkably. By structurally and functionally characterizing the ECD of RTKs, two major activation concepts have emerged: (1) entirely ligand mediated dimerization/oligomerization (e.g. nerve growth factor), and (2) entirely receptor mediated dimerization/oligomerization (e.g. epidermal growth factor) (Lemmon and Schlessinger, 2010). Activation of the FGF receptors, c-Kit, and also of VEGFRs are processes that involve additional features. Ligand binding to c-Kit or VEGFRs induces receptor dimerization, but additional entirely receptor mediated interactions stabilize this complex. In the case of FGF receptors it has been shown that dimerization is receptor mediated. However, the FGFs interact with both receptors in the dimeric complex.

In the following review article we discussed the mechanism of VEGFR activation that has emerged from structural and functional studies of VEGFRs and related RTKs. The structure of the individual domains, the ECD, the

membrane domain, the juxtamembrane domain, and the kinase domain and their role in receptor activation are highlighted. Concluding these data, we propose a mechanism of activation that should not give a final statement, but rather induce further discussion.

5.5   Aims of the thesis

Angiogenesis and vasculogenesis are important in the development of the lymphatic and blood vasculature and their deregulation is implicated in a number of pathological conditions. In angiogenesis and vascularization the members of the VEGF/VEGFR signaling system are key regulators. VEGFs bind to VEGFRs, leading to receptor dimerization, followed by exact positioning of the intracellular kinase domain, enabling its activation and subsequent autophosphorylation of intracellular tyrosine residues. The phosphorylated tyrosine residues act as docking sites for intracellular signaling molecules. The VEGF family consists of 5 members in humans that bind to three different receptors. Depending on the ligand/receptor complex, distinct signaling pathways are activated. Although there are several high resolution structures available, the mechanisms of ligand binding specificity and of the subsequent ligand dependent phosphorylation of tyrosine residues still need to be elucidated. At the onset of this thesis only a low resolution structure of the VEGFR-2 ECD in complex with VEGF-A was known. This structure showed that ligand binding promotes additional receptor/receptor interactions. In order to shed more light on these interactions, the first aim was to determine the high resolution structure of the membrane-proximal Ig-homology domain 7 of VEGFR-2 and its biochemical and biophysical characterization. During the course of this project a competing research group published this structure, supporting the hypothesis based on the low resolution VEGFR-2 ECD/VEGF-A structure. This motivated us to analyze the structure of the VEGFR-1 ECD using low and high-resolution structural methods. Structural information gained from VEGFR-1 ECD/VEGF complexes would help to understand ligand specificity, the role of the ECD in the activation mechanism, and to facilitate drug development for VEGFR-1 inhibitors. As a third aim, we wanted to analyze whether or not homotypic receptor/receptor interactions that are formed upon ligand binding can be targeted by designed ankyrin repeat proteins (DARPins) with the goal to inhibit VEGFR-2 signaling.

6   Structure of the VEGFR ECD

6.1   Introduction

When this project was initiated, only limited or no structural information of the VEGFR-1 and VEGFR-2 ECD, respectively, was available. The crystal structures of VEGFR-1 D2 in complex with VEGF-A and PlGF gave first insights into the ligand binding mechanism (Wiesmann et al., 1997; Christinger et al., 2004). Furthermore, an EM analysis of the VEGFR-2 ECD in complex with VEGF-A revealed Ig-homology domain 7 interactions in the ligand-bound complex (Ruch et al., 2007). However, a detailed understanding of the mechanism of receptor activation was still missing. Thus, gaining structural data for multidomain fragments of the VEGFR ECD is expected to lead to novel insights into the molecular mechanism of receptor activation. In addition, detailed knowledge of the structural arrangement of VEGFRs in the ligand-bound state may open new opportunities to target VEGFR signaling and to block pathological angiogenesis.

Based on the hypothesis that VEGF binding to VEGFR-2 induces the formation of homotypic receptor/receptor interactions in the membrane-proximal Ig-homology domain 7, we wanted to gather structural information to reveal the molecular basis of these interactions. To reach this goal, we designed predimerized VEGFR-2 D7 proteins and analyzed them using small-angle X-ray scattering (SAXS) and X-ray crystallography.

VEGFR-2 is the best characterized VEGFR, mainly owing to its important role in regulating physiological and pathological angiogenesis. However, VEGFR-1 malfunction is also implicated in pathological conditions. Little is known about the structure and the activation mechanism of VEGFR-1. Hence, we aimed at expressing the VEGFR-1 ECD to gain structural information using SAXS, EM, and X-ray crystallography. Furthermore, we wanted to elucidate the role of Ig-homology domains 4-7 in receptor activation using isothermal titration calorimetry (ITC), multi-angle light scattering (MALS), and EM.

6.2   Materials and methods

6.2.1 Construction of expression plasmids

The expression plasmids for scFv-like constructs were cloned using classic restriction digestion/ligation enzymes. First, a pcDNA3 plasmid carrying the cDNA encoding VEGFR-2 D6-7 was cloned by PCR-subcloning as described using the primers listed in Table A-1 (Geiser et al., 2001). A glycine-serine linker and a Kpn2I restriction site were then introduced using the same technique. Individual Ig-homology domains 4 or 7 were PCR amplified using Phusion high Fidelity DNA polymerase (Finnzymes) and the specified primers. The PCR products and the plasmid backbone were digested with KpnI, Kpn2I, EcoRI, and/or BamHI (Fermentas). The digested PCR fragments were ligated into the plasmid using standard T4- ligase (Fermentas).

All other pcDNA3 expression vectors were cloned using ligase-independent cloning by PCR (Geiser et al., 2001). Briefly, the coding sequences of the proteins of interest were amplified by PCR using primers that contain sequences homologous to the desired insertion sequence of the plasmid backbone (Table A-1). The PCR amplicon was then used as a primer for a second PCR step to amplify the plasmid backbone linked to the insert. The linear amplified plasmids were closed by addition of Tsc-ligase (Roche).

The pFL-plasmids containing several VEGFR-1 ECD variants were cloned by ligase-independent cloning using the CloneEZ-kit (GenScript). Briefly, the insert and the vector backbone were amplified by PCR using primers that contain homologous sequences at their 5'-end (Table A-1). The linear insert and plasmid backbone were *in vitro* recombined using the CloneEZ-kit. The recombined plasmid was then transformed into *Escherichia coli* (*E. coli*) DH10β-cells for amplification and selection.

The sequence encoding VEGFR-2 D7 linked to a GCN4 coiled coil was amplified by PCR using primers listed in Table A-1. The PCR-product and the *Pichia pastoris* expression plasmid pPICZαA (Invitrogen) were digested with EcoRI and SalI (Fermentas). The digested fragments were ligated using T4-ligase (Fermentas).

Pichia pastoris expression constructs encoding the ligands VEGF-A$_{121}$, VEGF-A$_{165}$, VEGF-A$_{165B}$, and PlGF-1 as well as insect cell expression plasmids pFASTBAC1 encoding VEGFR-1 D1-7 and D1-3 were already available in the laboratory.

6.2.2 Production and purification of recombinant proteins

VEGF-A$_{121}$, VEGF-A$_{165}$, VEGF-A$_{165B}$, and PlGF-1 were produced in *Pichia pastoris* by Thomas Schleier, Paul Scherrer Institute Villigen, Switzerland. VEGF-B was kindly provided by Veli-Matti Leppanen from the University of Helsinki, Finland.

All VEGFR-1 ECD variants and PlGF-1-1fzv (residues 19-221) were expressed in Sf21 or HighFive™ insect cells. Briefly, Sf21 and HighFive™ cells (Invitrogen) were maintained in suspension in serum-free InsectXpress medium (Lonza) or ExpressFive medium (Invitrogen), respectively, at 27°C and 90 rpm. As soon as the cells reached a density of 10^6 cells/ml, they were infected with recombinant baculovirus at high multiplicity. Three days after infection the supernatant was harvested by centrifugation at 900 g and concentrated using a tangential flow ultrafiltration device with a 10 kDa cut-off membrane (Schleicher & Schuell). The buffer was exchanged to 20 mM sodium-phosphate buffer (PBS) pH 7.4, 500 mM NaCl, and 10 mM imidazole by dialysis or by dilution of the concentrated medium followed by another concentration round. The conditioned medium was then loaded onto an immobilized metal ion chromatography (IMAC) column (GE Healthcare). The hexa histidine-tagged (His$_6$) protein was eluted with a gradient of 40-500 mM imidazole and further purified by size exclusion chromatography (SEC) on a Superdex200 HR 16/60 column (GE Healthcare) equilibrated in 25 mM HEPES pH 7.5 and 500 mM NaCl. For VEGFR-1 ECD/VEGF-A$_{121}$ complex formation, an equimolar amount of receptor and ligand were mixed and the complex was then purified by SEC as described above. If needed, the proteins were concentrated using centrifugal protein concentrators (Sartorius Stedim Biotech).

VEGFR-2 D7-GCN4, VEGFR-2 D7 and VEGFR-2 D6-7 were produced in transiently transfected HEK293T cells as described (Aricescu et al., 2006). In

brief, when the cells reached ~90% confluency, the medium was changed from DMEM (BioConcept) containing 10% fetal bovine serum to DMEM containing 0.5% fetal bovine serum. For a 15 cm tissue culture dish 50 µg DNA were incubated with 75 µg polyethylenimine (PEI, 25 kDa branched, Sigma-Aldrich) in 5 ml serum-free DMEM for 10 min at room temperature. After the incubation the DNA:PEI complex was added to the cells. Three days after transfection the medium was harvested, cleared by centrifugation, and concentrated using a 350 mL Amicon ultrafiltration device (Millipore). The buffer was exchanged to 20 mM PBS pH 7.4, 500 mM NaCl, and 10 mM imidazole. The His$_6$-tagged proteins were purified by IMAC as described for the VEGFR-1 ECD variants. The buffer was exchanged to 25 mM HEPES pH 7.5, 150 mM NaCl using centrifugal protein concentrators (Sartorius Stedim Biotech). Proteins produced for crystallization screens or SAXS analysis were further purified by SEC using a Superdex75 10/30 column (GE Healthcare), equilibrated in 20 mM Tris pH 7.5, and 150 mM NaCl.

For the production of VEGFR-2 D7-GCN4 in *Pichia pastoris*, X33 or KAI3 strains positive for protein expression were grown in BMGY medium. After 24 h at 30°C and 220 rpm, the medium was exchanged to BMMY to induce protein expression. Additional methanol was added every 12 h after expression induction to a final concentration of 0.5%. After 48 h the supernatant was harvested by centrifugation at 1500 g, supplemented with 8x IMAC binding buffer (160 mM PBS pH 7.4, 4 M NaCl, 80 mM imidazole) to a final concentration of 1x, and the proteins were purified over an IMAC column (GE Healthcare).

6.2.3 Deglycosylation

Proteins were analytically deglycosylated using EndoF1 or PNGaseF, both recombinantly produced as a GST-fusion protein in *E. coli* (Grueninger-Leitch et al., 1996). Endoglycosidases were added in a 1:20 (w/w) ratio to the glycosylated proteins in the purification buffer. The reactions were incubated at 4°C and/or room temperature for 1 h and overnight. The enzymatic reaction was stopped by adding 4x SDS-PAGE sample buffer. Subsequently, the proteins

were separated on a SDS-PAGE gel and the gels were stained either with Coomassie for proteins or with periodic acid-Schiff to stain sugar moieties.

VEGFR-1 ECD proteins produced in Sf21 cells were deglycosylated in preparative amounts using 1:100 (w/w) PNGaseF. The proteins were incubated with the enzymes overnight at 4°C. The reaction buffer was the same as the purification buffer, consisting of 25 mM HEPES pH 7.5, and 500 mM NaCl. The completeness of the enzymatic reaction was assessed using SDS-PAGE. The endoglycosidase was removed by another step of SEC as described above.

6.2.4 Isothermal titration calorimetry

All measurements were performed at 20°C in 25 mM HEPES pH 7.5, and 500 mM NaCl (ITC-buffer) using an iTC200 calorimeter (MicroCal®, GE Healthcare). All proteins were purified over a Superdex200 SEC column (GE Healthcare) equilibrated in ITC-buffer and dialysed against the ITC-buffer overnight at 4°C prior to the experiments. The calorimeter cell contained VEGFR-1 D1-7 or VEGFR-1 D1-3 at concentrations ranging from 4.4 to 30 µM and the ligands VEGF-A$_{121}$, VEGF-A$_{165}$, VEGF-A$_{165B}$, and PlGF-1 were used in the syringe at concentrations ranging from 22.5 to 100 µM. Protein concentrations were determined spectrophotometrically at 280 nm using theoretical extinction coefficients estimated by the ExPASy tool ProtParam (Gasteiger et al., 2003). All samples were equilibrated to the measurement temperature and degassed prior to the ITC experiments. The following settings were applied: one initial injection of 1 µl followed by 15 injections of 2.6 µl at an injection speed of 1 µl*s^{-1} with a data filter of 1 s and 300 s recovery time between each peak. In order to fully saturate the reaction and to accurately estimate the unspecific heat, overtitrations were conducted when needed. The software ConCat (MicroCal®) was used to merge the data from overtitration measurements and Origin 7.0 (OriginLab®) was employed for data analysis.

6.2.5 Multi-angle light scattering

The SEC coupled multi-angle light scattering (MALS) experiments were conducted on an Agilent 1100 HPLC-system (Agilent Technologies) with an

analytical-grade Superdex 200HR 10/30 column (GE Healthcare) coupled to the Wyatt miniDAWN Tristar (Wyatt Technologies). The system was equilibrated in 25 mM HEPES pH 7.5, 500 mM NaCl at 20°C prior to the experiments. The cell contents of the ITC experiments were concentrated to 110 µl in Vivaspin500 centrifugal protein concentrators with a molecular weight cut-off of 10 kD (Sartorius Stedim Biotech). For the MALS experiments, 100 µl of the concentrated proteins were loaded onto the SEC column. For the measurement of individual proteins, a total amount of 100 ug was loaded onto the SEC column. The elution profiles were recorded as UV-absorbance at 280 nm and as the intensity of Rayleigh scattering at three different angles. The ASTRA^{TM} software (Wyatt Technologies) was used to calculate the weight average molecular masses (Mr).

6.2.6 Electron microscopy

VEGFR-1 ECD/VEGF-A$_{121}$,   VEGFR-1 ECD/PlGF-1,   and   VEGFR-1 ECD/VEGF-B samples were prepared for electron microscopy (EM) using a conventional negative staining protocol (Ohi et al., 2004). Briefly, 5 µl of protein sample were adsorbed to a glow-discharged carbon-coated copper grid, washed with 2 drops of deionized water, and stained with one drop of 2% (w/v) uranyl acetate. For the grid preparation we used protein concentrations in the range of 1-3 µg/ml. The samples were imaged at room temperature with a CM10 electron microscope (Philips) equipped with a LaB6 filament and operated at an acceleration voltage of 80 kV. Images of specimens were recorded with a side-mounted Veleta 2k x 2k CCD camera (Olympus Soft Imaging Solutions) using low-dose procedure at a magnification of 92,000.

The display program X3D (Conway et al., 1996) was used for selecting and picking particles. For projection analysis, 6260 particles of VEGFR-1 ECD/VEGF-A$_{121}$, 2203 particles of VEGFR-1 ECD/PlGF-1, and 1234 particles of VEGFR-1 ECD/VEGF-B were interactively selected from 161, 39, and 39 images, respectively. The particles were windowed into 70 x 70 pixel images, stacked, centered, subjected to 10 cycles of multireference alignment, and classified into 50 output classes for the VEGFR-1 ECD/VEGF-A$_{121}$ complex

and 20 output classes for the VEGFR-1 ECD/PlGF-1 and VEGFR-1 ECD/VEGF-B complexes using the SPIDER program suite (Frank et al., 1996).

6.2.7 Small angle X-ray scattering

SAXS data acquisition was performed at the X12SA-beamline (cSAXS) at the Swiss Light Source at the Paul Scherrer Institute Villigen, Switzerland. The intensities of the scattered X-rays were recorded on a Pilatus 2M detector using a wavelength of $\lambda = 1$ Å. Data was collected in the scattering vector range of 0.008 Å^{-1} - 0.4 Å^{-1}, where the length of the scattering vector is given as $s = 4\pi \sin\theta/\lambda$ (2θ is the scattering angle). Silver behenate was used as a standard for calibration of the s-range (Huang et al., 1993). Three concentrations were measured per protein sample using quartz capillaries with a diameter of 1 mm (Hilgenberg GmbH). To record the background scattering, the protein buffer was measured in the same capillaries prior to the actual protein data acquisition. Exposures of 0.5 s were taken at ten different spots along the capillary. The data was monitored for radiation damage and all frames showing no radiation damage were merged and averaged for further data processing.

The collected SAXS data were integrated and radially averaged utilizing our own MATLAB-scripts (Missimer & Kisko). Using PRIMUS (Konarev et al., 2003) from the ATSAS-program package (Petoukhov et al., 2007), the background scattering was substracted and data of different concentrations were merged. In order to check the proper folding of all measured proteins Kratky-plots were calculated. The distance distribution function P(r) was calculated using GNOM and the program AUTOGNOM. We calculated the radius of gyration Rg from both the P(r) function as well as from the data in the linear Guinier-region. The programs DAMMIF and DAMMIN were used for *ab-initio* shape reconstructions from the P(r) functions. For all samples, between 10 and 20 independent DAMMIF runs were aligned, averaged, and filtered back to the original envelope volume using DAMAVER. For superimpositions of the SAXS envelopes with existing crystal structures the program SITUS was employed (Wriggers and Birmanns, 2001).

6.2.8 Protein crystallization

Protein crystallization screens were set up in Innovaplate^{TM} SD-2 (Innovadyne Technologies, Inc.) using the Crystal PHOENIX dispenser (Art Robbins Instruments). Proteins were first screened for the proper concentration range using the pHClear and pHClear II crystallization suites (QIAGEN). Crystallization drops containing a protein:precipitant ratio of 1:1 were pipetted using protein concentration ranges of 2-19 mg/ml. The JCSG-core suite (QIAGEN) was then used for further crystallization screening. Crystals of the VEGFR-1 ECD/VEGF-A$_{121}$ complex grew at 20°C in several conditions consisting of a buffer substance in the pH-range of 6-9, 0.2-1 M monovalent or bivalent salt, and 8-13% polyethyleneglycole (PEG) with a size between 2000 and 8000 Da. For crystal reproduction and refinement, 24-well plates (Greiner) were used, usually containing 500 µl reservoir solution and 1-2 µl drops of a protein:precipitant mixture at a ratio of 1:1 or 2:1.

For collection of diffraction data, the crystals were fished using nylon loops (Hampton Research). They were transferred to drops of mother liquor containing increasing concentrations of cryo-protectant. In each drop they were equilibrated for 1-5 min and then immediately flash frozen in liquid nitrogen. Crystal diffraction data was collected at the X06SA- or the X06DA-beamline at the Swiss Light Source, PSI Villigen, Switzerland.

6.3   Results

6.3.1 Expression and purification of VEGFR-2 ECD protein

EM images of VEGFR-2 ECD in complex with VEGF-A$_{121}$ revealed interactions between Ig-homology domains 7 of the two receptor chains that are incorporated in one complex. Furthermore, the structural knowledge of VEGFR ECDs was limited to one single Ig-homology domain of VEGFR-1 at the onset of this project. Hence, additional high resolution data of Ig-homology domain 7 would be helpful to elucidate the molecular mechanism of VEGFR activation and to understand the molecular basis of the receptor interactions observed in the EM images. To further confirm the interaction of Ig-homology domain 7, we

wanted to bring two such domains into close proximity either through a glycine-serine-linker, resembling a scFv-like molecule, or through the C-terminal attachement of a GCN4 coiled coil domain to induce dimerization (Fig. 10).
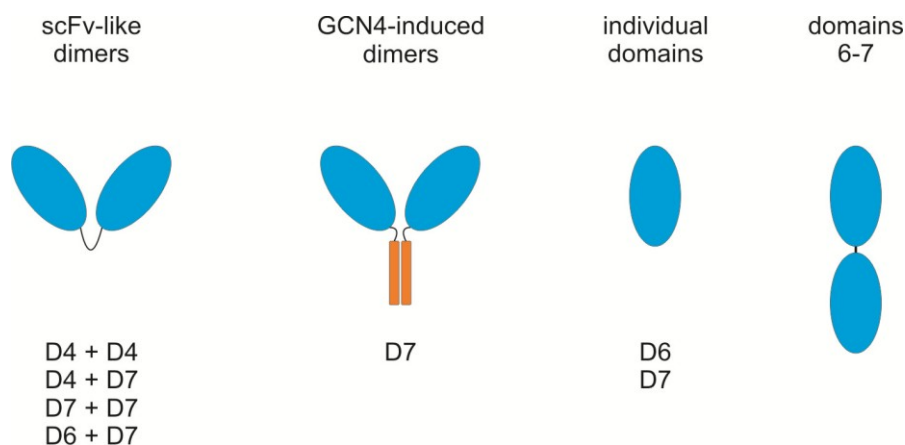
Fig. 10: Schematic representation of different strategies to gain structural knowledge on the VEGFR-2 ECD membrane proximal domains

Expression in HEK-cells

The coding sequences of the constructs shown in Fig. 10 were cloned into pcDNA3, a mammalian expression vector. All proteins were produced as secreted proteins carrying the native VEGFR-2 signal sequence. A C-terminal His$_6$-tag facilitated purification of the recombinant proteins from the expression medium. During the project, asparagine residues 704 and 721 were mutated to glutamine in order to prevent N-glycosylation giving rise to additional Ig-homology domain 7 and 7-GCN4 constructs.

Test expressions of the scFv-like dimeric Ig-homology domain constructs showed low expression in case of Ig-homology domain 7 linked to domain 6 and to another domain 7, while Ig-homology domain 7 linked to the GCN4 coiled coil showed a reasonable expression 72 hours post transfection (Fig. 11a). A dimeric Ig-homology domain 4 construct showed no expression at all. Because of the low expression levels compared to other constructs, I stopped this approach to study the homotypic interactions of Ig-homology domain 7.

Small scale test expressions were conducted to validate the production of recombinant VEGFR-2 ECD variants in HEK293T cells. Immunoblotting and

detection with anti-His$_5$ antibodies confirmed the presence of recombinant Ig-homology domains 6, 6-7, and 7 linked to GCN4 in the supernatant of transfected HEK293T cells (Fig. 11b). All of the expressed recombinant proteins appeared as several bands on SDS-PAGE owing to heterogenous N-glycosylation. Mutation of two glycosylation sites in the VEGFR-2 D7-GCN4 construct showed a shift to smaller molecular weights, confirming the presence of N-glycosylation (Fig. 11c).
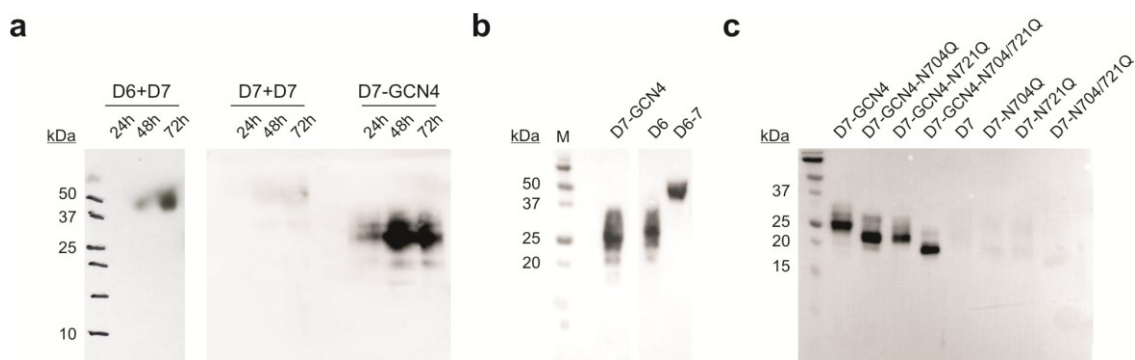
Fig. 11: Immunoblot analysis of His$_6$-tagged VEGFR-2 ECD variants expressed in HEK293T cells
Aliquots of the medium harvested from transfected HEK293T cells were subjected to SDS-PAGE and subsequent immunoblotting. Recombinant proteins were detected with an anti-His$_5$ antibody. scFv-like linked domains 6 and 7, 7 and 7, and domain 7 linked to a GCN4 coiled coil (a). Ig-homology domain 6 and 6-7 (b). Wild type Ig-homology D7 and D7-GCN4 and several asparagines mutants to prevent N-glycosylation (c).

Upscaled protein production was carried out in HEK293T cells in the absence and presence of Kifunensine and in HEK293S-GnTI$^-$ cells. Kifunensine is a α-mannosidase-I inhibitor, rendering proteins expressed in the presence of Kifunensine endo-H sensitive (Chang et al., 2007). HEK293S-GnTI$^-$ is a cell line that has been engineered to lack the enzyme N-acetylglucosaminyltransferase I (GnTI) (Reeves et al., 2002). These cells produce proteins that are homogenously glycosylated with five mannoses and two N-acetylglucosamines. Hence, proteins generated in HEK293S-GnTI$^-$ cells are endoglycosidase sensitive, which allows deglycosylation and may facilitate crystal growth.

Recombinant proteins were produced in transiently transfected HEK293T cells using either calcium-phosphate or PEI as the transfecting reagents. Expression of Ig-homology domain 6/7 variants in HEK293T cells resulted in protein yields

between 6-9 mg per liter of culture medium, whereas the expression in HEK293S-GnTI⁻ cells yielded only 1-2 mg protein per liter of culture medium. Stable cell lines expressing Ig-homology domain 7, 6, 6-7, or 7 linked to the GCN4 coiled-coil were generated, which increased the protein yield up to 3 mg/L.

The His$_6$-tagged proteins were purified directly from the cell supernatant via IMAC. The proteins were eluted from the column by increasing imidazole concentrations. The purity of the proteins was examined using SDS-PAGE. One step of IMAC purification resulted in sufficiently pure material for further experiments as judged by SDS-PAGE (Fig. 12). Proteins that were produced in HEK293T cells appeared as diffuse bands on SDS-PAGE owing to N-glycosylation, while proteins that were expressed in HEK293S-GnTI⁻ cells or lack 2 of 3 N-glycosylation sites run as discrete bands (Fig. 12). This results from the inability of HEK293S-GnTI⁻ cells to process the glycan precursors to complex-type glycans, which are very heterogenous (Reeves et al., 2002). However, in most cases several bands are observed for proteins produced in HEK293S-GnTI⁻ cells probably due to heterogenous glycosylation (Fig. 12).

For further applications, recombinant VEGFR-2 ECD variants were purified by SEC to remove aggregates. In addition, proteins were characterized by MALS and/or mass spectrometry (LC/ESI/MS).
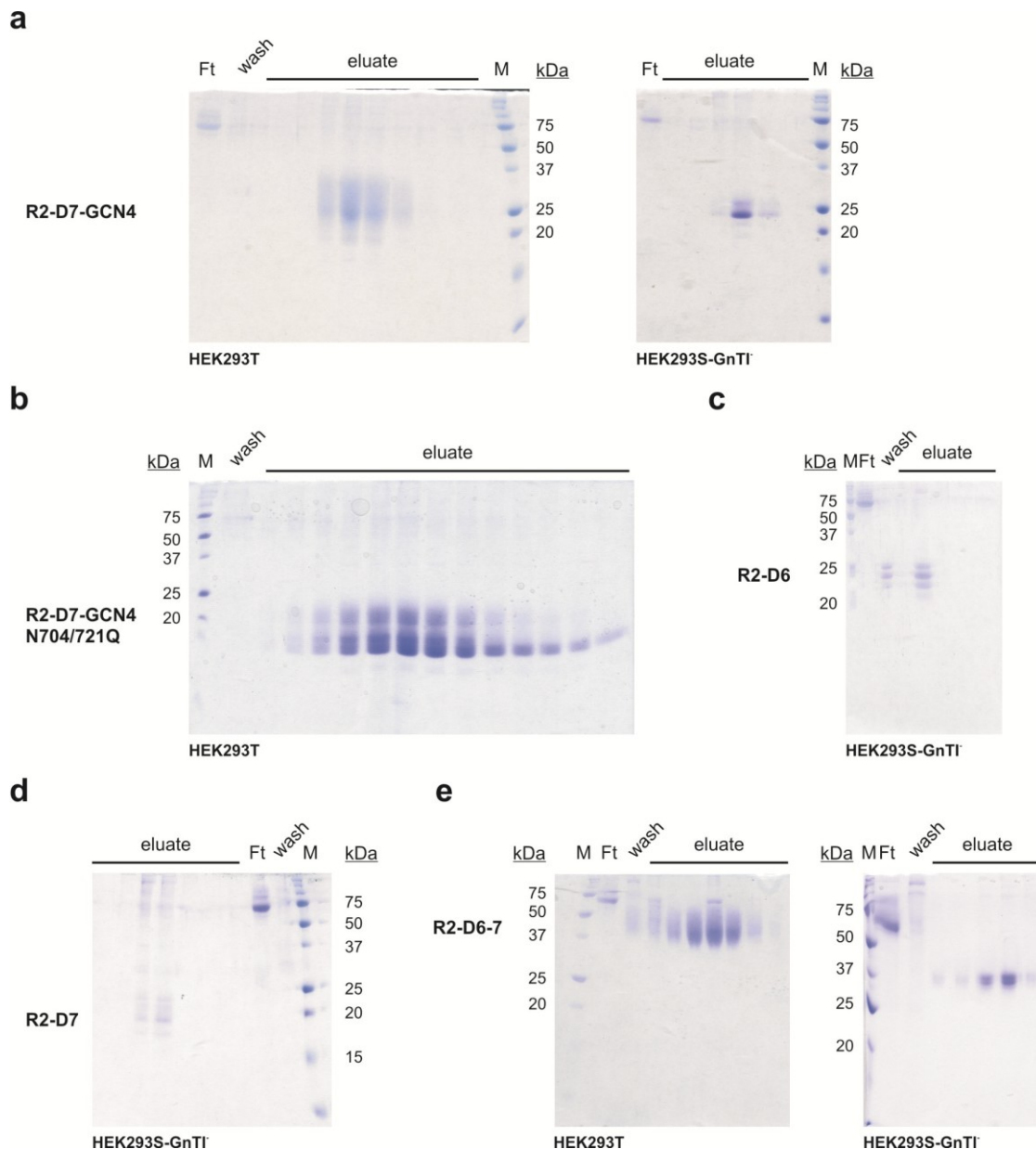
***Fig. 12: IMAC purification of VEGFR-2 ECD variants expressed in mammalian cells***
Proteins were produced in HEK293T or HEK293S-GnTI⁻ cells and purified by IMAC. Fractions of the IMAC were subjected to SDS-PAGE. Coomassie stained SDS-gels of VEGFR-2 D7-GCN4 (a), VEGFR-2 D7-GCN4-N704/721Q (b), VEGFR-2 D6 (c), VEGFR-2 D7 (d), and VEGFR-2 D6-7 (e).

Expression in *Pichia pastoris*

HEK293T cells possess the necessary cellular machinery to fully process recombinant proteins posttranslationally. However, expression in HEK293T cells is expensive and protein yields are often not very high. Hence, *Pichia pastoris* can be an alternative, since the cells are able to modify recombinant

proteins posttranslationally in particular by N-glycosylation, are very robust, and can be grown to high densities at production costs way below those of mammalian cells. Furthermore, multi-copy insertion of the expression plasmid into the genome is possible leading to higher expression yields.

The DNA sequence encoding VEGFR-2 D7 linked to a GCN4 coiled coil was transferred into an expression plasmid designed for the production of secreted proteins in *Pichia pastoris*. The wild type strain X33 and the mutated strain KAI3 were used for expression tests. KAI3 overexpresses the *Trichoderma reesei* α-1,2-mannosidase in the endoplasmatic reticulum and contains a disrupted OCH1 gene, which encodes a mannosyltransferase, enabling the expression of recombinant protein that is endoglycosidase-H sensitive (Vervecken et al., 2004). Immunoblot analysis of the supernatants of several expression clones shows two major bands at ~25 kDa and ~10 kDa (Fig. 13). While the 25 kDa band represents the full length VEGFR-2 D7-GCN4, the lower band is most likely a degradation product. Edman-sequencing of the 10 kDa band revealed that this protein carries the N-terminus RVRKEDE, which is the amino acid sequence found in the loop connecting β-strand E and F in Ig-homology domain 7. Unfortunately, protein production in an upscaled format showed the same digestion product, leading to a loss of ~50% of the protein (Fig. 13).
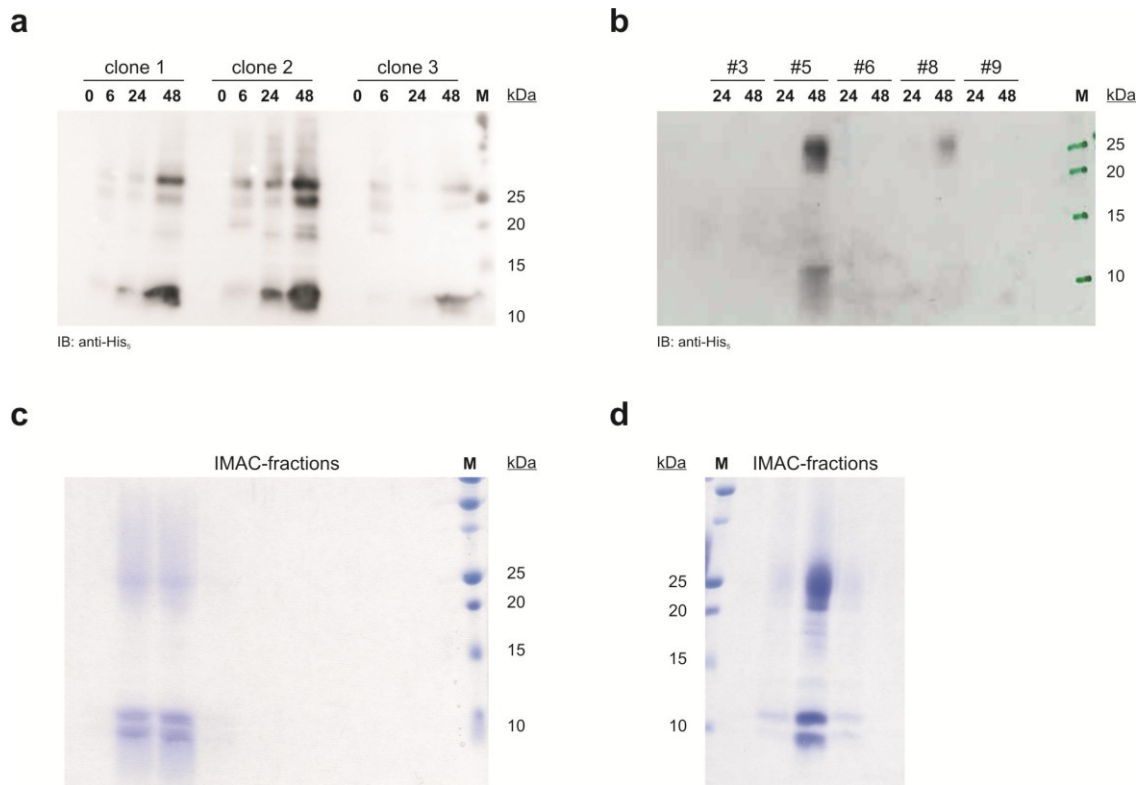
Fig. 13: Expression of VEGFR-2 D7-GCN4 in Pichia pastoris **leads to proteolysis**
Individual clones of Pichia pastoris *strain X33 (a) and KAI3 (b) were induced to express VEGFR-2 D7-GCN4 by addition of methanol. Aliquots of the media were harvested at the indicated time points and subjected to immunoblotting. Recombinant proteins were detected with anti-His$_5$ antibodies. Expression positive clones of Pichia pastoris strains X33 (c) and KAI3 (d) were grown in an upscaled format. Protein expression was induced by methanol addition. Recombinant VEGFR-2 D7-GCN4 was purified by IMAC. Individual IMAC fractions were subjected to SDS-PAGE, followed by Coomassie staining.*

6.3.2 Expression and purification of VEGFR-1 ECD protein

Expression in insect cells

At the beginning of the VEGFR-1 project, several expression plasmids encoding VEGFR-1 ECD variants were already available in the laboratory. These expression plasmids included the insect cell expression plasmid pFASTBAC-1 encoding VEGFR-1 D1, VEGFR-1 D2, VEGFR-1 D3, VEGFR-1 D1-3, and VEGFR-1 D1-7 and the mammalian expression plasmid pcDNA3.1 encoding VEGFR-1 D1-7 (Fig. 14). All constructs contain the endogenous VEGFR-1 signal sequence to trigger the secretion of the protein and a C-terminal His$_6$-tag.
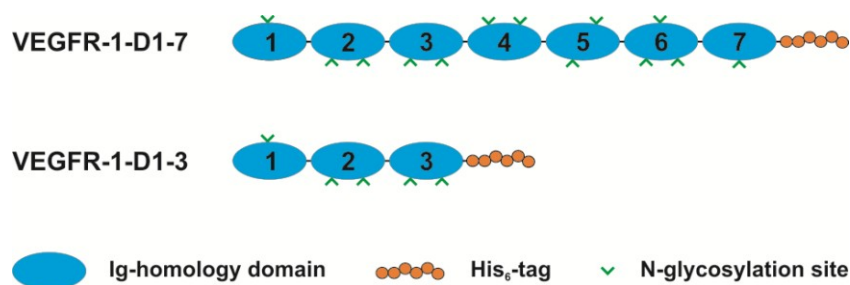
Fig. 14: Schematic representation of the VEGFR-1 constructs used for initial expressions

To date, there are three insect cell lines that are mainly used for recombinant protein expression, Sf9, Sf21, and High Five™ cells. Sf21 as well as Sf9 are ovarian cell lines from *Spodoptera frugiperda* (Vaughn et al., 1977) and High Five™ cells were isolated from adult ovarian tissue of *Trichoplusia ni* (Wickham et al., 1992). High Five™ cells have been reported to be more suitable for secreted protein expression (Davis et al., 1992). Thus, recombinant protein expression was compared between Sf21 and High Five™ insect cells for the constructs encoding VEGFR-1 D1-7 and VEGFR-1 D1-3. Aliquots of the supernatant were analyzed for its protein content by immunoblotting using His$_5$-tag specific antibodies. The peak of protein expression was observed 72-96 h postinfection (Fig. 15a). The medium was harvested at this time point in subsequent large scale productions of proteins. The expression of VEGFR-1 D1-7 in Sf21 and High Five™ cells showed no significant differences, while the expression of VEGFR-1 D1-3 was remarkably increased in High Five™ cells compared to Sf21 cells (Fig. 15b). Hence, High Five™ cells were used for VEGFR-1 D1-3 expression and Sf21 cells for VEGFR-1 D1-7 expression. Expression of VEGFR-1 D1-7 resulted in a ~100 kDa protein band and VEGFR-1 D1-3 runs as a ~50 kDa protein in SDS-PAGE, both are heavier than the theoretical values of 83.6 kDa and 36.6 kDa, respectively, that are calculated based on the amino acid sequence. Given the fact that proteins produced in insect cells have the advantage to carry all posttranslational modifications, the difference in molecular weight can be explained by N glycosylation. As a matter of fact, the ECD of VEGFR-1 contains 13 predicted N-glycosylation sites (Fig. 14).
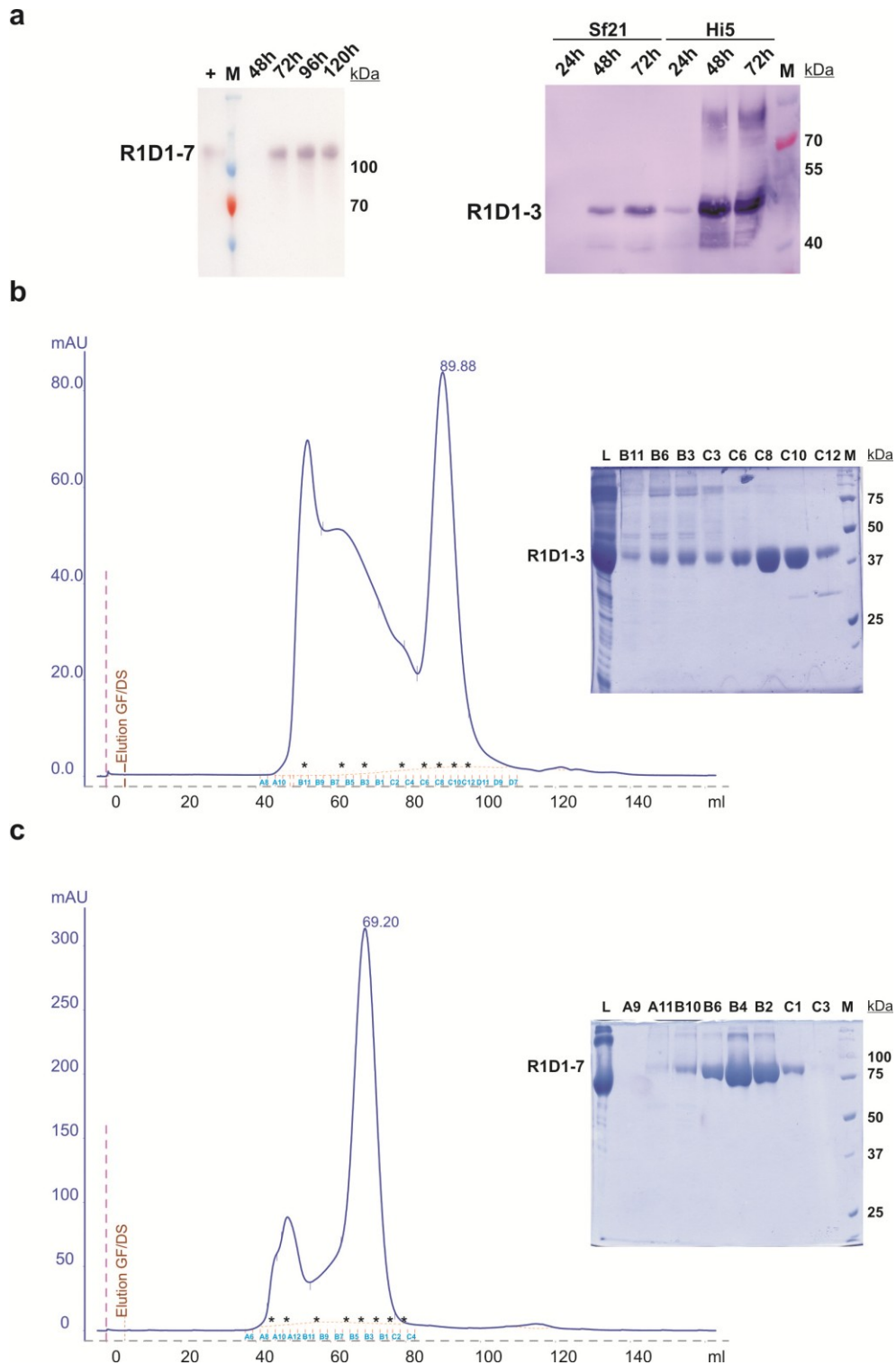
Fig. 15: Expression of VEGFR-1 D1-3 and D1-7 in insect cells
VEGFR-1 D1-7 (left) and VEGFR-1 D1-3 (right) expression was tested in Sf21 and High-Five™ cells. Supernatants were blotted onto PVDF membranes and recombinant protein was detected with anti-His$_5$ antibodies (a). UV-absorption profiles of SEC purified VEGFR-1 D1-3 (b) and VEGFR-1 D1-7 (c). SDS gels showing individual fractions (marked with asterisks) are shown in the insets.

In an upscaled format, protein yields ranged from 2-12 mg per liter of cultured cells. The optimal purification protocol comprised a first step of IMAC purification to remove major impurities and a second step using SEC columns to get rid of any aggregates and remaining impurities. This procedure resulted in at least 95% pure protein judged from SDS-PAGE (Fig. 15).

During the course of this project it became evident that additional constructs for insect cell expression are needed. The new constructs were supposed to encode VEGFR-1 ECD variants with varying domain boundaries. Several DNA fragments encoding different Ig-homology domains of the VEGFR-1 ECD were cloned into one expression cassette of the pFL plasmid. The pFL plasmid carries two expression cassettes allowing the production of multiprotein complexes (Berger et al., 2004). Future experiments coexpressing the VEGFR-1 ECD variants with ligands or coreceptors may be possible using this vector. All constructs contained the signal sequence of VEGFR-2 and a C-terminal His$_6$-tag that is removable with factor-Xa protease cleavage (Table 2). The VEGFR-2 signal sequence was used owing to the higher protein yield in VEGFR-2 productions compared to VEGFR-1 preparations.

Table 2: Expression constructs for recombinant VEGFR-1 ECD production in insect cells

Domain boundaries	Amino acids	
D1-7N27	27-750	
D1-6N27	27-660	
D1-5N27	27-554	
D1-4N27	27-420	
D1-3N27	27-331	
D1-7N32	32-750	
D1-6N32	32-660	
D1-5N32	32-554	
D1-4N32	32-420	
D1-3N32	32-331	
D2-7	132-750	
D2-6	132-660	
D2-5	132-554	
D2-4	132-420	
D2-3	132-331	
D4-7	343-750	
D4-6	343-660	
D4-5	343-554	

Ig-like domain ⬤   His$_6$-tag ⬤⬤⬤⬤⬤   N-glycosylation site ⌄

During the virus production aliquots of the supernatant were analyzed on immunoblots using anti-His$_5$ antibodies for immunodetection of the expressed proteins. All supernatants of the virus producing cells showed a band for the expressed proteins, except VEGFR-1 D1-5N27, VEGFR-1 D1-5N32, VEGFR-1 D1-3N27, and VEGFR-1 D2-6. Several of these constructs were expressed in an upscaled format. The yield of these protein preparations ranged from 1-6 mg per liter of cell culture medium. The purification protocol was applied as described above and a single purification step using IMAC columns resulted in pure protein (exemplary VEGFR-1 ECD variants are shown in Fig. 16).
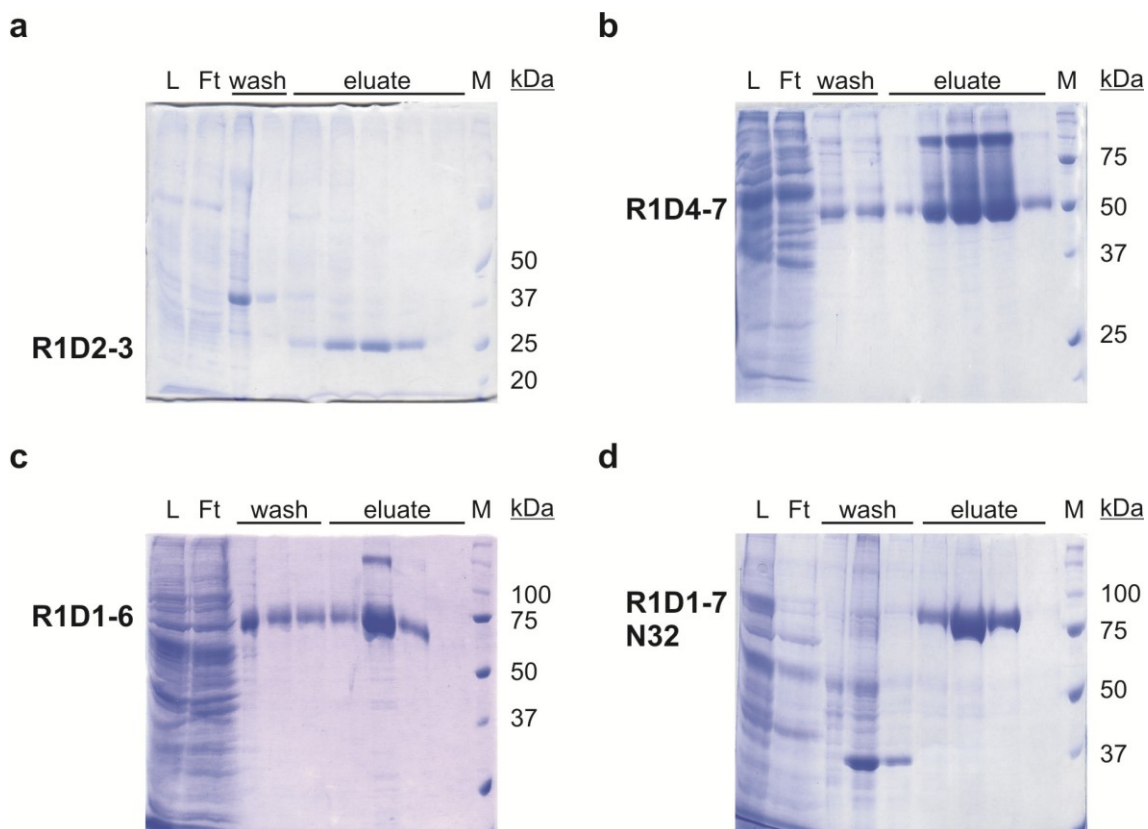
Fig. 16: IMAC purifications of VEGFR-1 ECD variants
Proteins were purified using IMAC and individual fractions were collected and subjected to SDS-PAGE. VEGFR-1 D2-3 (a), VEGFR-1 D4-7 (b), VEGFR-1 D1-6 (c), and VEGFR-1 D1-7N32 (d) are shown. L: loading; Ft: flow-through; M: protein size marker

Expression in mammalian cells

Although crystal structures of proteins containing N-linked glycosylations have been reported, crystal growth may be hampered by sugar moieties. Thus, removing these modifications can help in crystallization. Therefore, VEGFR-1 D1-7 expression was also assessed in HEK293S-GnTI⁻ cells.

Since transient expression of VEGFR-1 D1-7 in HEK293S-GnTI⁻ cells yielded only a low amount of protein, a stable cell line was generated. Cells transfected with the VEGFR-1 D1-7 expression plasmid underwent two rounds of antibiotic selection to assure the cells are monoclonal. Protein expression was analyzed by immunoblotting using His$_5$-tag specific antibodies. Several clones showed expression of VEGFR-1 D1-7 (Fig. 17). However, the expression level between the clones varied remarkably. One clone was selected for testing an upscaled

protein preparation. After purification using an IMAC column, only 0.8 mg protein per liter of cultured cells was recovered, a low amount of protein compared to the expression in insect cells.
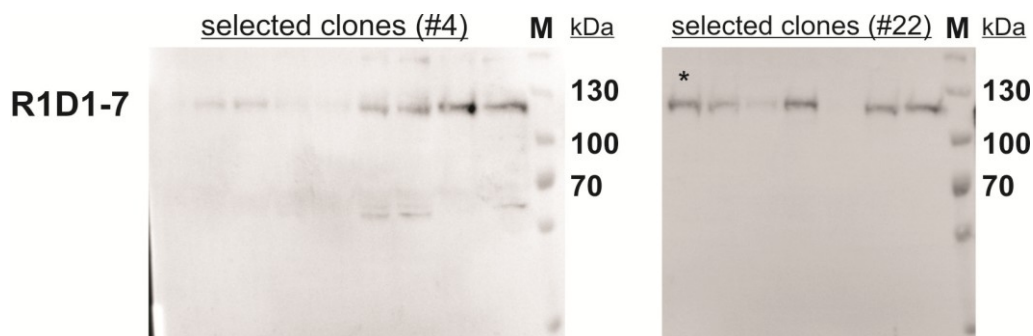
Fig. 17: Expression of VEGFR-1 ECD in HEK293S-GnTГ cells
The supernatants of individual HEK293S-GnTГ clones stably expressing VEGFR-1 D1-7 were analyzed for their recombinant protein content on immunoblots using antibodies against the His$_6$-tag. The clone selected for upscaled protein production is marked with an asterisk.

6.3.3 Deglycosylation

As sugar moieties linked to asparagines of the recombinant protein may impede crystal growth, one approach to improve crystal quality is to remove the glycosylations from the protein of interest. Insect cells share common first steps of the N-glycosylation pathway with mammalian cells by adding the same N-glycan precursor to asparagines. However, insect cells fail in elongating this precursor with galactose and sialic acid residues and they trim the precursors by one N-acetylglucosamine to produce paucimannose or high-mannose end products. This feature renders proteins produced in insect cells at least partially sensitive for native deglycosylation by glycosidases, such as EndoF1 or PNGaseF. EndoF1 cleaves between the two innermost N-acetylglucosamines, leaving one N-acetylglucosamine residue linked to the asparagines. PNGaseF cleaves between N-acetylglucosamine and asparagine, leaving no sugar moieties linked to the protein.

VEGFR-1 D1-7 was treated with EndoF1 and PNGaseF for 1h or overnight at room temperature or 4°C, respectively. The deglycosylation of VEGFR-1 D1-7 with either EndoF1 or PNGaseF resulted in a band shift towards a smaller Mr on SDS-PAGE (Fig. 18a), confirming that the protein is highly glycosylated. The

PNGaseF treated protein was only weakly observed by a faint band in the periodic acid-Schiff staining, while the EndoF1 treated protein gave rise to a strongly stained band (Fig. 18b). Furthermore, PNGaseF treatment led to a larger band shift than EndoF1. This indicates that either deglycosylation by EndoF1 is not complete or the remaining N-acetylglucosamine residues result in different electrophoretic characteristics of the protein in SDS-PAGE and are still heavily stained with periodic acid-Schiff. Another explanation would be that specific N-glycans are buried in the folded protein, rendering them inaccessible for EndoF1 cleavage. Treatment of the proteins for 1 h and 24 h did not result in any differences. Thus, the enzymatic reactions can be considered as completed. Since PNGaseF resulted in bigger band shift and a weakly stained band using periodic acid-Schiff, indicating an almost completely deglycosylated protein, it appears that paucimannose glycans produced by insect cells are not fully removable by EndoF1.
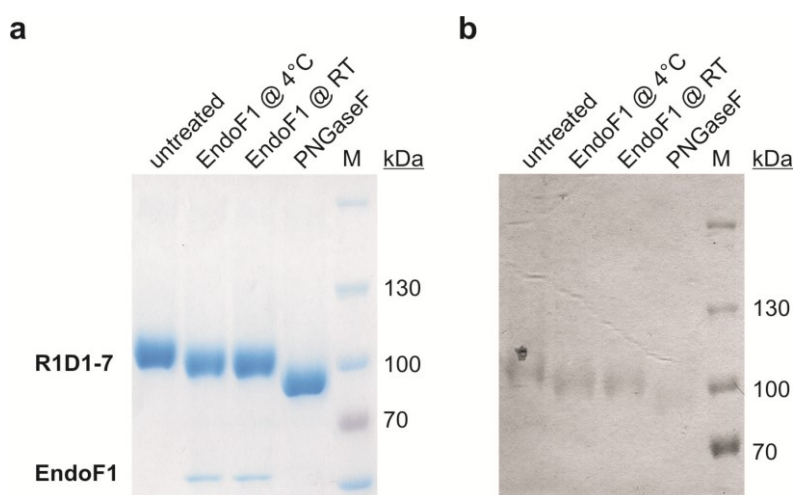
Fig. 18: Analytical deglycosylation of VEGFR-1 D1-7
Coomassie-staining (a) and periodic acid-Schiff staining (b) of untreated and deglycosylated VEGFR-1 D1-7 separated on SDS-PAGE.

6.3.4 Crystallization of VEGFR ECDs

Recombinantly produced proteins underwent extensive crystallization screens using commercial 96-well format screens (Table 3). For initial screenings several drop ratios of protein:precipitant were used.

Table 3: Used screens for the assessment of crystal growth of VEGFR ECD proteins
The protein or protein complex analyzed for crystal growth is given accompanied with the used concentrations (c) and crystal screen conditions.

Protein	c [mg/ml]	Screens	Remarks
VEGFR-2 D6-7	4.5; 9; 12.7	pHClear	
	12.7	AmSO$_4$ suite; PEG suite	
	5.8	pHClear	Protein produced in the presence of kifunensine and deglycosylated with EndoF1
	9.5	JCSG-Core suite; JCSG+ suite; PACT suite;PEG suite	Protein produced in the presence of kifunensine and deglycosylated with EndoF1
	19.1	pHClear; JCSG-Core suite	Deglycosylated with EndoF1 and PNGaseF
	14.9	PEG suite	Produced in HEK293S-GnTI- cells and deglycosylated with EndoF1
VEGFR-2 D7	2	AmSO$_4$ suite; PEG suite	
VEGFR-2 D7-GCN4	7	pHClear; Classics	
	5.1	pHClear II	
	6.6	pHClear; Classics; JCSG+; JCSG core suite	
VEGFR-2 D7-GCN4 N704/721Q	5.8	JCSG core suite	
VEGFR-1 D1-7	2.6; 5; 7.4; 10	pHClear	
	7	JCSG core suite	
	5.7	JCSG core suite	Methylated lysines
	6	JCSG core suite	Deglycosylated with PNGaseF
VEGFR-1 D1-3	7.1	JCSG core suite	Methylated lysines
VEGFR-1 D4-7	2.2		Deglycosylated with PNGaseF
VEGFR-1 D1-3 /VEGF-A$_{121}$	4; 8; 11.3; 14.8	pHClear	
	8	JCSG core suite	
VEGFR-1 D1-7 /VEGF-A$_{121}$	2; 3.8; 7.5; 9.6	pHClear	
	5.5; 9.6	JCSG core suite; Additive screen HT; silver bullets additive screen	
	5.5	JCSG core suite	+ EndoF1 or α-chymotrypsin
	5.9	JCSG core suite	Methylated lysines
	5.4	JCSG core suite; Additive screen HT	Deglycosylated with PNGaseF
VEGFR-1 D2-7 /VEGF-A$_{121}$	4.5	JCSG core suite	Deglycosylated with PNGaseF

Crystallization screening of VEGFR-2 D7 alone, linked to a GCN4 coiled coil, or D6-7 did not result in crystal growth. In most cases different forms of precipitates were observed, especially in ammonium-sulphate containing conditions. Refined screens were set up for promising conditions without any success in crystal growth.

VEGFR-1 ECD variants were screened for crystallization alone as well as in complex with VEGF-A$_{121}$. While the receptor ECD alone did not yield any crystals, the VEGFR-1 D1-7/VEGF-A$_{121}$ complex crystallized in several conditions. The crystals initially grew to 0.1-0.2 µm in an almond like shape (Fig. 19a). The buffers leading to crystal growth varied from pH 5 to pH 9 and the precipitant concentration ranged from 8-13% PEG. PEGs from 2000-8000 Da were the most effective precipitants. In addition, most conditions comprised monovalent salts such as sodium chloride or lithium chloride varying in concentrations from 0.1-1 M. The crystals were fished and transferred into drops of mother liquor containing increasing concentrations of cryo-protectant and immediately flash frozen in liquid nitrogen. Unfortunately, the frozen crystals diffracted only up to ~10 Å. In addition, diffraction spots were only observed when shooting the crystals with full intensity leading to radiation damage and rapid loss of diffraction.

In order to improve crystal quality, deglycosylated protein was analyzed for its crystallization characteristics. It crystallized in similar conditions as fully glycosylated protein. However, the crystal morphology changed to clusters of rods or plates depending on the precipitant concentration (Fig. 19b & c). Although the protein crystallized in a different crystal shape, the diffraction behavior did not change at all (Fig. 19b). SDS-PAGE and immunoblot analysis using anti-His$_5$ antibodies assured that the crystals contain at least VEGFR-1 protein and most likely also VEGF-A$_{121}$ (Fig. 19c).
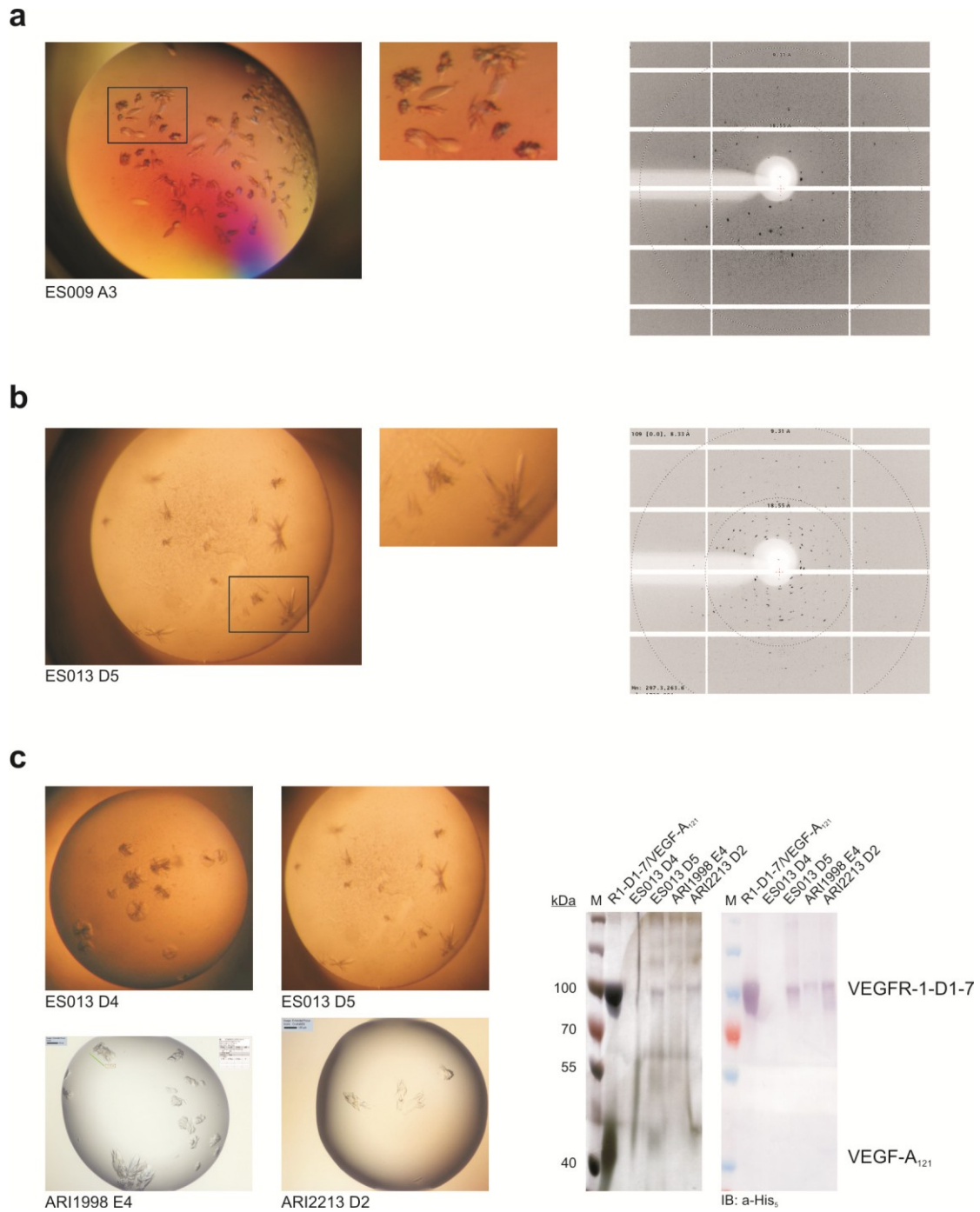
Fig. 19: Crystallization of VEGFR-1 D1-7/VEGF-A$_{121}$
Images of crystallization drops containing crystals of glycosylated (a) and deglycosylated (b) VEGFR-1 D1-7 in complex with VEGF-A$_{121}$, together with their diffraction pattern. Silver-stained SDS-gel and immunoblot of VEGFR-1 D1-7/VEGF-A$_{121}$ crystals containing deglycosylated (top) and glycosylated (bottom) VEGFR-1 D1-7 (c).

In addition to modifications in the glycosylation pattern of the used protein, I tried additive screens, lysine methylation (Walter et al., 2006), partial proteolysis with α-chymotrypsin (Dong et al., 2007), in drop deglycosylation, different cryo conditions followed by dehydration of the crystal, chemical crosslinking of the protein in the crystal, and initial seeding tests to induce growth of single rods or plates. However, none of these methods yielded crystals with improved diffraction characteristics.

6.3.5 Characterization of ligand-binding to VEGFR-1 ECD

In order to assess the quality and the functionality of the recombinant VEGFR-1 ECD proteins, its ligand binding ability was used as an assay. VEGFR-1 D1-7 or VEGFR-1 D1-3 was incubated with VEGF-A$_{121}$ at a 2:1, 1:1, and 1:2 molar ratio (receptor:monomeric ligand). The complexes were purified over a SEC column and analyzed by SDS-PAGE. Addition of two-fold higher amount of VEGFR resulted in a UV-profile showing two peaks, the VEGFR/VEGF complex eluting earlier (12.4 ml for VEGFR-1 D1-7 & 14.1 ml for VEGFR-1 D1-3) and the excess receptor protein eluting at a bigger elution volume (13.5 ml for VEGFR-1 D1-7 & 15.4 ml for VEGFR-1 D1-3). The chromatograms of the 1:1 complex and the 1:2 complex look very similar, showing one major peak at 12.1 ml elution volume and 14.1 ml for the VEGFR-1 D1-7/VEGF-A$_{121}$ and the VEGFR-1 D1-3/VEGF-A$_{121}$ complex, respectively (Fig. 20). Compared with a molecular weight standard, these elution volumes correspond to a Mr of 195 kDa for the VEGFR-1 D1-7/VEGF-A$_{121}$ complex and 99 kDa for the VEGFR-1 D1-3/VEGF-A$_{121}$ complex, which is very close to the theoretical values of 196.8 and 103.6 kDa, respectively. This indicates that the recombinant VEGFR-1 ECD variants are fully functional and bind to VEGF-A$_{121}$ in a 1:1 ratio, considering the VEGF-A$_{121}$ as a monomer.

74
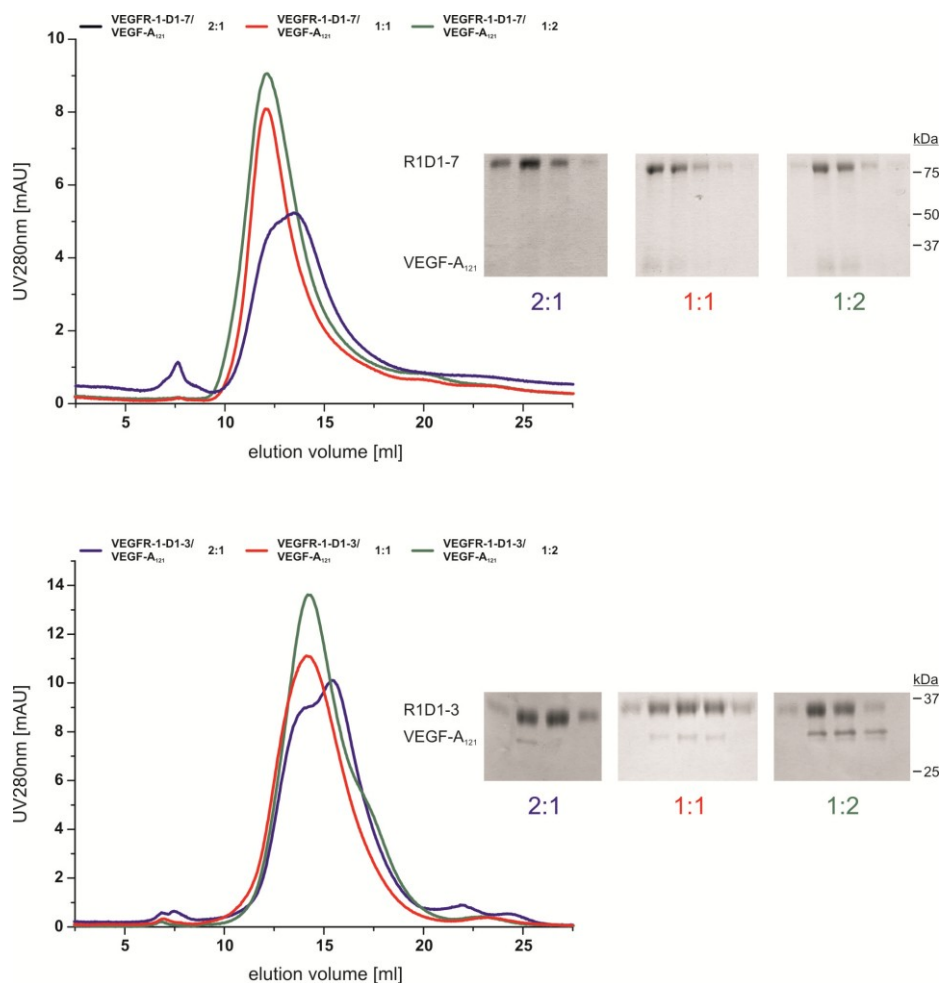
Fig. 20: SEC of VEGFR/VEGF complexes
UV-profiles of SEC purifications of VEGFR-1 D1-7/VEGF-A$_{121}$ (top) and VEGFR-1 D1-3/VEGF-A$_{121}$ (bottom). The complexes were mixed at a molar ratio of 2:1 (blue), 1:1 (red), and 1:2 (green). SDS-gels showing selected fractions of the SEC purifications are displayed in the insets.

In order to validate these results, purified VEGFR/VEGF complexes were loaded onto a SEC column connected to a MALS instrument to estimate the molecular masses of the recombinant proteins. MALS of proteins allows calculating the Mr in a shape independent manner. The loading of VEGFR-1 D1-7 gave rise to a single peak with a calculated mass of 90 kDa (Fig. 21). Adding VEGF-A$_{121}$ caused a shift of this peak towards earlier elution volumes with a calculated mass of 206 kDa. The experimentally determined Mrs are slightly bigger than the theoretical values of 83 kDa for the VEGFR-1 D1-7 alone and 197 kDa for the ligand/receptor complex. This can be explained by the sugar moieties that are still linked to the proteins, resulting in higher Mrs in MALS experiments. The same explanation is valid vor VEGFR-1 D1-3 alone.

However, the experimentally determined Mr of the VEGFR-1 D1-3/VEGF-A$_{121}$ complex (88 kDa) is smaller than the theoretical value of 99 kDa (Fig. 21). The peak of the VEGFR-1 D1-3/VEGF-A$_{121}$ complex in the UV-profile shows a long tail, suggesting that a heterogenous mixture of 2:1 and 1:1 receptor:ligand complexes is present.

	Mr (theor) [kDa]	Mr (MALS) [kDa]
VEGFR-1-D1-7	83.25	89.71
VEGFR-1-D1-7/VEGF-A$_{121}$	196.8	206.3
VEGFR-1-D1-3	36.62	39.03
VEGFR-1-D1-3/VEGF-A$_{121}$	99.34	87.96
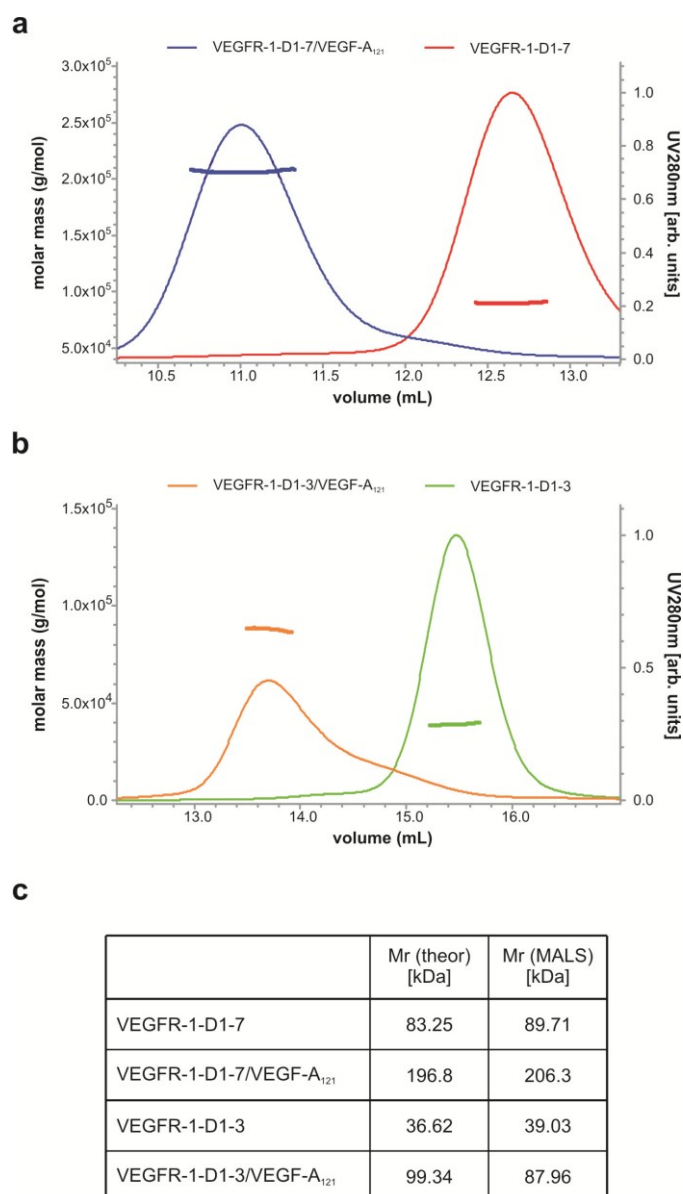
Fig. 21: SEC coupled MALS of VEGFR-1 ECD variants alone and in complex with VEGF-A$_{121}$
The UV-profiles of VEGFR-1 D1-7 alone and in complex with VEGF-A$_{121}$ (a) and VEGFR-1 D1-3 alone and in complex with VEGF-A$_{121}$ (b) are shown along with the mass distribution of each peak calculated from the MALS data. Table comparing the experimental Mr with the theoretical Mr (c).

6.3.6 Thermodynamic profile of VEGFR-1 ECD/ligand complex formation

In a recent study conducted in our laboratory, we showed that the presence of VEGFR-2 Ig-homology domain 4-7 reduced the free energy for all ligand/receptor interactions (Brozzo et al., 2011, submitted). Hence, the membrane-proximal Ig-homology domains seem to prevent receptor self dimerization in the absence of ligand.

In order to further characterize the VEGFR-1 ECD proteins ITC experiments were performed. ITC allows to determine binding parameters, such as dissociation constant (K_d), enthalpy (ΔH), and stoichiometry (N). Furthermore, by comparing ligand binding to the minimal ligand binding domain (VEGFR-1 D1-3) and to the full length ECD (VEGFR-1 D1-7), the contribution of the membrane-proximal Ig-homology domains 4-7 to the ligand binding can be estimated. Four ligands were analyzed for their receptor binding characteristics: VEGF-A$_{121}$, VEGF-A$_{165}$, VEGF-A$_{165B}$, and PlGF.

Table 4: Thermodynamic parameters of the VEGFR-1 ECD/ligand interaction determined by ITC
Stoichiometry (N), dissociation constant (K_d), Gibbs free energy (ΔG), enthalpy (ΔH), entropy (ΔS), and c-value (calculated as: $c = N*[R1]/K_d$) are given.

	N	K_d [µM]	ΔG [kcal*mol^{-1}]	ΔH [kcal*mol^{-1}]	-TΔS [kcal*mol^{-1}]	c-value
VEGF-A$_{121}$/R1-D1-7	1.93	0.012	-10.6	-11.9	1.3	759
VEGF-A$_{165}$/R1-D1-7	1.91	0.033	-10.0	-15.4	5.4	267
VEGF-A$_{165B}$/R1-D1-7	1.82	0.020	-10.3	-12.8	2.5	440
PlGF/R1-D1-7	2.03	0.038	-10.0	-12.5	2.5	234
VEGF-A$_{121}$/R1-D1-3	2.37	0.098	-9.4	2.0	-11.3	408
VEGF-A$_{165}$/R1-D1-3	2.01	0.069	-9.6	2.3	-11.9	583
VEGF-A$_{165B}$/R1-D1-3	2.13	0.172	-9.1	1.7	-10.7	267
PlGF/R1-D1-3	ND		ND	ND	ND	ND

The ITC measurements confirmed that VEGF binds to VEGFR with a stoichiometry of 2, meaning VEGF (as a dimer) can bind two receptor molecules. The binding affinities of the used ligands for VEGFR-1 D1-3 ranged

from 69-172 nM, whereas the binding affinities for the full length ECD showed lower values and varied from 12-38 nM (Fig. 22 & Table 4). The higher affinity for the full length ECD of VEGFR-1 suggests that Ig-homology domains 4-7 have a positive effect on ligand binding, possibly owing to receptor/receptor interactions. Interestingly, the binding of VEGFs to the full length ECD of VEGFR-1 is enthalpically driven, whereas the binding to Ig-homology domains 1-3 is dominated by entropic contributions (Fig. 22 & Table 4). Hence, Ig-homology domains 4-7 show a strong effect on the enthalpy of VEGF binding. Although the different ligands (VEGF-A_{121}, -A_{165}, -A_{165B}, and PlGF) bind with different binding constants, the thermodynamic mechanism of ligand binding is the same, shown by similar ΔΔ-values (ΔΔG, ΔΔH, and −TΔΔS). Surprisingly, PlGF showed high affinity binding to the full ectodomain of VEGFR-1, but no binding to the minimal ligand binding domain of VEGFR-1 consisting of Ig-homology domains 1-3. This is in contrast to the binding characteristics of VEGF-A.

To confirm VEGFR/VEGF complex formation in the ITC cell, specific samples were loaded onto a SEC column coupled to a MALS instrument. The chromatograms of the SEC step as well as the calculated Mrs showed complex formation of VEGFR-1 D1-7 with all ligands. VEGFR-1 D1-3 formed the complex only with the VEGF-A variants but not with PlGF, which is apparent when comparing the UV-profile of the individual proteins and the sample of the ITC experiment (Fig. 23a). The separation of the ITC cell content of the VEGFR-1 D1-3/PlGF complex formation resulted in two peaks with the apparent Mr of 59.6 and 39.1 kDa, close to the Mr of PlGF (54 kDa) and VEGFR-1 D1-3 (40.4 kDa) when loaded separately onto SEC-MALS. The VEGFR-1 D1-3/VEGF-A_{121} complex on the other hand resulted in two peaks with a Mr of 95.8 and 30.7 kDa, which are similar to the theoretical values of the complex (103.6 kDa) and the VEGF-A_{121} (30.3 kDa). PlGF alone does not elute as a monodisperse peak from the SEC column, probably due to the heterogeneity of the sugar moieties present on the protein. Since PlGF was produced in *Pichia pastoris*, the protein gets heavily glycosylated. Deglycosylation with EndoF1 shows a significant shift of the diffuse band observed for the glycosylated form to a more discrete band on SDS-gels (Fig. 23b). Interestingly, VEGFR-1 D2-3

mixed with PlGF and loaded onto the SEC-MALS eluted as one peak with a calculated Mr of 81 kDa, resembling the theoretical value of 81.5 kDa for a 2:1 complex, considering the PlGF dimer as one molecule (Fig. 23).

	ΔΔG [kcal*mol⁻¹]	ΔΔH [kcal*mol⁻¹]	-TΔΔS [kcal*mol⁻¹]
VEGF-A₁₂₁	-1.4	-13.9	12.6
VEGF-A₁₆₅	-0.4	-17.7	17.3
VEGF-A₁₆₅b	-1.2	-14.5	13.2
PlGF			
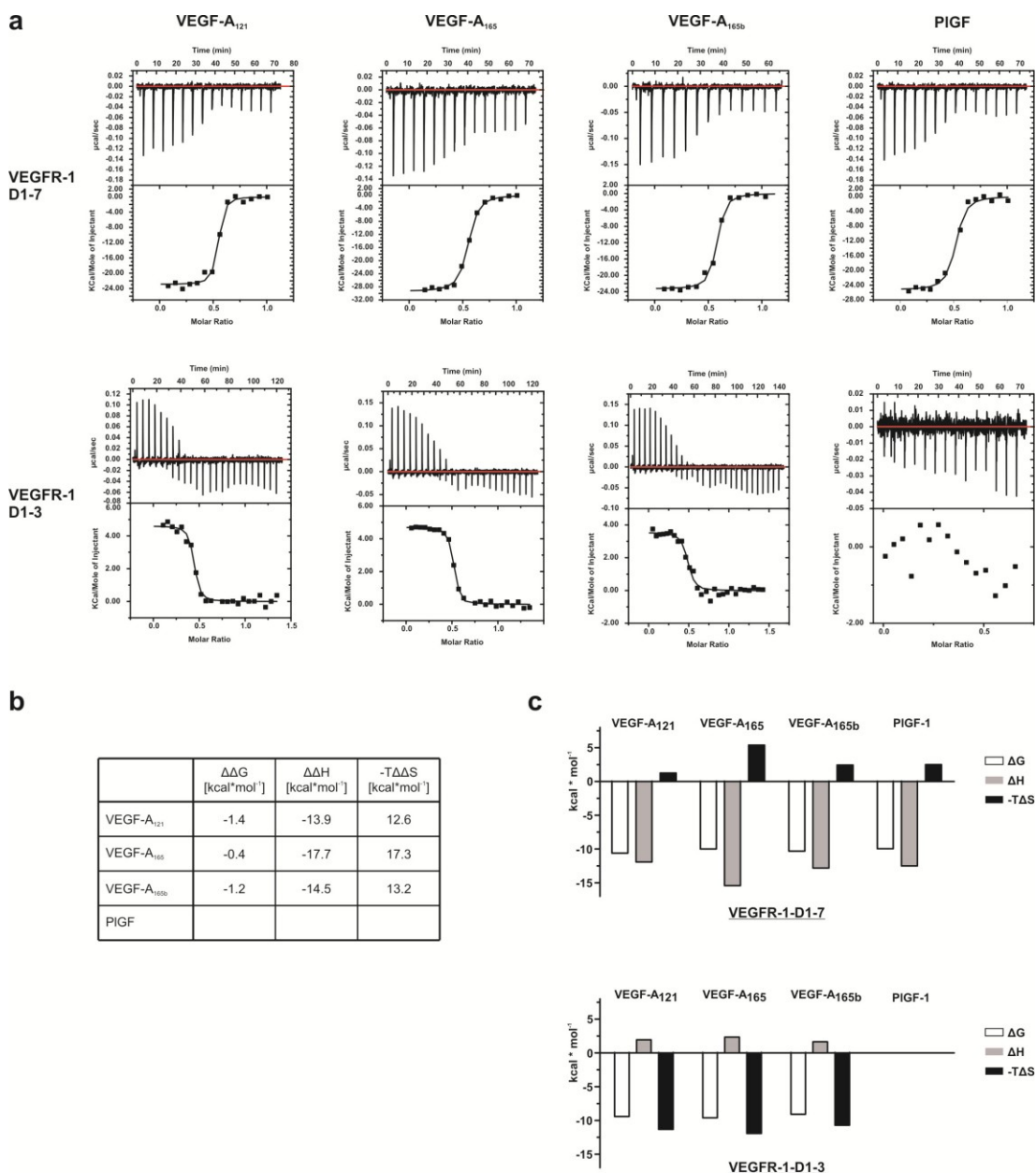
Fig. 22: Representative thermodynamic characterization of the VEGFR-1 ECD/ligand interaction
Raw titration data and the corresponding integrated and concentration normalized isothermograms (a). The solid lines represent the best fit according to the "One Site Model". Table representing the thermodynamic parameters ΔΔG, ΔΔH, and –TΔΔS (b). Graphical representation of the thermodynamic parameters Gibbs free energy (ΔG), enthalpy (ΔH), entropy (-TΔS) of the VEGFR-1 ECD/ligand interaction (c).
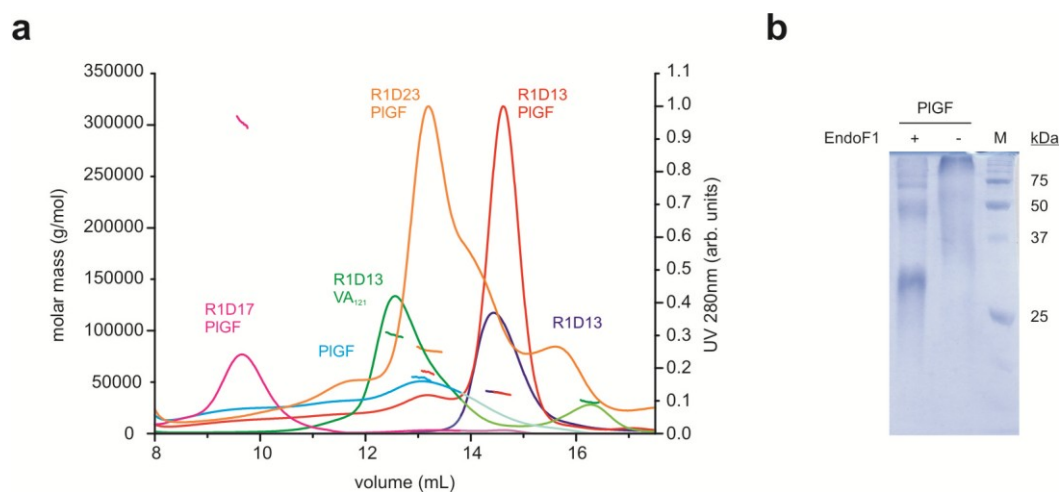
Fig. 23: MALS analysis of VEGFR-1 ECD/VEGF complex formation in ITC experiments
UV-profiles of SEC-MALS experiments conducted with selected ITC cell contents, PlGF and VEGFR-1 D1-3 alone as controls, and the VEGFR-1 D2-3/PlGF complex (a). Coomassie-stained SDS-gel of fully glycosylated and deglycosylated PlGF (b).

6.3.7 Structure of predimerized VEGFR-2 Ig-homology domain D7 determined by SAXS

SAXS gives access to low resolution structures of macromolecules in solution by *ab-initio* modeling. The following parameters can be easily obtained using SAXS: Rg, Dmax, hydrated particle volume, and Mr (Mertens and Svergun, 2010). While the Dmax represents the maximum intramolecular distance, the Rg is defined as the root-mean-squared distance of all elemental scattering volumes from their center of mass weighted by their scattering densities (Jacques and Trewhella, 2010). The Fourier-transformation of the scattering intensities gives rise to the P(r) function. The P(r) function illustrates the distribution of intramolecular distances. The Rg is accessible from both the liniear Guinier-region (scattering intensities plotted against s^2) and the P(r) function. From the P(r) function three-dimensional shapes can be retrieved through *ab-initio* modeling.

As indicated in the EM images of the VEGFR-2 ECD/VEGF-A complex, the membrane-proximal Ig-homology domains 7 interact with each other in the

80

ligand bound receptor complex (Ruch et al., 2007). To further characterize these interactions I predimerized individual domains 7 through a C-terminal GCN4 coiled coil. Keeping two Ig-homology domains 7 in close proximity would trigger them to form homotypic interactions as observed in the EM images. SAXS was used as an initial low resolution method to analyze whether or not the two Ig-homology domains 7 interact.

The SAXS analysis showed a relatively flat intensity curve with no apparent features (Fig. 24a). The Kratky-plot confirmed that the protein is folded and the linear Guinier-region showed that no higher order aggregates are formed (Fig. 24b & c). The P(r) function showed a maximum distance (Dmax) of 120 Å (Fig. 24d). The asymmetric shape of the P(r) function with a maximum at around 35 Å and a longer tail indicates that the overall structure of the protein is elongated. *Ab-initio* modeling resulted in an elongated envelope structure with dimensions of 120x90x45 Å that has a bigger volume at one end, narrowing down to the other end (Fig. 24e). The overall shape of the SAXS model is bigger than the crystal structures of the Ig-homology domain 7 dimer and the GCN4 coiled coil (Fig. 24f). SAXS, in contrast to X-ray crystallography also takes into account the hydration shell of the protein since analysis is performed in solution, leading to bigger overall shapes. Furthermore, the proteins used for the SAXS study still contain all N-glycosylations, while the proteins shown in the crystal structures have been produced in *E. coli*, giving rise to unglycosylated proteins. In summary, the *ab-initio* model of the VEGFR-2 D7-GCN4 protein shows that two Ig-homology domains 7 interact with each other when arranged in close proximity.
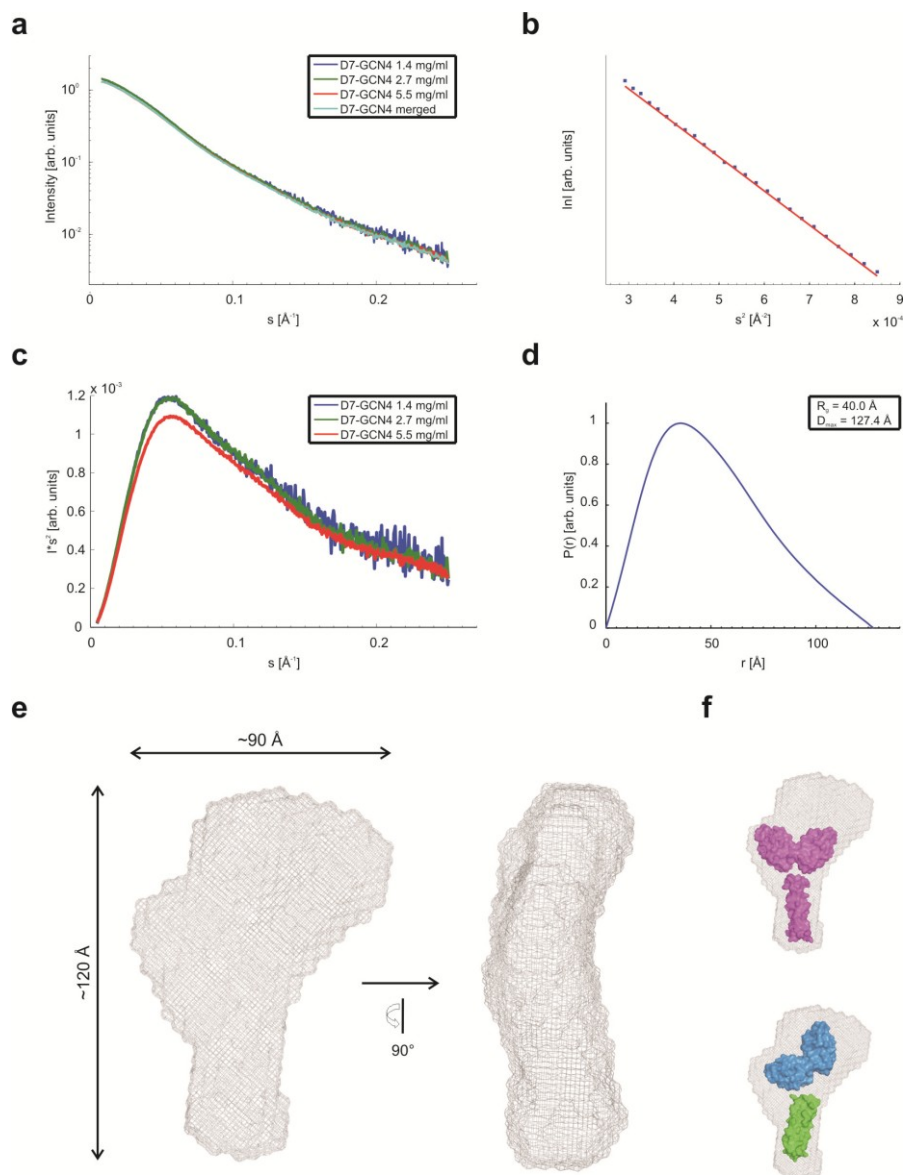
Fig. 24: SAXS results of VEGFR-2 D7-GCN4
The intensity plotted as a function of s (a). The linear Guinier region (b). The Kratky-plot (c). The P(r) function of as calculated from AUTOGNOM (d).The averaged model of VEGFR-2 D7-GCN4 as retrieved from ab-initio modeling (e). SITUS generated (top) and manual (bottom) superimposition of the ab-initio model (grey) with the dimeric Ig-homology domain 7 (PDB: 3KVQ) and a GCN4 coiled coil (PDB: 2ZTA) (f).

6.3.8 Structure of the VEGFR-1 ECD/VEGF-A complex in solution

Using SAXS, I wanted to gain insight on the overall structure of monomeric VEGFR-1 ECD as well as complexed with its ligand VEGF-A$_{121}$. The scattering intensity curves of monomeric and complexed VEGFR-1 ECD show no remarkable features, but they differ at low angles showing that the VEGFR-1

ECD/VEGF-A$_{121}$ complex has a bigger size than the monomeric receptor (Fig. 25a). This is verified by the P(r) function indicating a shifted maximum towards higher distances when VEGFR-1 is bound to the ligand and a Dmax of 255 Å for the receptor/ligand complex and 220 Å for the monomeric receptor (Fig. 25d & Table 5). The shifted maximum of the P(r) function reflects a thicker overall body in the complex compared to the monomeric VEGFR-1 ECD. The Kratky-plot and the linearity of the Guinier region document the presence of properly folded protein (Fig. 25b & c).

Table 5: SAXS analysis of samples
All values were calculated from data of the individual concentrations using AUTOPOROD. Errors were estimated from the differences between the individual concentrations.

Protein sample	Concentrations [mg/ml]	Rg [Å]	Dmax [Å]	Vol x10^3 [Å^3]
VEGFR-1 ECD (glycerol)	2.8; 3.4	66.7 ± 6.5	214 ± 22	268 ± 99
VEGFR-1 ECD (DTT)	1.5; 2.0; 2.9	66.0 ± 0.7	221 ± 2	214 ± 13
VEGFR-1 ECD (EDTA)	2.0; 2.4; 3.3	66.9 ± 2.8	231 ± 21	223 ± 34
VEGFR-1 ECD/ VEGF-A121 (glycerol)	1.3; 3.1; 5.7	82.4 ± 3.2	270 ± 9	632 ± 22
VEGFR-1 ECD/ VEGF-A121 (DTT)	2.2; 2.8; 3.1	76.9 ± 1.1	260 ± 7	596 ± 10
VEGFR-1 ECD/ VEGF-A121 (EDTA)	2.0; 2.4; 3.6	81.2 ± 1.4	272 ± 17	685 ± 8
VEGFR-1 ECD/ VEGF-A121 (ascorbic acid)	2.5; 5.0	74.7 ± 2.5	256 ± 12	574 ± 52
VEGFR-1 ECD/ VEGF-A121 (sucrose)	2.7; 5.0	75.4 ± 1.3	253 ± 2	557 ± 18
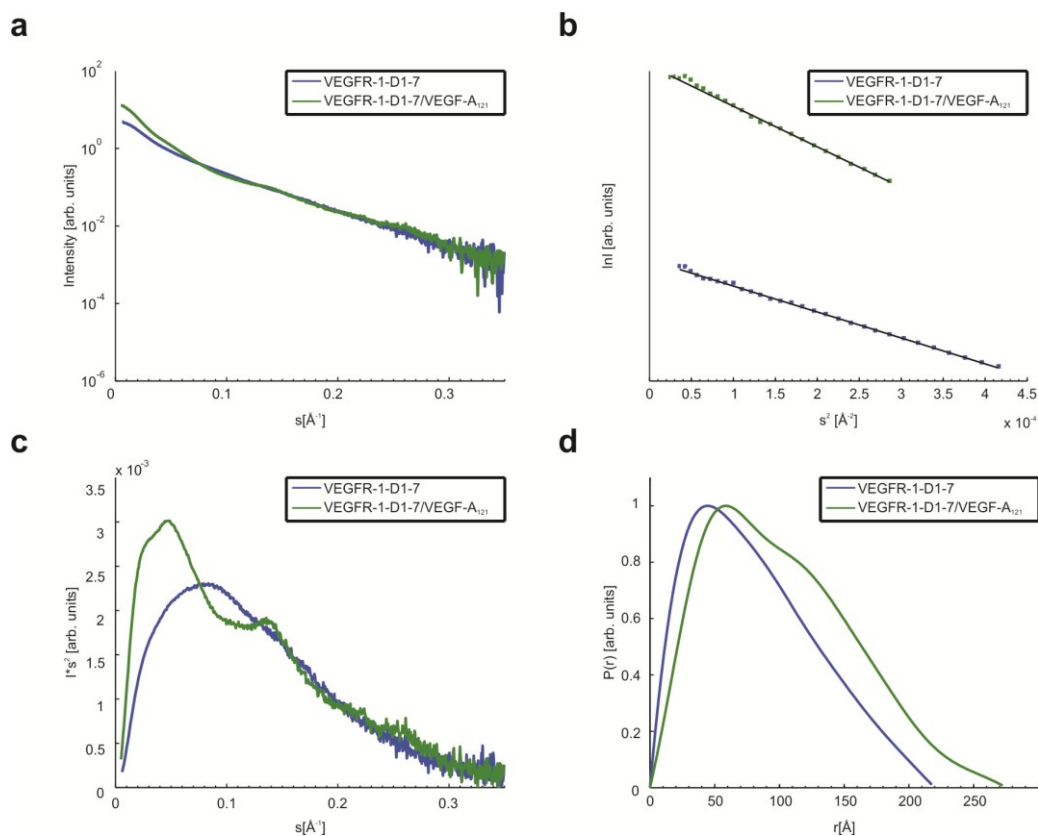
Fig. 25: SAXS results for VEGFR-1 ECD alone and in complex with VEGF-A$_{121}$
The intensity as a function of s (a), the linear Guinier regions (b), the Kratky-plot (c) and the P(r) function (d) are shown for VEGFR-1 D1-7 and the VEGFR-1 D1-7/VEGF-A$_{121}$ complex.

Ab-initio shape reconstruction of the monomeric VEGFR-1 ECD resulted in an elongated tube like shape that is bent twice along the molecule (Fig. 26a). The VEGFR-1 ECD shape is 220 Å long and 65 Å wide. Superimposition of the obtained SAXS shape with VEGFR-2 D2-3 (PDB 2X1W) showed that it fits nicely into the shape leaving space for the remaining Ig-homology domains (Fig. 26b). The VEGFR-1 ECD/VEGF-A$_{121}$ complex can be described as a Y-like shape with dimensions of 255 Å in length and 140 Å in width. The end with the bigger mass presumably represents the ligand binding domain with Ig-homology domains 1-3 and the ligand VEGF-A$_{121}$ (Fig. 26c). Towards the other end, the shape becomes thinner, implying receptor/receptor interactions between Ig-homology domains 4-7. The overall topology of the VEGFR-1 ECD/VEGF-A$_{121}$ suggests an asymmetric complex in solution. In contrast, the crystal structure of the c-Kit ECD in complex with its ligand SCF

shows a similar shape but with a P2-symmetry along the receptor chains
(Yuzawa et al., 2007). However, the c-Kit/SCF crystal structure did not
superimpose well with the 'most typical' model of VEGFR-1 D1-7/VEGF-A$_{121}$
(Fig. 26d). The application of P2-symmetry for *ab-initio* shape reconstructions
resulted in models where the symmetry axis was placed across, instead of
along, the receptor molecules.
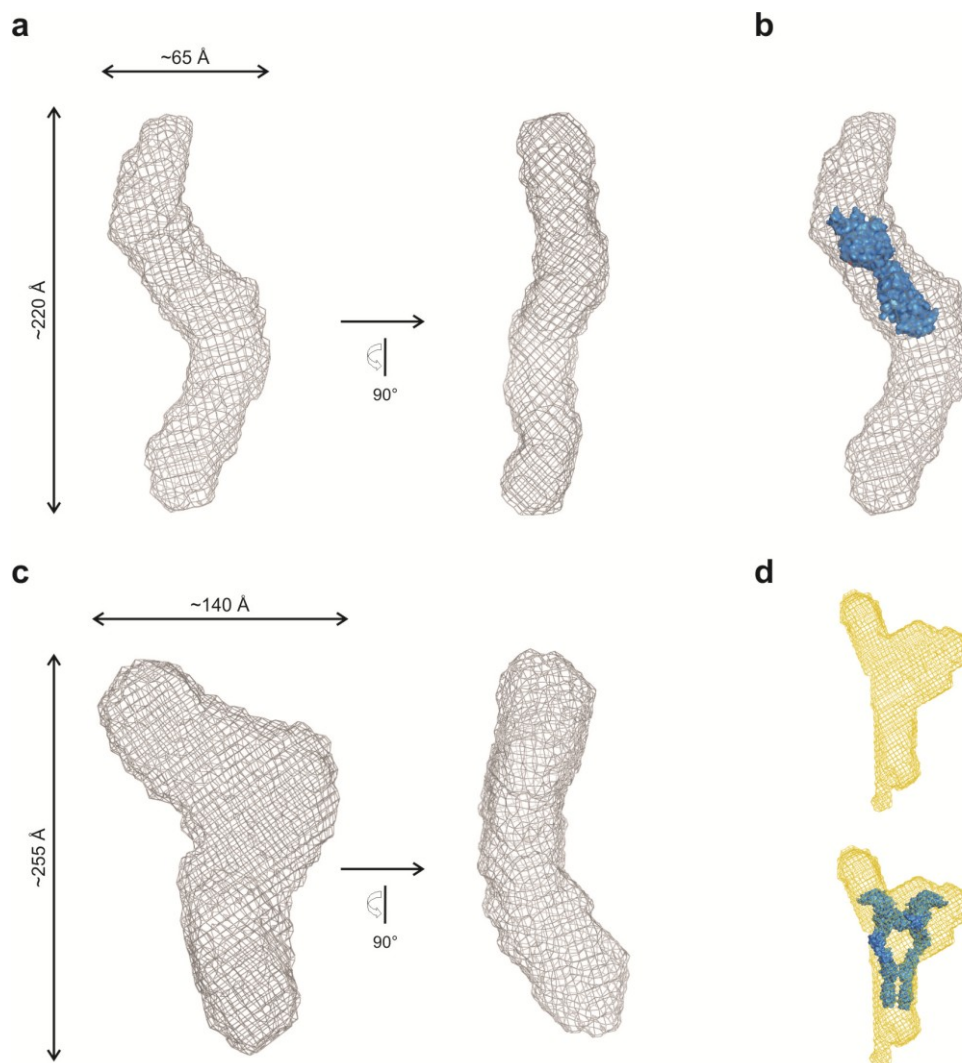
Fig. 26: **Ab-initio** *shape reconstruction of VEGFR-1 ECD and VEGFR-1*
ECD/VEGF-A$_{121}$
The averaged and filtered model of VEGFR-1 ECD (a) and its superposition
with VEGFR-2 D2-3 (blue; PDB-entry: 2X1W) using SITUS (b). The averaged
and filtered model of VEGFR-1 ECD in complex with VEGF-A$_{121}$ (c). The 'most
typical' model of VEGFR-1 D1-7 in complex with VEGF-A$_{121}$ (wheat) and its
*superposition with the c-Kit/SCF (blue; PDB-entry: 2E9W) crystal structure (d).*

6.3.9 Structure of the VEGFR-1 ECD/ligand complexes determined by EM

Negative stain EM provides quick access to the overall shape of the analyzed macromolecule, especially for bigger complexes that may be problematic for X-ray crystallography. Here, isolated proteins are embedded in a layer of dried heavy metal solution on a carbon support film. The recorded images of a negative stained specimen can be computationally averaged to allow finer details to be visualized.

VEGFR-1 is activated by VEGF-A, VEGF-B, and PlGF. Whereas VEGF-A also binds to VEGFR-2, VEGF-B and PlGF bind exclusively to VEGFR-1. VEGF-A and PlGF have been shown to cause the phosphorylation of distinct tyrosine residues (Autiero et al., 2003). Depending on the ligand type that binds to the receptor, different conformations of the intracellular kinase domain may be induced. This in turn may regulate the accessability of specific tyrosine residues to the active site of the kinase. Using EM, we wanted to analyze the different VEGFR-1 ECD/ligand complexes.

The VEGFR-1 ECD alone showed a highly flexible structure, making it difficult to average single particles into classes. However, we observed that the unliganded receptor was monomeric and did not show intermolecular interactions (Fig. 27). The seven Ig-homology domains were mostly stretched out to an elongated chain with a maximum length between 200 and 250 Å. The EM class averages of the ligand/receptor ECD complexes showed molecules that are 100 Å in width and 250 Å in length. Most class averages of all three complexes show conformations where two receptor molecules are bridged by extra density most likely representing the ligand, which binds Ig-homology domains 2 and 3 (Fig. 27). Thus, the density pointing away from the ligand has to be Ig-homology domain 1, which is bent by almost 90° compared to the other Ig-homology domains. This prominently bent Ig-homology domain 1 is present in almost all class averages and is often seen only on one receptor molecule. The individual receptor chains were often oriented in a parallel fashion and only in some class averages they showed an intertwined shape, as seen in the VEGFR-2/VEGF-A complex (Ruch et al., 2007). Furthermore, some class averages indicate receptor/receptor interactions in the region of Ig-homology

domains 4 to 7. The homotypic interaction of Ig-homology domain 7, which has been described for VEGFR-2, is also seen in over 50% of the images of VEGFR-1, independent of the bound ligand type. However, there are also molecules showing the region around Ig-homology domain 4 and 5 of the two receptor chains in very close proximity, suggesting further homotypic interactions that may stabilize the VEGFR/VEGF complex. When comparing the complexes of the three ligands with the receptors, no significant differences were observed. Hence, all ligands for VEGFR-1 form similar complexes with the ectodomain of VEGFR-1, indicating similar binding mechanisms.
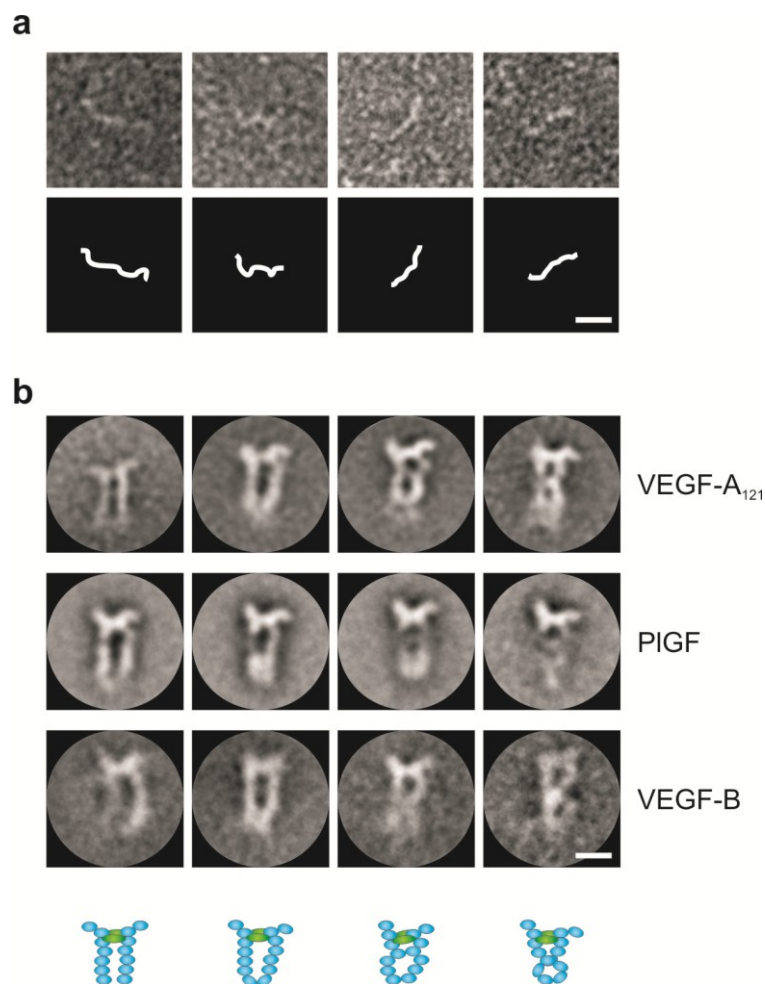
Fig. 27: Electron microscopy of monomeric VEGFR-1 ECD and of VEGFR-1 ECD/ligand complexes
Raw images and schematic representations of the monomeric VEGFR-1 ECD (a). Class averages and graphic representations of the VEGFR-1 ECD in complex with VEGF-A$_{121}$, PlGF, and VEGF-B (b). All scale bars, 15 nm.

Comparing the SAXS shape with the EM images, some differences can be noticed. While the shape of the VEGFR-1 ECD/VEGF complex obtained using SAXS implies an asymmetric conformation, the EM images show more symmetrical complex conformations. In EM, Ig-homology domain 1 of both receptor chains points outwards, whereas in SAXS this feature is less prominent. Furthermore, the EM images indicate several different conformations, either with both receptor chains oriented parallel to each other or arranged in an intertwined manner. Since the SAXS shape represents an average over all conformations found in solution, these details can not be observed in the SAXS derived VEGFR-1 D1-7/VEGF-A$_{121}$ structure.

6.4   Discussion

VEGFs and their receptors, the VEGFRs, are major regulators of angiogenesis, vasculogenesis, and lymphangiogenesis. Their dysfunction has been linked to a number of pathological conditions, making VEGFs and VEGFRs prominent drug targets. During this project, a major goal was to determine the structure of VEGFR ECD variants using high and low resolution methods. In this chapter I described the successful expression, purification, characterization, and crystallization of VEGFR ECD variants. The capability of complex formation of the recombinant proteins was assessed and thermodynamic parameters of ligand binding were determined. ITC and MALS experiments showed that VEGFR-1 D1-7 has a higher affinity for VEGF-A and PIGF-1 than VEGFR-1 D1-3. In fact, PIGF-1 did not bind to VEGFR-1 D1-3 but to VEGFR-1 D2-3, suggesting a regulatory role of Ig-homology domain 1 for PIGF binding. Furthermore, structural information obtained by SAXS using predimerized VEGFR-2 Ig-homology domain 7 confirmed that two of these domains form low affinity interactions presumably when they are brought into close proximity. SAXS and EM images of the VEGFR-1 ECD/ligand complex resulted in a dimeric receptor/ligand complex that is further stabilized by homotypic interactions in the region of Ig-homology domains 4-7. These interactions are characteristic for all three VEGFR-1 ligands: VEGF-A, VEGF-B, and PIGF. Overall, the study presented establishes low affinity homotypic interactions

induced upon ligand binding as a common feature for type V RTK activation.

Recombinant receptor protein expression was conducted in mammalian cells, insect cells, and *Pichia pastoris*, yielding protein amounts in the range of milligrams. However, only the mammalian and insect cell expression system resulted in full length proteins, whereas *Pichia pastoris* expression gave rise to protein degradation. While the protein yield in HEK293T, Sf21, and HighFive™ cells was sufficiently high, protein production in HEK293S-GnTI⁻ cells showed high protein yield only when generating stable cell lines. Protein expression in *E. coli* was not assessed due to the fact that earlier expression trials in the laboratory resulted in unfolded protein in inclusion bodies. However, it is arguable whether or not *E. coli* is the right expression system for single Ig-homology domains. In fact, all crystal structures of single VEGFR Ig-homology domains have been solved with protein expressed in *E. coli* that was later refolded (Wiesmann et al., 1997; Christinger et al., 2004; Iyer et al., 2010; Yang et al., 2010). In order to produce larger VEGFR ECD fragments, eukaryotic expression systems represent a more suitable strategy to gain correctly folded recombinant proteins. Several crystal structures of Ig-homology domain proteins have been solved using insect cell produced material (Yuzawa et al., 2007; Leppanen et al., 2010b). However, proteins produced in insect cells can lead to heterogeneously glycosylated protein. Thus, expression in HEK293S-GnTI⁻ cells is a promising option in order to obtain homogenously glycosylated proteins. As a matter of fact, there is an increasing number of structures of RTK ECDs deposited in the PDB database reporting expression in HEK293S-GnTI⁻ cells (Hye-Ryong Shim et al., 2010; Verstraete et al., 2011). In order to overcome low expression yields in HEK293S-GnTI⁻ cells, the BacMam-system has been developed (Dukkipati et al., 2008). Here, virus produced in insect cells is able to infect mammalian cells. Infection of HEK293S-GnTI⁻ with this virus is characterized by an improved gene delivery compared to classical transfection methods. Furthermore, this method has been already successfully applied to solve the structure of the PDGFR Ig-homology domains 1-3 in complex with PDGF (Hye-Ryong Shim et al., 2010). Therefore, the BacMam-system should be evaluated in the future to obtain reasonable expression yields of VEGFR ECDs in HEK293S-GnTI⁻ cells.

Expressed VEGFR-1 and VEGFR-2 ECD proteins underwent extensive screening for crystallization. While VEGFR-2 ECD domains did not result in any crystal growth, VEGFR-1 D1-7 in complex with VEGF-A$_{121}$ showed crystal growth in a number of conditions. Both glycosylated and deglycosylated proteins were used for crystallization screening resulting in different crystal forms. However, all crystals showed only poor diffraction. One possible explanation that comes to mind is that N-glycosylation affected the crystal growth or diffraction quality of the crystals. In fact, researchers who successfully solved the crystal structure of VEGFR-2 Ig-homology domain 7 used non glycosylated protein produced in *E. coli* (Yang et al., 2010). In a recent project at the PSI solving the structure of a vitamine B12 transporter, the protein was treated with EndoH leaving one N-acetylglucosamine at asparagine residues (Frei et al., personal communication). Some of the remaining N-acetylglucosamines formed crystal contacts, showing that residual sugars may even be beneficial for crystallization. Since deglycosylation did not improve diffraction characteristics of VEGFR-1 D1-7/VEGF-A$_{121}$ crystals, it appears that the proteins themselves are very flexible or contain flexible regions resulting in loosely packed crystals. Thus, new constructs with redefined domain boundaries or newly engineered loop and linker regions would be helpful. Other strategies I did not pursue during my thesis include tag-cleavage, mutation of the N-glycosylation sites, and the employment of other ligands for crystallization screening. Furthermore, the existing crystals can be used for extensive seeding screens to support crystal growth in conditions that did not result in crystals before. This strategy can possibly lead to a different crystal packaging, thereby improving diffraction quality.

Using SAXS and predimerized Ig-homology domains 7, I was able to confirm that these domains form homotypic interactions. Initially, I believed, that Ig-homology domain 7 only dimerizes upon local concentration through a glycine-serine linker or a coiled coil domain. Surprisingly, the structure of this domain alone showed dimers in the crystal held together through salt bridges formed by the conserved amino acids R726 and D731 (Yang et al., 2010). Thus, the single Ig-homology domain 7 would have been sufficient for crystallization trials in order to characterize the reported receptor/receptor

interactions (Ruch et al., 2007). However, for low resolution methods such as SAXS, the local concentration of this Ig-homology domain through dimerization by a coiled coil is needed. In analytical ultracentrifugation, individual Ig-homology domains 7 indicated dimerization starting at a concentration of 0.1 mM (Yang et al., 2010). For SAXS studies a homogenous distribution of the analyte is an absolute requirement. Hence, very high concentrations would have been needed to obtain a homogenous dimeric solution of the single Ig-homology domain 7, which we did not achieve.

The ability of the VEGFR-1 ECD to form a complex with VEGF-A and PlGF was characterized by several methods in this thesis. SEC, MALS, and ITC confirmed that VEGFR-1 ECD and ligands form a complex in a 2:1 stoichiometry, considering the disulfide linked ligand as one molecule. Binding affinities of the ligands for VEGFR-1 D1-7 were in the range of 12-33 nM, while the binding affinities for VEGFR-1 D1-3 decreased 2 to 8-fold. Higher affinities have been reported in the literature thus far. Using Biacore, Christinger and colleagues showed that concentrations of 24 pM VEGF and 435 pM PlGF are required to displace 50% VEGFR-1 D1-7 bound to VEGF (Christinger et al., 2004). Furthermore, 0.114 nM VEGF and 1.1 nM PlGF are sufficient to displace 50% of bound VEGFR-1 D2-3. Similar values were reported by Park and colleagues, who determined an IC_{50} value of 250 pM for VEGF binding to a dimeric VEGFR-1 D1-7 fusion protein (Park et al., 1994). Predimerization of VEGFR-1 proteins can explain the higher measured affinities in this case. However, another group determined the binding affinities of VEGF and PlGF to recombinantly produced VEGFR-1 ECD variants (Tanaka et al., 1997). They immobilized the VEGFR-1 ECD variants in 96-well plates and quantified the amount of bound radiolabeled ligand. With this assay, they showed that VEGF bound VEGFR-1 D1-7 and D1-3 with K_ds of 17 pM and 6.5 pM, respectively. PlGF on the other hand showed K_d values of 193 and 447 pM for VEGFR-1 D1-7 and D1-3 binding, respectively. The different experimental setup used in these studies explains the differences to our measured K_d values. Most of the research groups determined binding parameters by immobilizing one reaction partner on a solid surface leading perhaps to locally concentrated protein and favorable conformations of the binding partner. In the thesis presented, we were

the first determining binding of VEGF ligands to VEGFR-1 in solution using ITC. However, in our experimental setup, ITC is able to determine K_d values only in the millimolar to nanomolar range. The VEGFR-1 ECD/ligand reaction shows affinities that are very close to the detection limit. In order to more accurately determine K_d values with ITC, a competitive binding setup would be more suitable.

The determination of the thermodynamic binding parameters using ITC revealed that Ig-homology domains 4-7 have a positive effect on ligand binding shown by lower K_d values for binding to VEGFR-1 ECD compared to D1-3. This effect is mainly owing to a large enthalpic contribution of Ig-homology domains 4-7 to the ligand binding reaction. In contrast, the presence of VEGFR-2 Ig-homology domains 4-7 result in reduced binding affinities for the ligands to VEGFR-2 ECD (Brozzo et al., 2011 manuscript submitted). These findings suggest that VEGFR-2 D4-7 acts as a control module to prevent self association of VEGFR-2 in the absence of ligand. The fact that these four membrane proximal Ig-homology domains enhance ligand binding to VEGFR-1 support the hypothesis that VEGFR-1 acts as a decoy receptor for VEGF-A. In fact, several knock out studies in mice showed that VEGF-A concentrations need to be spatially and temporally tightly controlled (Fong et al., 1995; Fong et al., 1999; Hiratsuka et al., 1998; Hiratsuka et al., 2005). In addition, sVEGFR-1, whose sole function is to sequester free ligand, is comprised of Ig-homology domains 1-6, supporting the importance of Ig-homology domains 4-6 for ligand binding (Kendall and Thomas, 1993).

Interestingly, PlGF did not bind VEGFR-1 D1-3 in contrast to the studied VEGF-A isoforms. However, removing Ig-homology domain 1 enabled PlGF-1 binding, as shown in MALS experiments. Barleon and colleagues were the first to analyze the binding characteristic of VEGFR-1 ECD domains (Barleon et al., 1997). Both VEGF-A and PlGF-1 showed binding to VEGFR-1 ECD variants containing at least Ig-homology domains 1-3. However, the immobilized receptor molecules were preincubated with radiolabeled VEGF-A. After addition of increasing amounts of non-labeled VEGF-A or PlGF-1, the remaining radioactivity was measured. In this setup the preincubation step with radiolabeled VEGF-A might favor the ligand-bound conformation of VEGFR-1

ECDs, thus facilitating PlGF-1 binding. In addition, immobilization of the VEGFR-1 ECDs might trigger the molecules to adopt a favorable conformation for ligand binding. Several other studies showed PlGF binding to VEGFR-1 D1-3 (Davis-Smyth et al., 1996; Davis-Smyth et al., 1998). However, in these studies VEGFR-1 ECD proteins were predimerized through a C-terminal Fc-tag. In this setup the Fc-tag might mimick the presence of Ig-homology domains 4-7 and thereby facilitate PlGF binding. Davis-Smyth and colleagues also reported that mutation of E137 to A affected PlGF but not VEGF binding (Davis-Smyth et al., 1998), although the crystal structure of VEGFR-1 D2 in complex with PlGF does not show a direct interaction of this amino acid with the ligand (Christinger et al., 2004). However, E137 is located close to the N-terminus of Ig-homology domain 2 and might be involved in the D1/2 interface and thereby indirectly regulating PlGF binding. Furthermore, binding studies of the VEGFR-2 ECD/VEGF complex suggest a regulatory role of Ig-homology domain 1 (Shinkai et al., 1998). Constructs comprising Ig-homology domain 1-7 showed a lower k_{on} for VEGF binding than constructs comprising Ig-homology domains 2-7, 2-5, and 2-4. In summary, I suggest that Ig-homology domain 1 of VEGFR-1 plays a regulatory role in ligand binding by favoring VEGF-A over PlGF binding.

Using SAXS and EM, the overall structure of VEGFR-1 D1-7 alone and in complex with one of its ligands was characterized. While the ECD alone has an elongated shape that shows a moderate flexibility, the structure of the ECD in complex with one of its ligands is more rigid. Both SAXS and EM revealed that ligand binding to Ig-homology domain 2-3 induces additional receptor/receptor interactions in the membrane-proximal domain 7. Some class averages of VEGFR-1 ECD in complex with VEGF-A suggested further homotypic interactions in the region of Ig-homology domains 4-5. Furthermore, no remarkable differences were observed between VEGFR-1 ECD in complex with VEGF-A, VEGF-B, or PlGF, indicating that all three ligands share a common mechanism of activation (Fig. 28).

Ligand binding to Ig-homology domains 2-3 leads to receptor dimerization without affecting the overall topology of these two Ig-domains. The high local concentration of dimerized receptor molecules enables low affinity interactions

between Ig-homology domains 4-7. These interactions lock the ligand/receptor complex in a defined conformation that brings the transmembrane, juxtamembrane, and the kinase domain into a specific conformation allowing autophosphorylation and activation of the kinase.
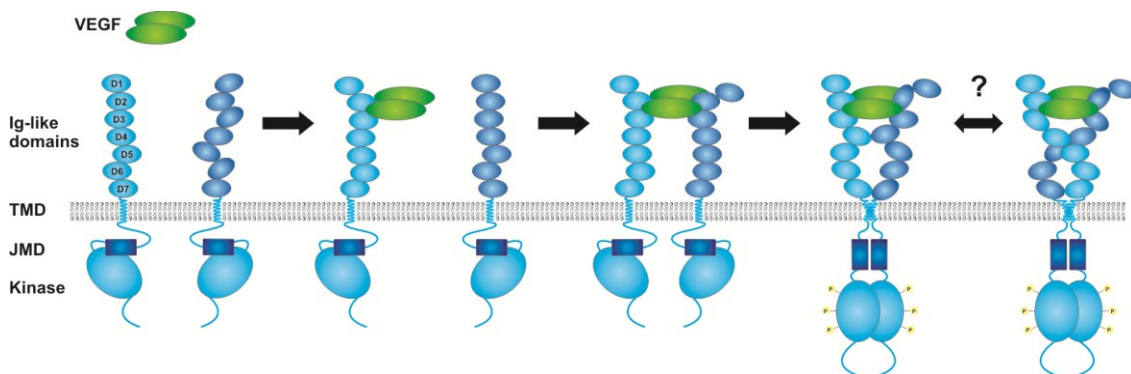
Fig. 28: Schematic model of VEGFR activation
Ligand (green) binding induces receptor dimerization, followed by a conformational arrangement of the VEGFR ECD allowing Ig-homology domains 7 to interact with each other. These interactions stabilize the active conformation enabling proper positioning of the transmembrane (TMD), the juxtamembrane (JMD), and the kinase domain to allow autophosphorylation in the intracellular receptor kinase.

Similar activation mechanisms were shown for VEGFR-2 (Ruch et al., 2007; Yang et al., 2010), another type-V RTK, c-Kit (Yuzawa et al., 2007), and PDGFR-β (Yang et al., 2008), both members of type-III RTKs, which contain only five Ig-homology domains in the ECDs. For c-Kit, both the crystal structures of the unbound monomeric receptor and the ligand-bound receptor complex were solved (Yuzawa et al., 2007). It was shown that ligand binding to Ig-homology domains 1-3 occurs without any remarkable conformational changes in this region. However, ligand binding is accompanied by a conformational rearrangement of Ig-homology domains 4 and 5. This enables E386 and R381, located in Ig-homology domain 4, to form salt bridges. Mutation of these residues resulted in decreased phosphorylation of the intracellular kinase domain. A similar motif was found in PDGFR-β and VEGFR-2 (Yang et al., 2008; Yang et al., 2010). In VEGFR-2, this pair of acidic and basic residues is located in the most membrane proximal Ig-homology domain 7. The crystal structure of VEGFR-2 Ig-homology domain 7 showed D731 and R726 forming

salt bridges (Yang et al., 2010). Thus, homotypic interactions between the extracellular domains seem to be a common mechanism within type III and V RTKs to stabilize the activated receptor complex. Surprisingly, the crystal structure of the Fms-like tyrosine kinase 3 ECD in complex with its ligand suggested a novel ligand binding mechanism that does not result in any receptor/receptor interactions (Verstraete et al., 2011).

Several studies showed that receptor dimerization is required but not sufficient for kinase activation (Bell et al., 2000; Dell'Era Dosch and Ballmer-Hofer, 2010). Rather, the two kinase domains in the dimer need to be in a specific orientation relative to each other to be fully functional. An artificially engineered transmembrane domain allows the rotation of the kinase domains with respect to each other. Tyrosine kinase activation of Neu RTK, PDGFR-β, and VEGFR-2 can only be detected in specific orientations indicating a tight linkage between kinase activity and the orientation of the two kinase domains in the receptor dimer (Bell et al., 2000; Dell'Era Dosch and Ballmer-Hofer, 2010). Hence, homotypic receptor interactions in the RTK ECD may be important for fixing the transmembrane and the kinase domain in a distinct orientation that allows autophosphorylation.

EGFRs have been shown to form dimers in living cells in the absence of ligand (Chung et al., 2010; Nagy et al., 2010). These dimers were inactive and existed for a finite lifetime (Chung et al., 2010). Our SAXS and EM studies of soluble VEGFR-1 ECD without ligand clearly showed only monomeric receptor molecules suggesting that VEGFRs do not form dimers without ligand. In agreement, FGFR3, consisting of three Ig-homology domains in the ECD, does not dimerize in the absence of FGF-1 (Chen et al., 2010). However, for VEGFRs the existence or absence of such preformed ligand-independent receptor dimers still needs to be proven in living cells.

In conclusion, the ITC, SAXS, and EM data presented in this study show that the VEGFR-1 ECD can be divided in two separate functional segments as suggested by the Schlessinger group for c-Kit (Yuzawa et al., 2007). Ig-homology domains 1-3 constitute the rather rigid segment 1, whose sole function is to bind the ligand. This is supported by the crystal structures of VEGFR-1 Ig-homology domain 2 in complex with VEGFR-1 ligands, which are

strikingly similar suggesting, that the ligands share a common binding mechanism to VEGFR-1 (Wiesmann et al., 1997; Christinger et al., 2004; Iyer et al., 2010). Furthermore, the solution structure of the free VEGFR-1 Ig-homology domain 2 showed no significant conformational changes compared to the ligand bound form (Starovasnik et al., 1999). Segment 2 is composed of Ig-homology domains 4-7. This segment is thus more flexible and provides additional interactions to the receptor/ligand complex, thereby stabilizing the activated complex.

7   Allosteric inhibition of VEGFR-2 signaling

Structural studies of the ECD of type III and type V RTKs suggest a common mechanism of activation. Ligand binding to the N-terminal 3 Ig-homology domains brings two receptor molecules together. The local concentration of the receptors leads to homotypic receptor interactions, thereby stabilizing the activated receptor/ligand complex, but also bringing the transmembrane and the intracellular domains into close proximity to allow autophosphorylation.

VEGFR-2 signaling is implicated in several pathological conditions such as cancer or retinopathic diseases. Several different strategies to tackle pathologic VEGFR-2 activation have been developed, including antibodies against VEGF-A or VEGFR-2 as well as small molecule inhibitors against the kinase domain.

As described in chapter 6 for the VEGFR family of RTKs homotypic interactions in the membrane proximal Ig-homology domains 4-7 are induced upon ligand binding. Based on similar data for VEGFR-2 (Ruch et al., 2007), we wanted to test whether or not these interactions can be targeted by Designed Ankyrin Repeat Proteins (DARPins) without disturbing the formation of the ligand/receptor complex.

In collaboration with Molecular Partners AG, we raised DARPins against VEGFR-2 D1-7. Several ribosome display screens resulted in 18 DARPins, of which 3 showed inhibitory effects on VEGFR-2 kinase phosphorylation in the presence of VEGF. While one DARPin bound the VEGFR-2 ectodomain very unspecifically, DARPins 6C8 and 6G9 bound the receptor at Ig-homology domain 4 or 2-3, respectively. We showed that DARPin 6G9 prevented ligand binding to the receptor, whereas 6C8 did not disturb the ligand/receptor complex integrity. Furthermore, downstream signaling was decreased in the presence of both DARPin 6C8 and 6G9. We further analyzed the effect of the inhibitors on the sprouting of endothelial cell spheroids. When preincubated with 6C8 or 6G9, embryoid bodies were not able to build sprouts upon VEGF application. In summary, we present a novel mechanism to target pathological VEGFR-2 signaling without disturbing ligand/receptor complex formation.

Furthermore, these data show that receptor dimerization alone does not drive VEGFR-2 activation and that a specific conformation in the region of Ig-homology domains 4-7 is necessary for full functionality of VEGFR-2.

This research project was conducted in collaboration with the PhD-student Alexandra Giese and Molecular Partners AG, Schlieren, Switzerland. My contribution to the project included production and purification of all proteins needed for the generation, verification, and determination of binding specificities of the DARPins. In addition, I performed the SEC-MALS experiments to show that 6C8 does not prevent VEGFR-2/VEGF complex formation. Furthermore, I was involved in designing and cloning the mutant VEGFR-2 constructs to functionally characterize the VEGFR-2 ECD.

Inhibition of receptor activation by Designed Ankyrin Repeat Proteins specific for the Ig-homology domain 4 of VEGFR-2 extracellular domain

Alexandra Giese[1][%], Edward Stuttfeld[1][%], Kaspar Binz[2] and Kurt Ballmer-Hofer[1][*]

[1]BiomolecularResearch, Molecular Cell Biology, Paul Scherrer Institute, CH-5232 Villigen PSI, Switzerland and [2]Molecular Partners AG, Wagistrasse 14, 8952 Zürich-Schlieren, Switzerland

[%] These authors equally contributed to this paper

*To whom correspondence should be addressed:

Phone: +41 56 310 4165

Fax: +41 56 310 5288

e-mail: kurt.ballmer@psi.ch

Abstract

Vascular Endothelial Growth Factors (VEGFs) regulate blood and lymph vessel formation by activating three receptor tyrosine kinases, VEGFR-1, -2, and -3. The extracellular ligand-binding domain of VEGFRs consists of seven immunoglobulin homology domains (Ig-domains) connected by a transmembrane helix to the intracellular tyrosine kinase domain. VEGF family ligands interact with Ig-domains 2 and 3 thereby inducing receptor dimerization. Low resolution structural information and biophysical data show that specific orientation of receptor monomers in active dimers is further controlled by homotypic receptor contacts mediated through membrane-proximal Ig-domains. Ig-domains 4 and 7 are required for properly aligning receptor monomers in active dimers and are thus indispensable for kinase activation. We then developed Designed Ankyrin Repeat Proteins (DARPins) specifically binding to the extracellular receptor domain. DARPins specific for Ig domains 2 and 3 inhibited ligand binding while DARPins specific for Ig domain 4 prevented kinase activation without interfering with dimerization. These data reveal a crucial role for the membrane-proximal receptor domain in ligand-mediated activation of VEGFR-2.

Introduction

Receptor tyrosine kinases (RTKs) accomplish functions in a wide variety of biological processes such as cell growth, differentiation, migration, and survival. Regulation of RTKs is the subject of intense research since it holds promise for the development of new drugs aiming at diseases caused by deregulation of RTK activity. Vascular Endothelial Growth Factors, VEGFs, comprise a family of proteins interacting with three type V RTKs, VEGFR-1 (Flt-1), VEGFR-2 (KDR/Flk-1), and VEGFR-3 (Flt-4) (Pajusola et al., 1992; Terman et al., 1991; Shibuya et al., 1990). VEGFs promote endothelial cell survival, migration, proliferation, and differentiation, and are thus indispensable for blood and lymph vessel formation and homeostasis. In addition, VEGFs regulate endothelial cell permeability and vessel contraction. Like all RTKs, VEGFRs are activated following ligand-induced structural changes in the receptor extracellular domain

(ECD) (Grünewald et al., 2010; Stuttfeld and Ballmer-Hofer, 2009). VEGFR-2 is the major mediator of angiogenic signaling in endothelial cells (Shalaby et al., 1995) and its activity is regulated at multiple levels. We have also shown that receptor dimerization is necessary, but not sufficient, for receptor kinase activation (Dell'Era Dosch and Ballmer-Hofer, 2010). These data establish that specific orientation of receptor monomers in the active dimers is mandatory to instigate transmembrane signaling and kinase activation.

High resolution structures of ligand-receptor complexes of VEGFRs show that Ig-homology domains 2 and 3 comprise the ligand binding site (Wiesmann et al., 1997; Christinger et al., 2004; Leppanen et al., 2010b; Iyer et al., 2010). Our low resolution electron microscopy structure of the full length ECD of VEGFR-2 bound to VEGF showed that ECD domains 4-7 form homotypic receptor contacts (Ruch et al., 2007). This was recently confirmed by a structural model derived from a small angle X-ray scattering (SAXS) analysis (Kisko et al., FASEBJ 2011). Taken together, our data demonstrate that receptor monomers are not only held together by ligand binding to Ig-domains 2 and 3, but by additional homotypic receptor contacts formed by the membrane-proximal part of the ECD.

Here we complement our structural studies by a functional characterization of the role of the individual extracellular Ig-domains in ligand binding (Shinkai et al., 1998) and receptor activation and signaling (Tao et al., 2001; Yang et al., 2010). We further analyzed the function of Ig-homology domains D4-7 in receptor dimerization and activation using a series of receptor ECD mutants expressed in tissue culture cells. Mutation or deletion of D4 and D7 drastically reduced receptor activity. Based on these results we developed new ECD binders, Designed Ankyrin Repeat Proteins (DARPins), specifically interacting with individual Ig-domains. By testing these reagents for inhibition of ligand-stimulated receptor activity we identified several DARPins binding to D2-3 and thereby blocking ligand binding and receptor activation. Most interestingly, DARPins binding to D4 efficiently inhibited receptor activation without interfering receptor dimerization. These new reagents will be useful for *in vivo* studies aiming at imaging or inhibiting VEGFR-2.

Materials and methods

Cloning of VEGFR-2 mutants

The pcDNA5/FRT vector (Invitrogen) was used for the expression of VEGFR-2 mutants in HEK293 and COS-1 cells. The pcDNA5/FRT VEGFR-2 3/5 construct was generated by PCR-subcloning (Geiser et al., 2001). Ig-domain D5 was PCR-amplified from the pcDNA3.1 VEGFR-2 wt construct (in-house) using the primers listed in Table 7-1 and subcloned into the pcDNA5 FRT VEGFR-2 wt plasmid to replace D4. The pcDNA5 FRT VEGFR-2 Δ4 and K868M constructs were kindly provided by Claudia Ruch (in-house).

Mutations R726A, D731, RD/AA, and xD7EF were introduced into the pcDNA5 FRT VEGFR-2 wt construct by PCR-subcloning (Geiser et al., 2001) with primers containing the mutations (Table 7-2).

The pLIB vector derived from Moloney murine leukemia virus was used for the retroviral transduction of PAE cells. The pLIB LN VEGFR-2 and the pVSV-G plasmids were kindly provided by Ralph Graeser (ProQinase GmbH Freiburg, Germany). For generating pLIB LN VEGFR-2 wt, 3/5, R, D, RD, and xD7EF constructs, the sequences were PCR-amplified from the respective constructs in the pcDNA5/FRT vector by simultaneously introducing a SalI restriction site. Primers are listed in Table 7-3. Insert and pLIB LN vector were joined by standard ligation process.

Mutations RRR/AAA, RRRK/AAAS, ED/AA, and EDE/AAA were introduced into both the pcDNA5 FRT VEGFR-2 wt and pLIB LN VEGFR-2 wt constructs by PCR-subcloning (Geiser et al., 2001) with primers containing the mutations (Table 7-3).

Mammalian expression plasmids for recombinant production of VEGFR-2 D7 (aa 663-764) and VEGFR-2 D6-7 (aa 549-764) were generated using PCR-subcloning (Geiser et al., 2001). Ig-domain 7 was PCR-amplified from pcDNA3-VEGFR-2-D7-GCN4 using the forward primer 5'-ATGGAGAGCAAGGTGCTGC-3' and the reverse primer 5'-GTGATGCTGGAAGTAGAGGTTCTCCAAGTTCGTCTTTTCCTGGGC-3'. Ig-domains 6-7 were amplified from pcDNA3-VEGFR-2-D1-7 using the forward primer 5'- CGCCTCTGTGGGTTTGCCTAGGGGTCCTGAAATTACTTTGC-3' and the

reverse   primer   5'-GTGATGCTGGAAGTAGAGGTTCTCCAAGTTCG
TCTTTTCCTGGGC-3'. The PCR-products were then subcloned back into the
templates used for the amplification reaction, thereby deleting Ig-domains 1-5 or
the sequence coding for a GCN4-zipper. VEGFR-2 D1-7 (residue 1-764) was
cloned into the pFASTBAC plasmid (Invitrogen) for expression in Sf21 cells as
described (Brozzo et al., 2011, submitted).

Cell culture

Human embryonic kidney epithelial cells 293 (HEK 293), COS-1 monkey kidney
cells and bovine aortic endothelial cells (BAECs) were grown in Dulbecco's
modified Eagle's medium (DMEM, BioConcept) supplemented with 10% fetal
bovine serum (FBS) or 10% newborne calf serum (NCS) in the case of the
BAECs. Porcine aortic endothelial cells (PAE cells) were maintained in Ham's
F12 medium (BioConcept) containing 10% FBS. Cells were grown in a
humidified atmosphere at 37 °C and 5% CO_2.

Transfection of HEK293 and COS-1 cells

Transfection of HEK293 cells or COS-1 cells with FuGENE (FuGENE HD
Transfection Reagent, Roche) was performed according to manufacturer´s
protocol. For the DNA titration experiments, different amounts of DNA were
used to form the transfection complex.

Generation of stably transfected PAE-cells by retroviral transduction

HEK293 Ampho (5×10^6) cells were plated in 10 cm cell culture dishes and
cultured in DMEM (Sigma) supplemented with 10% FBS. Cells were transfected
with 10 µg pLib LN VEGFR-2 plasmid and 10 µg pVSV-G plasmid by $Ca_3(PO_4)_2$
precipitation. Cells were then transferred to an BL2 laboratory. Medium was
replaced 5 h later with 20 ml of fresh DMEM. Target PAE cells were seeded in
10 cm cell culture dishes in Ham's F12 medium (BioConcept) containing
10% FBS. After 24 h, the supernatant of the transfected HEK293 Ampho cells
was filtered through a 45 µm-nitroacetate filter and added to the PAE cells. To

increase the efficiency of infection, polybrene (Hexadimethrinebromide, Sigma H9268) was added to a final concentration of 4 µg/ml. Fresh DMEM was added to the HEK293 Ampho cells. Infection of PAE cells was repeated the next day. After 48 h, PAE cells were split 1/6 and selected with 1 mg/ml G418. Selection medium was added every 3 days. After 2 weeks, cells were checked for expression.

VEGF receptor activity test

HEK293 (5×10^5) cells were plated into 6 cm cell culture dishes, grown for 24 h in DMEM with 10% FBS, and transfected with $Ca_3(PO_4)_2$ precipitation. Cells were starved overnight in DMEM supplemented with 1% BSA 30 h after transfection. Transfected cells were stimulated with 1.5 nM VEGF-A$_{165}$ for 10 min at 37°C. Cells were rinsed once with ice-cold PBS followed by lysis in 200 µl lysis buffer (50 mM Tris, pH 7.5; 100 mM NaCl; and 0.5% w/v Triton X-100) containing protease inhibitor cocktail (Roche), phosphatase inhibitors (200 µM Na_3VO_4, 10 mM NaF, 10 mM sodium pyrophosphate, 30 mM paranitrophenylphosphate, 80 mM glycerophosphate, and 20 µM phenylarsine oxide), and 10% glycerol. Cell lysates were boiled in Lämmli buffer (20 mM Tris, pH 6.8; 5% SDS; 10% mercaptoethanol; and 0.02% bromophenol blue) and resolved on 8% SDS gels, blotted to PVDF membranes, and immunodecorated with phospho-specific antibody pY1175 or VEGFR-2 specific antibody (Cell Signaling). All experiments were performed in triplicates and immunoblots were quantified by densitometric scanning using the ImageQuant TL software (Molecular Dynamics, GE Healthcare).

Immunocytochemistry

HEK293, COS-1, or stably transfected PAE cells were grown on glass coverslips to a density of approximately 60%. HEK293 and COS-1 cells were transfected with the VEGFR-2 constructs. Cells were fixed with 3.7% formaldehyde in PBS for 10 min at 37°C followed by extensive washing with PBS. Cells were permeabilized with 1% NP40 in PBS for 10 min at RT. The first antibody diluted in PBS was added to the cells for 2 h at room temperature

followed by incubation with fluorescently labeled secondary antibody for 1 h. Samples were washed with PBS before they were embedded in gelvatol (15% gelvatol, 33% glycerol, 0.1% sodium azide). Images were acquired on an Olympus IX81 epifluorescence microscope and processed using 3D deconvolution and spectral unmixing software (Olympus Cell^R).

Sprouting of BAECs

BAECs were cultured in DMEM supplemented with 10% normal calf serum (NCS). A total of 500 cells were used to generate one hanging drop. Hanging drops were incubated upside down at 37 °C. After 24 h, spheroids were collected and pooled by centrifugation (100 rcf, 3 min). On ice, 8 volumes of collagen I stock (BD Biosciences) were mixed with one volume of 10x PBS and 0.023 volumes of 1 N NaOH. Basal medium was added up to ten volumes. Spheroids were resuspended in basal growth medium with inclusion of DARPin (100 nM) and mixed 1:1 with the collagen-containing medium. Spheroids were transferred to a prewarmed 24-well plate (500 µl, 20 spheroids per well) and polymerization was induced by incubation at 37°C for 2 h. Gels were overlaid with 500 µl of normal growth medium supplemented with 1% FCS and VEGF-A$_{165}$ (1.5 nM final concentration) and incubated for 24 h. Spheroids were fixed with 3.7% formaldehyde at 37 °C o/n. After washing with PBS spheroids were stained with Rhodamin labeled Phalloidin (Cell Signaling) and imaged. In the spheroid assay the length and number of sprouts was determined using the Image J software (NIH). Sprouts from two independent experiments were statistically analyzed for each condition.

Production and purification of recombinant proteins

VEGFR-2 ECD was produced and purified as described (Brozzo et al., 2011 submitted). Briefly, Sf21 cells, maintained in serum-free Insect-Express (Lonza) media at 27 °C, were used to produce recombinant virus. When the cells reached a density of 10^6 cells/ml, they were infected with recombinant baculovirus at high multiplicity. Three days after infection, the supernatant was harvested by centrifugation at 900 g, concentrated, and dialyzed against 20 mM

sodium-phosphate buffer pH 7.4 and 500 mM NaCl. The conditioned medium was loaded onto an IMAC column (GE Healthcare). The hexa-histidine tagged (His$_6$) protein was eluted with a gradient from 40-500 mM imidazole and further purified by gel filtration on a Superdex 200HR 10/30 column (GE Healthcare) equilibrated with 25 mM HEPES pH 7.5 containing 150 mM NaCl.

VEGFR-2 D7 and VEGFR-2 D6-7 were produced in transiently transfected HEK293T cells as described (Aricescu et al., 2006). In brief, when cells reached ~90% confluency, the medium was exchanged from DMEM (BioConcept) containing 10% fetal bovine serum to DMEM containing 0.5% fetal bovine serum. The preincubated DNA-polyethylenimine complex (at a 1:1.5 ratio) diluted in serum-free DMEM was added to the cells. Three days after transfection the medium was harvested, cleared by centrifugation, and concentrated. The His$_6$-tagged proteins were purified by IMAC as described above. The buffer was exchanged to 25 mM HEPES pH 7.5, 150 mM NaCl using centrifugal protein concentrators (Sartorius Stedim Biotech).

Size exclusion chromatography coupled multi-angle light scattering (SEC-MALS)

The SEC-MALS experiments were conducted on an Agilent 1100 HPLC-system (Agilent Technologies) with an analytical-grade Superdex 200HR 10/30 column (GE Healthcare) coupled to the Wyatt miniDAWNTristar (Wyatt Technologies). The system was equilibrated in 25 mM HEPES pH 7.5, 150 mM NaCl at 20°C prior to the experiments. For each run 100 µg of VEGFR-2 ECD alone, VEGF-A$_{121}$ alone, VEGFR-2 ECD/VEGF-A$_{121}$ complex, VEGFR-2 ECD/6C8/VEGF-A$_{121}$ complex, and VEGFR-2-ECD/6G9/VEGF-A$_{121}$ were loaded onto the SEC-column. The elution profiles were recorded as UV-absorbance at 280 nm and as the intensity of Rayleigh scattering at three different angles. In the case of VEGFR-2 ECD/6C8/VEGF-A$_{121}$ and VEGFR-2 ECD/6G9/VEGF-A$_{121}$, VEGFR-2 ECD was mixed with the inhibitor at a 1:3 molar ratio and incubated for 60 min at 4°C. VEGF-A$_{121}$ was added to the receptor at a molar ratio of 1:1.1 (receptor:ligand). The ASTRA^{TM} software (Wyatt Technologies) was used to calculate the weight average Molecular masses (Mr).

Ribosome display

Ribosome display was performed by Molecular Partners AG,Schlieren, as described in (Zahnd et al., 2007) and (Binz et al., 2004).

Epitope-mapping ELISA

Epitope-mapping ELISA was performed by Molecular Partners AG, Schlieren, using Surface Plasmon Resonance (ProteOn XPR36, Biorad, Switzerland) (Reference: Dr. Kaspar Binz, Molecular Partners AG, Zürich-Schlieren, Switzerland).

Results

Role of membrane-proximal Ig-homology domains 4 and 7 in receptor activation

In the crystal structure of the c-Kit receptor, two amino acids R381 and E386 in the E-F loop of D4 were identified that form salt bridges mediating homotypic interaction of receptor monomers. Sequence alignment showed that this dimerization motif is conserved among several type III and type V RTKs and is also found in D7 of VEGFR-2. Based on this alignment, we generated a series of VEGFR-2 D7 mutants where parts of or the entire loop containing this dimerization motif were mutated (Fig. 7-1).
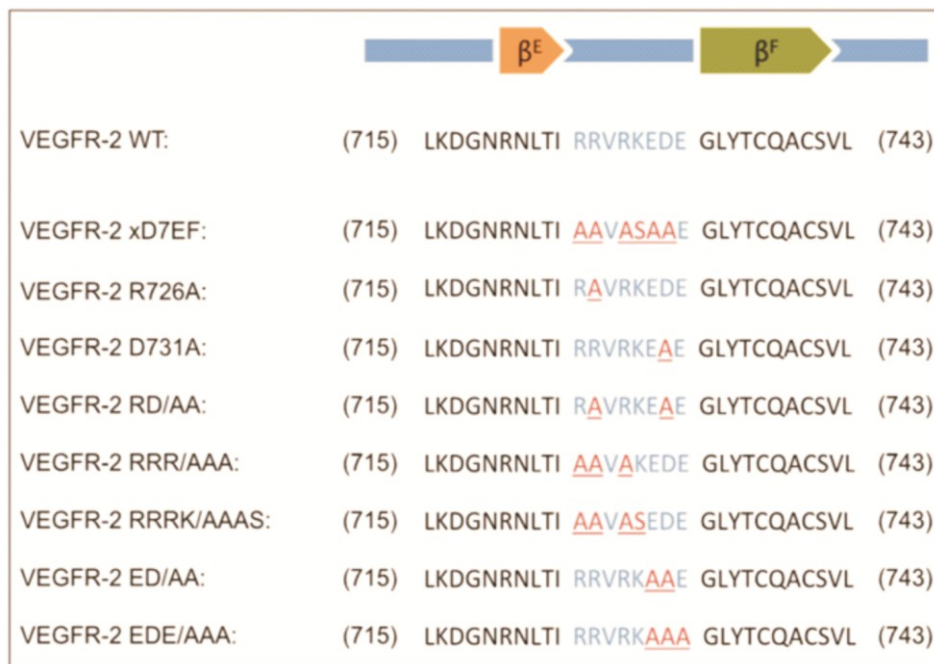
Fig. 7-1: Schematic representation of the βE-βF loop in VEGFR-2 D7 and sequences of generated mutants
Mutated amino acids are indicated in red, wild type amino acids in blue

We transiently expressed these mutant receptors in HEK293 cells and generated stably expressing retrovirus-infected PAE cell lines. To create amphitropic retroviruses, VEGFR-2 constructs were cloned into the pLIB retroviral expression vector providing a ψ+ packaging signal. The packaging cell line HEK293 Ampho expressing the viral gag, pol, and env genes, was transfected with the retroviral expression vector. The viral genomic transcript containing the target gene and a selectable neomycin resistance marker was packaged into infectious virus and subsequently used to infect PAE cells.

Transiently or stably transfected cells were starved, stimulated with VEGF-A$_{165}$ for 10 min, and lysed. Ligand-induced VEGFR-2 activation was determined by immunoblotting with anti-phosphoY1175 and anti-VEGFR-2 antibodies. All mutants except mutant xD7EF, whose phosphorylation was completely blocked, retained some autophosphorylation activity both in stable (Fig. 7-2) and in transiently transfected cells (Fig.7-12). The ratio of phosphorylation normalized to total VEGFR-2 compared to wt (wt value set to 1.0) was: RRRK: 0.49 ± 0.09; RR: 0.53 ± 0.05; R: 0.53 ± 0.13; EDE: 1.55 ± 0.04; ED: 1.07 ± 0.53; D: 1.06 ± 0.67; xD7EF: 0.02.
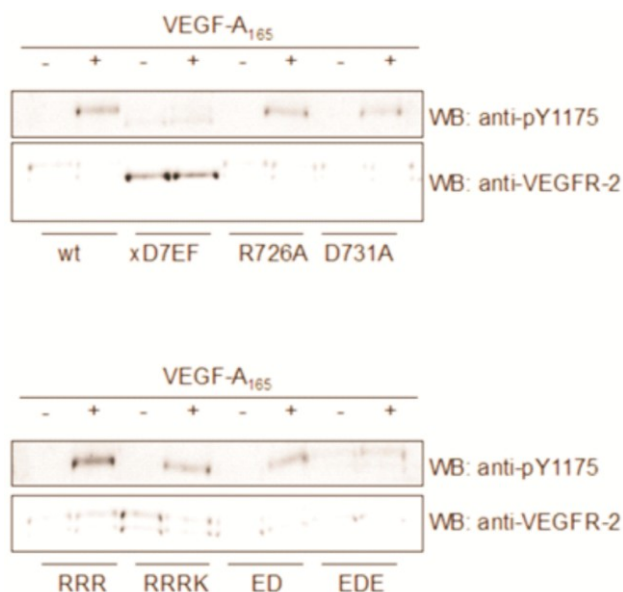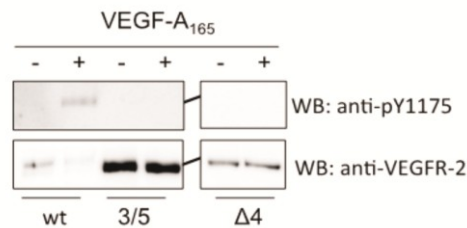
Fig. 7-2: The conserved dimerization motif in D7 is crucial for ligand-induced activation of VEGFR-2
Ligand-induced activation of VEGFR-2 is compromised by mutation of the EF-loop in D7. PAE cells stably expressing the indicated VEGFR-2 mutants were generated by retroviral transduction. Cells were stimulated with 1.5 nM VEGF-A$_{165}$ for 10 min at 37°C. Cell lysates were analzed on immunoblots with phospho-specific antibody pY1175 and anti-VEGFR-2 antibody.

Point mutations of these sites gave rise to partially defective receptors presumably due to compensatory interactions mediated by other charged amino acids in the βE-F loop. Mutation of all charged amino acids in the βE-F loop completely blocked receptor activation in both transiently and stably transfected cell lines and thus showed that D7 interaction plays an essential role in receptor activation. These data show that the homotypic interactions between D7 in receptor dimers revealed in the published VEGFR-2 D7 structure (Yang et al., 2010) are indispensable for receptor activation.

For D4, which may also be involved in receptor dimerization (Ruch et al., 2007) but has not yet been as extensively studied as D7, we generated mutants where the entire domain was either replaced by D5 of VEGFR-1 (3/5) or deleted (Δ4). Mutants were transiently or stably transfected into HEK293 and PAE cells. Both mutants were completely inactive in the phosphorylation assay (Fig. 7-3, Fig. 7-13, and Fig. 7-14). The ratio of phosphorylation normalized to total VEGFR-2 compared to wt (wt value set to 1.0) was: 3/5: 0.06; Delta4: 0.01. These data show that D4 is also required for correctly positioning receptor monomers in active dimers.

Fig. 7-3: Ligand-induced activation of VEGFR-2 is compromised by mutation of D4
PAE cells stably expressing VEGFR-2 3/5 or VEGFR-2 Δ4 were stimulated with 1.5 nM VEGF-A$_{165}$ for 10 min at 37°C. Cell lysates were analyzed on immunoblots with phospho-specific antibody pY1175 and anti-VEGFR-2 antibody.

Isolation and characterization of Ig-homology domain-specific DARPins

To test whether VEGFR-2 activation can be blocked with reagents specifically binding to D4 or D7, we selected DARPins binding to single Ig-domains of the VEGFR-2 ECD. The selected DARPins were verified on recombinant VEGFR-2 ECD protein. A total of 18 DARPins was isolated and their affinities determined by surface plasmon resonance (confidential data, Molecular Partners AG, Schlieren). All DARPins bound the receptor with high affinity with K_ds below 10 nM. To determine the specificity of each DARPin, an ELISA with distinct ECD proteins encompassing various Ig-homology domains was performed. DARPin 6G9 bound to D1-7, D2-3, and D2-4. DARPin 6C8 was shown to be specific for D1-7 and D2-4. DARPin 7H4 bound to D1-7 and D7 (Fig. 7-4). In conclusion, DARPin 6G9 is specific for D2-3, DARPin 6C8 for D4, and DARPin 7H4 for D7.
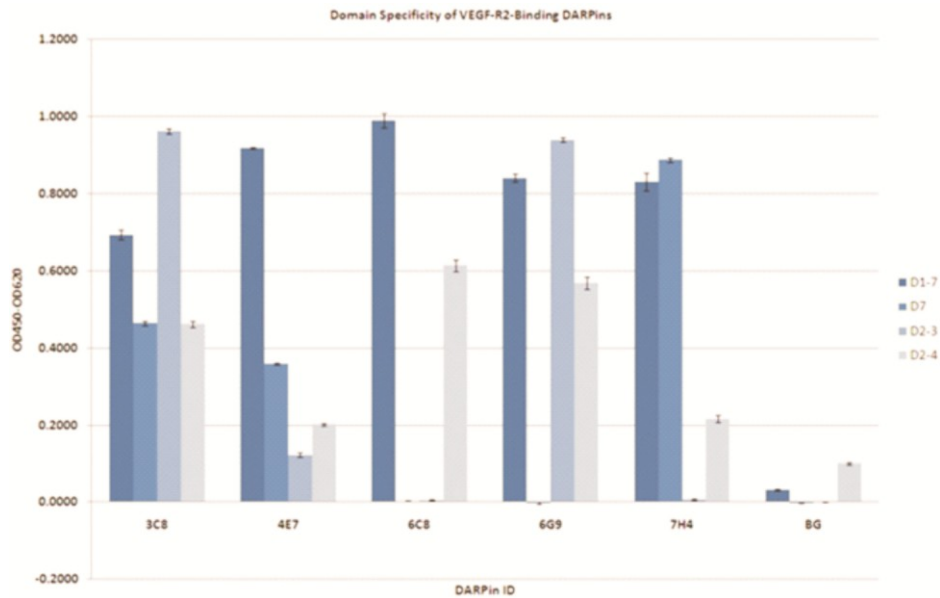
Fig. 7-4: DARPin specificity for VEGFR-2 ECD
Specificity of DARPins 3C8, 4E7, 6C8, 6G9, and 7H4 against VEGFR-2 ECD
was determined by ELISA. Proteins used were: D1-7, D7, D2-3, and D2-4.
BG: background signal.

To verify that these DARPins recognized VEGFR-2 also when expressed on cells, we analyzed receptor binding by fluorescence microscopy using a series of distinct receptor-expressing cells. HEK293 cells expressing wt or mutant VEGFR-2 (VEGFR-2 Δ4) were fixed, permeabilized, and incubated with DARPins. DARPins were labeled with anti-His$_5$ and fluorescently labeled anti-mouse antibodies. DARPins 6C8 and 6G9 both recognized the receptor on the cell surface as well as in intracellular vesicles following ligand stimulation (Fig. 7-5). As expected, 6G9 bound both wt as well as D4 deleted VEGFR-2. In agreement with the epitope-mapping ELISA, 6C8 only recognized wt VEGFR-2, but not D4 deleted receptor. Control are shown in Fig. 7-15.
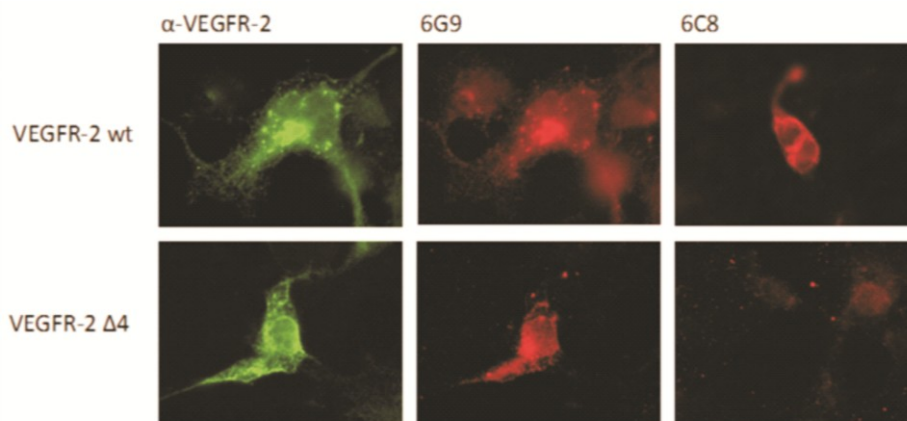
Fig. 7-5: DARPin 6C8 binds to D4 and DARPin 6G9 to D2-3
HEK293 cells were transiently transfected with VEGFR-2wt (top) or Delta4
mutant (bottom), fixed, and stained with DARPin 6G9 or 6C8, anti-His, and
anti-mouse Cy3 antibodies (red). As a control (left panels), cells were stained
with a commercially available anti-VEGFR-2 antibody and an Alexa488 labeled
secondary antibody (green).

Effect of DARPins on ligand-mediated receptor dimerization

Next, we analyzed whether inhibitors of D4 affected ligand-mediated receptor dimerization. Receptor dimerization was determined by MALS using recombinant receptor ECD protein incubated with ligand in the presence or absence of DARPins. DARPin 6G9 specific for D2-3 completely blocked receptor dimerization (Fig. 7-6). Incubation of VEGFR-2-ECD with the DARPin 6G9 showed three peaks with calculated Mrs of 110.6, 28.7, and 18.7 kDa, corresponding to one VEGFR-2 ECD molecule in complex with the DARPin 6G9, unbound VEGF-A$_{121}$, and unbound DARPin 6G9, respectively. On the other hand, the D4-specific DARPin 6C8 incubated with VEGFR-2 ECD and ligand gave rise to two peaks with apparent Mrs of 217.2 and 20.4 kDa. The 20.4 kDa species represented the unbound DARPin 6C8, the 217.2 kDa species consisted of VEGFR-2 ECD bound to the DARPin and to VEGF-A$_{121}$. This is supported by the fact that the elution volume of VEGFR-2 ECD/6C8/VEGF-A$_{121}$ shifts to a lower value compared to VEGFR-2 ECD/VEGF-A$_{121}$ alone. This complex apparently contains one or two DARPin molecules since the theoretical Mrs of the individual components are expected to form complexes of 235 kDa for a 2:2:2 (VEGFR-2/VEGF/DARPin) complex and 217 kDa for a 2:2:1 complex. These results clearly show that DARPin 6G9

inhibits ligand binding of VEGFR-2, whereas DARPin 6C8 does not.
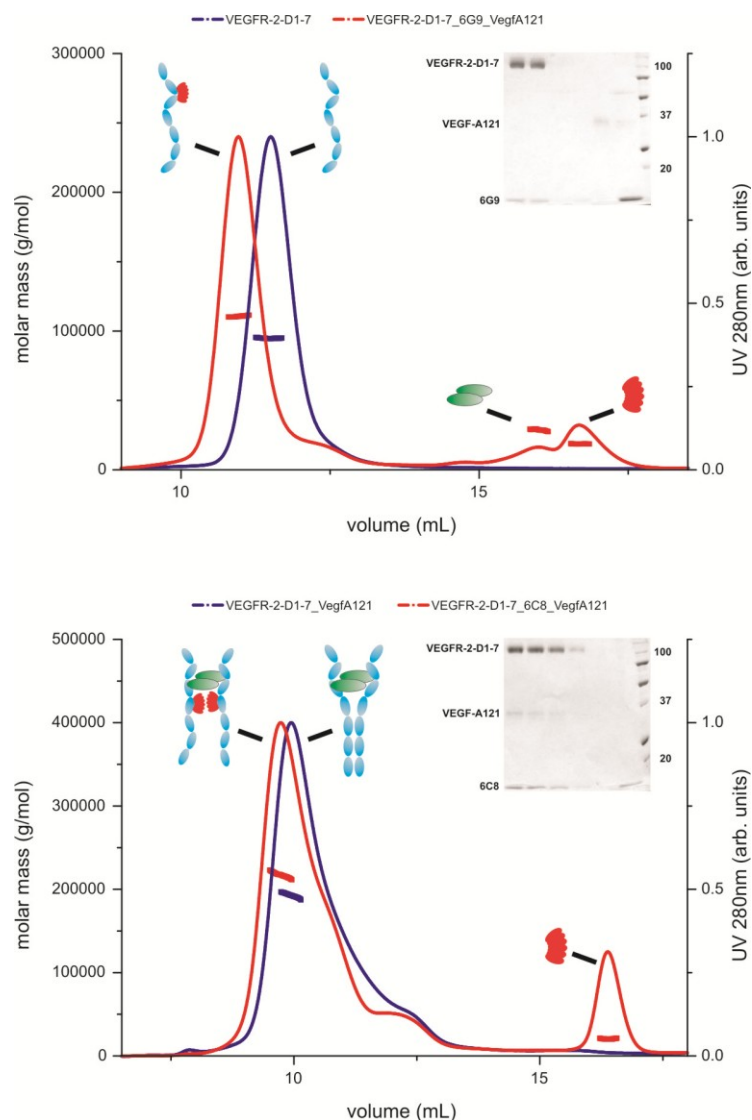
Fig. 7-6: DARPin 6C8 does not interfere with dimerization of VEGFR-2 ECD whereas DARPin 6G9 prevents dimerization in the presence of VEGF
Receptor ECD proteins were incubated with ligand in the presence of DARPin 6G9 (top panel) or 6C8 (bottom panel) an analyzed by MALS. After MALS analysis, proteins were analyzed by SDS-PAGE to confirm their identity.

Functional characterization of receptor-inhibitory DARPins

All 18 DARPins specifically binding to the ECD of VEGFR-2 were tested for their ability to inhibit VEGFR-2 activation (Fig. 7-16). PAE cells expressing VEGFR-2 were incubated with DARPins for 30 min before stimulation with VEGF-A$_{165}$ (Fig. 7-7 top). DARPin 6G9 completely blocked receptor kinase activation. Most interestingly, the D4-specific DARPin 6C8, which does not

block ligand binding, also inhibited receptor phosphorylation. Furthermore, DARPin 6G9 completely inhibited VEGF-A$_{165}$ induced PLCγ1 phosphorylation whereas 6C8 led to a significant decrease in phosphorylation (Fig. 7-7 bottom).
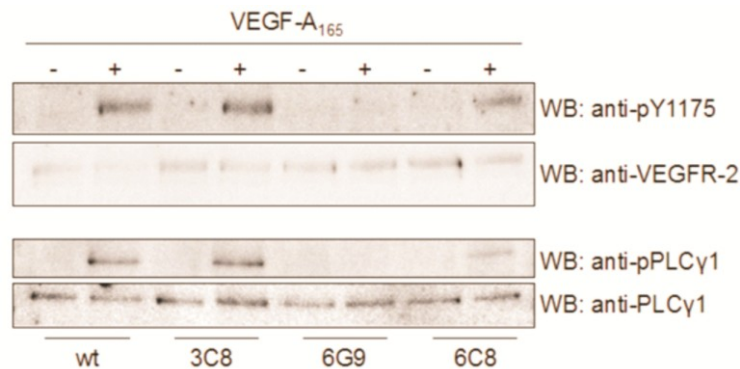
Fig. 7-7: DARPins 6G9 and 6C8 inhibit VEGFR-2 activation and downstream signaling
PAE-VEGFR-2 cells were incubated with 100 nM DARPins for 30 min at 37°C and subsequently stimulated with 1.5 nM VEGF-A$_{165}$ for 10 min at 37°C. Cell lysates were analyzed on immunoblots with phospho-specific antibody pY1175, anti-VEGFR-2 antibody (top) and phospho-PLGγ1, anti-PLCγ1 antibody (bottom).

Immunofluorescence of VEGFR-2 expressing PAE cells incubated with DARPins 30 min prior to stimulation showed that the receptor was retained on the cell surface (Fig. 7-8), while receptor was rapidly internalized in the absence of DARPins following ligand stimulation. Therefore, both DARPin 6C8 and 6G9 blocked internalization of the receptor and were thus functional in live cells.
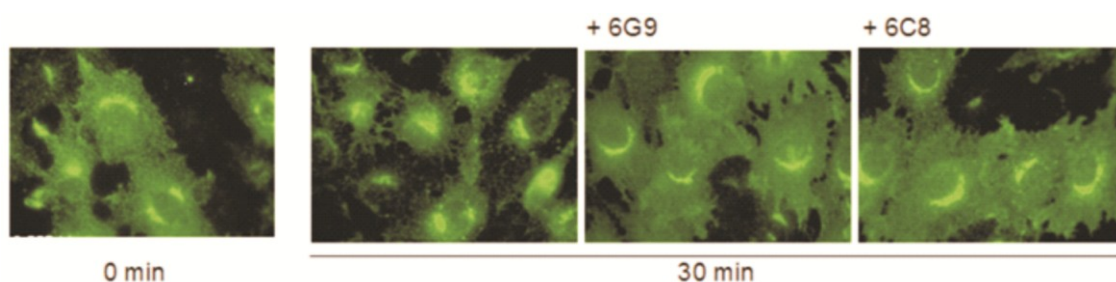
Fig. 7-8: DARPins 6G9 and 6C8 inhibit VEGFR-2 internalization after stimulation
PAE-VEGFR-2 cells were incubated with DARPin 6G9 or 6C8 30 min prior to ligand stimulation. Cells were fixed before stimulation (left panel) or 30 minutes after stimulation with 1.5 nM VEGF-A$_{165}$ (three right panels). Membrane-bound and internalized VEGFR-2 was detected with an anti-VEGFR-2 antibody.

To analyze the effect of the inhibitory DARPins on endothelial cell sprouting, we embedded BAEC spheroids in collagen gels containing 100 nM of DARPins. Both DARPins led to significantly decreased relative sprouting compared to controls which clearly showed VEGF-dependent sprouting (Fig. 7-9).
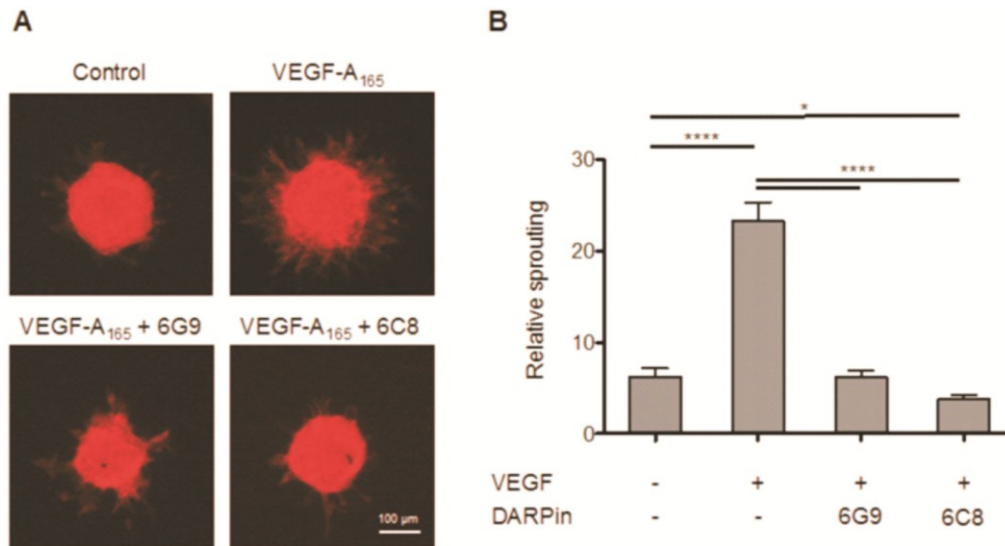
Fig. 7-9: DARPins6G9 and 6C8 inhibit sprouting of BAECs in the EC spheroid sprouting assay
(A) BAECs were embedded in collagen gels containing 100 nM DARPins. Collagen gels were overlaid with 1.5 nM VEGF-A$_{165}$ and sprouting was analyzed after 24h.Cells were fixed and visualized with a TRITC-labeled anti-phalloidin antibody. (B) Relative sprouting (number x average length of sprouts), *p < 0.05, ****p < 0.0001. Error bars represent $\pm$ SEM.

We further monitored endothelial cell sprouting by live-cell imaging. Spheroids stimulated with VEGF-A$_{165}$ were incubated in the presence or absence of DARPin 6C8 and monitored for 16 h. Representative pictures are presented in Fig. 7-10 (without DARPin) and Fig. 7-11 (with DARPin 6C8) and confirmed inhibition of BAEC sprouting by DARPin 6C8.
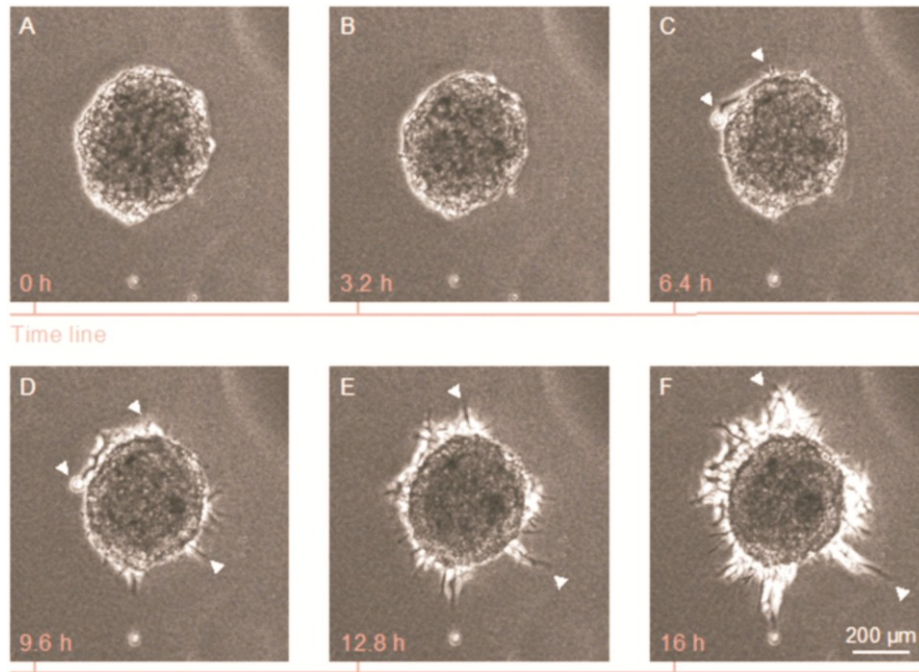
Fig. 7-10: Live cell imaging of endothelial cell sprouting
Sprouting of BAEC spheroids was monitored over 16 h after adding 1.5 nM VEGF-A$_{165}$. Figures show six representative time points (A: 0 h, B: 3.2 h, C: 6.4 h, D: 9.6 h, E: 12.8 h, F: 16 h). Arrowheads indicate emerging and growing sprouts.
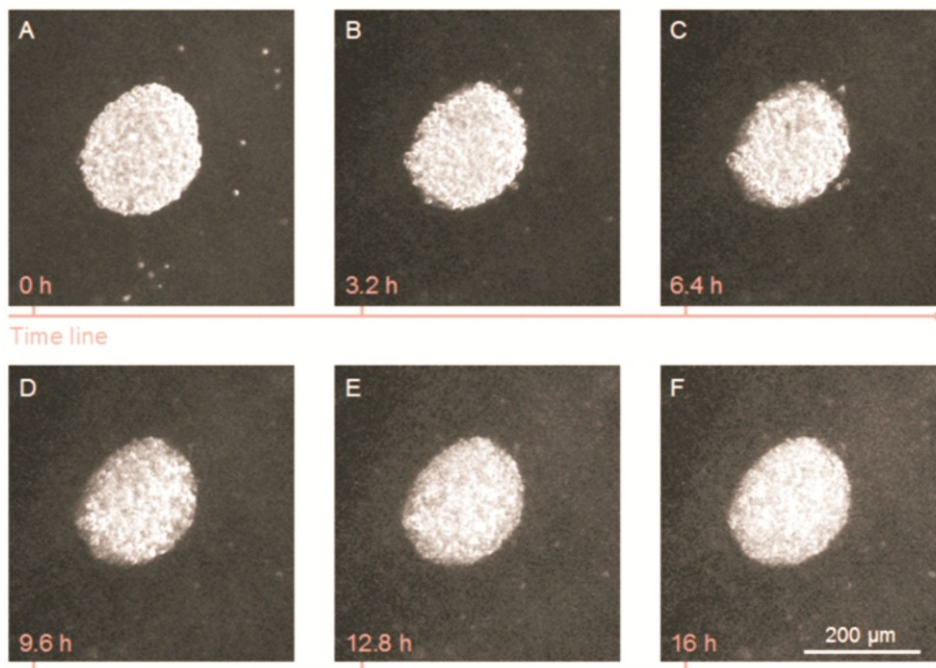
Fig. 7-11 Inhibition of endothelial cell sprouting by DARPin 6C8
Sprouting of BAEC spheroids was monitored over 16 h after VEGF-A$_{165}$ incubation in the presence of DARPin 6C8. Figures show six representative time points (A: 0 h, B: 3.2 h, C: 6.4 h, D: 9.6 h, E: 12.8 h, F: 16 h).

116

Discussion

We demonstrated that homotypic interactions between D7 previously indicated in the VEGFR-2 D7 structure (Yang et al., 2010) are required for receptor activation. These interactions are mediated by a conserved pair of basic and acidic amino acids in the loop linking the βE and βF strands. Point mutation of these residues gave rise to only partially defective receptors presumably due to compensatory interactions mediated by other charged amino acids in the loop. Mutation of the entire βE-F loop, however, completely blocked receptor activation in both transiently and stably transfected cell lines and thus confirmed that D7 interactions play essential critical roles in receptor activation. Our results are partially contradictory to the recently published functional data (Yang et al., 2010). Yang *et al* showed that also point mutations in the βE-F loop are sufficient to strongly compromise the ligand-induced activation of VEGFR-2, whereas our data show this only when the entire loop was mutated. There are various explanations for this observation: the cells used by Yang *et al.* for the generation of stable lines are NIH-3T3 cells, a non-endothelial fibroblast cell line not involved in angiogenesis. We believe that our PAE cells are more representative of endothelial cells and thus better suited for functional analysis. In addition, some of the receptor mutants employed in the study were chimeric receptors composed of the VEGFR-2 ECD linked to the transmembrane and the cytoplasmic domain of PDGFR. The regulation of such chimeric receptors might differ from that of authentic receptors and not adequately reproduce the *in vivo* situation in developing vessels expressing wild type VEGFR receptors.

The EM structure of the ECD of VEGFR-2 published by our laboratory revealed that, in addition to D7, D4 may also be involved in homotypic interactions between ligand-bound receptor dimers (Ruch et al., 2007). In agreement with functional data published earlier on VEGFR-1 (Barleon et al., 1997), we suggest that D4 is also involved in stabilizing receptor dimers. To investigate the role of D4 in receptor activation and in intracellular signaling, we generated PAE cells stably expressing VEGFR-2 mutants where D4 was either deleted (Δ4-mutant) or replaced by D5 of VEGFR-1 (mutant 3/5), a domain which up to now has not been shown to play a specific role in receptor activation. Receptor phosphorylation assays demonstrated that, in contrast to the wild type

VEGFR-2, D4 mutants were not active upon VEGF-A stimulation, showing that this domain is indispensable for receptor activation. By manual sequence alignment, Yang *et al.* identified a conserved amino acid sequence motif, "D/E-x-G", in D4 that was similar to the dimerization motif in D4 of c-Kit and PDGFR (Yang et al., 2010). In their study, mutation of the conserved D392 to A did not lead to receptor inactivation, neither did the mutations of residues E387 and R391, which they claimed to be the non-conserved pair of amino acids with opposite charges responsible for the generation of salt bridges in D4 (similar to R726 and D731 in D7). We propose that similar to the D7 mutants, compensatory interactions are mediated by other charged amino acids in this loop, such as for example E390. Furthermore, D4-D4 interactions might be mediated through different interfaces, as proposed earlier (Yang et al., 2008). This seems highly probable since the sequence identity between D4 of PDGFR-α and VEGFR-2 is only 20% making a definitive conclusion based on sequence alignment nearly impossible. The results obtained with our D4-specific inhibitor clearly confirm the essential role of this domain in receptor activation and show that the membrane-proximal domains of the ECD act as allosteric regulators of VEGFR-2.

We showed earlier that activation of VEGFR-2 requires specific positioning of two intracellular kinase domains relative to each other in response to conformational changes mediated by the TMD (Dell'Era Dosch and Ballmer-Hofer, 2010). Dimerization is hence necessary but not sufficient for receptor activation and downstream signaling, and requires exact positioning of the kinase domains relative to each other in receptor dimers. We now show that such an orientation requires also homotypic interactions between the membrane-proximal Ig-homology domains in the ECD in the full length receptor. As proposed for D4 of the c-Kit receptor (Lemmon and Ferguson, 2007), we suggest that the weak interactions between ECD domains D4 and D7 in dimeric VEGFR-2 are important for proper alignment of receptor monomers and assume that the specific orientation resulting from ECD-mediated dimerization resulting from ligand binding leads to a conformational reorganization of the juxtamembrane domain and subsequently of the intracellular kinase domain, leading to kinase activation.

In this study we provide functional evidence for the findings described in our earlier EM structure of the VEGFR-2 ECD (Ruch et al., 2007). We demonstrate the importance of ECD Ig-homology domains D4 and D7 in VEGFR-2 activation and signaling. As a result, we conclude that interference with these homotypic contacts in the VEGFR-2 ECD might represent a novel and effective way of inhibiting VEGFR-2 signaling. In a next step, we therefore developed specific binders for Ig-homology domains D4 and D7 of the VEGFR-2 ECD. The advantage of such VEGFR-2 inhibitors over those targeting the receptor ligand-binding domain or VEGF itself is that they bind to the receptors with high specificity and are not competed by excessive amounts of ligand secreted by neighboring cells. This allows for distinct targeting of VEGFR-2 and we anticipate less side effects than those reported for the commercially available angiogenesis inhibitors targeting VEGF-A (Mack, 2009). The clinically most advanced VEGFR-2 inhibitor so far is Ramucirumab (IMC-1121) (Spratlin, 2011), a chimeric antibody against the ligand-binding domain of VEGFR-2. Although this antibody is currently in phase III clinical trials (http://clinicaltrials.gov/ct2/results?term=ramucirumab), the nature of its mechanism of action reduces its specificity and affinity. This is due to the fact that the ligand-binding domain of all VEGFRs is relatively conserved and that such molecules actively compete with the natural ligand.

To test our hypothesis *in vitro* we screened DARPin libraries against the entire ECD of VEGFR-2 and identified a number of compounds that targeted the ligand-binding domain of VEGFR-2. As expected, these DARPins completely abolished ligand-induced VEGFR-2 activation and were subsequently used as a positive control in our experiments. Furthermore, we identified DARPin 6C8 which binds specifically to D4 of the ECD. Incubation of cells expressing VEGFR-2 with the inhibitor prior to stimulation with VEGF led to significantly decreased receptor activation. In addition, downstream signaling to PLCγ1 was also compromised and sprouting of multicellular spheroids was significantly reduced. We have thus discovered a potent mechanism of inhibition of VEGFR-2 activation which is independent of natural ligand concentration.

To further define the binding mode of this inhibtor, we investigated the dimerization status of ECD proteins in the presence of DARPin 6C8. As

expected, the DARPin still enabled ligand binding. More importantly, 6C8 did not interfere with receptor dimerization. This confirms that homotypic interactions in the ECD are dispensable for receptor dimerization as shown for RTKs such as c-Kit (Yuzawa et al., 2007), PDGFR (Yang et al., 2008), and VEGFR-2 (Yang et al., 2010), but dimerization itself is not sufficient for activation of VEGFR-2 (Dell'Era Dosch and Ballmer-Hofer, 2010).

Our inhibitor apparently suppresses VEGF-mediated receptor activation and downstream signaling by interfering with the correct three dimensional organization of receptor monomers in active dimers. This is a novel approach of receptor inhibition. The only related inhibitor in clinical trials so far is the dimerization blocking inhibitor Pertuzumab, an antibody against ErbB2 (Franklin et al., 2004; Badache and Hynes, 2004). Pertuzumab blocks ErbB2 heterodimerization with other members of the ErbB family. At the time of writing, Tvorogov et al. reported a monoclonal antibody against D5 of VEGFR-3 which, by inhibiting VEGFR-2/VEGFR-3 heterodimerization, suppresses signal transduction, migration, and sprouting of microvascular endothelial cells (Tvorogov et al., 2010). In addition, Kendrew et al. generated a human antibody in a Xenomouse which binds to D4-7 of VEGFR-2 and suppresses VEGFR-2 activation (Kendrew et al., 2011). However, they did not demonstrate the antibody's mode of action and did not investigate its binding stoichiometry and epitope.

In summary, we have identified a high affinity inhibitor specific for D4 of VEGFR-2 that shows exquisite binding specificity for this receptor and functions independently from ligand binding. Potent high affinity inhibitors targeting D4 of VEGFR-2 ECD could in the future be employed in clinical applications such as tumor vasculature imaging or anti-angiogenic treatment in diseases such as cancer or macular degeneration.

Supplementary Information
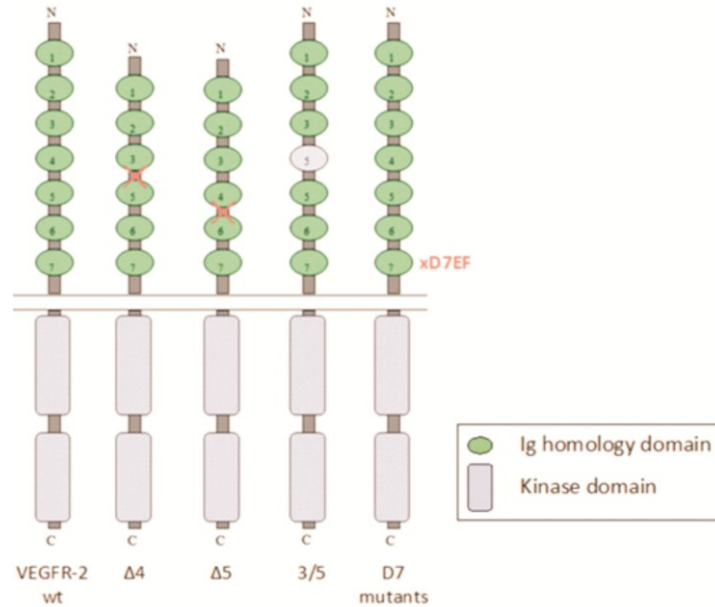
Fig. 7-12: Schematic representation of VEGFR-2 mutants.
Green spheres represent the Ig-homology domains in the ECD of VEGFR-2.
Shown are VEGFR-2 wt, VEGFR-2 Delta4, VEGFR-2 Delta5, VEGFR-2 3/5,
and VEGFR-2 D7 mutants.
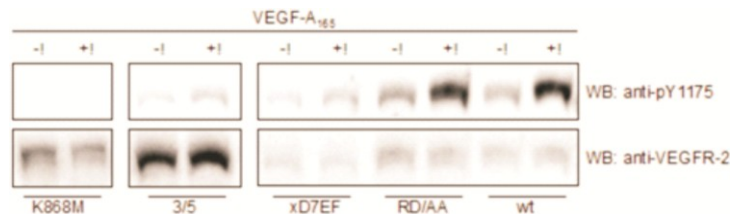
Fig. 7-13: Ligand-induced activation of VEGFR-2 is compromised by
mutation of D4 and D7
HEK293 cells were transiently transfected with the indicated VEGFR-2 mutants
and stimulated with 1.5 nM VEGF-A165 for 10 min at 37°C. Cell lysates were
analysed on immunoblots with phospho-specific antibody pY1175 and
anti-VEGFR-2 antibody.
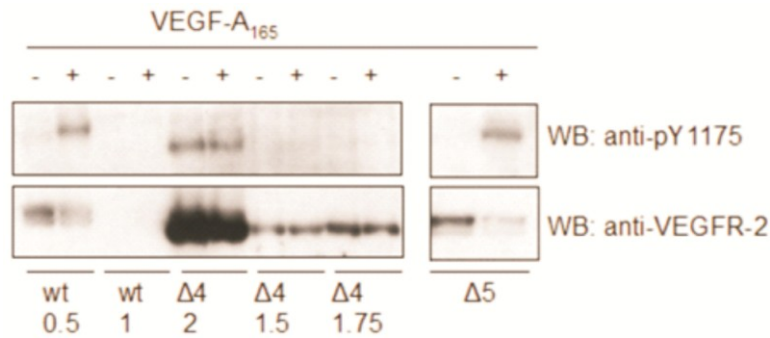
Fig. 7-14: Ligand-induced activation of VEGFR-2 is compromised by mutation of D4.
We adjusted the expression level of the VEGFR-2 mutant constructs by titrating the amount of DNA used for transfection. HEK293 cells were transiently transfected with the indicated VEGFR-2 mutants. Amount of DNA used for transfection was varied to obtain a comparable expression level between the mutants. Amounts were 0.5 and 1 µg for the wt construct and 2, 1.5, 1.75 µg for Delta 4. Cells were stimulated with 1.5 nM VEGF-A165 for 10 min at 37°C. Cell lysates were analysed on immunoblots with phospho-specific antibody pY1175 and anti-VEGFR-2 antibody.
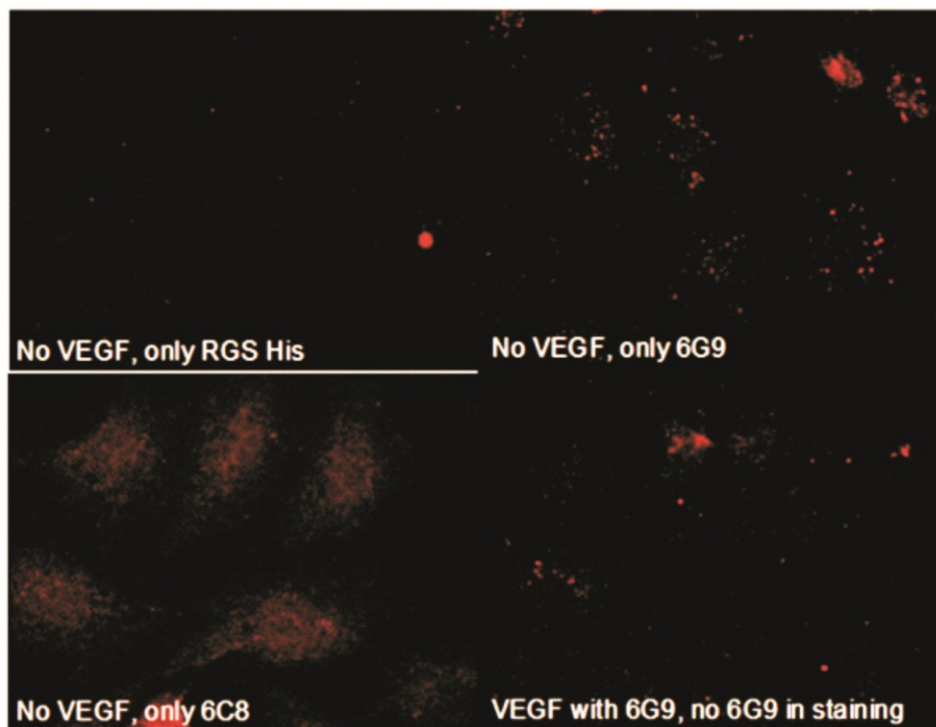
Fig. 7-15: Stainings of VEGFR-2 on cells with DARPins are specific.
Control stainings were performed. DARPins and antibodies used are indicated in white writing on the figure.
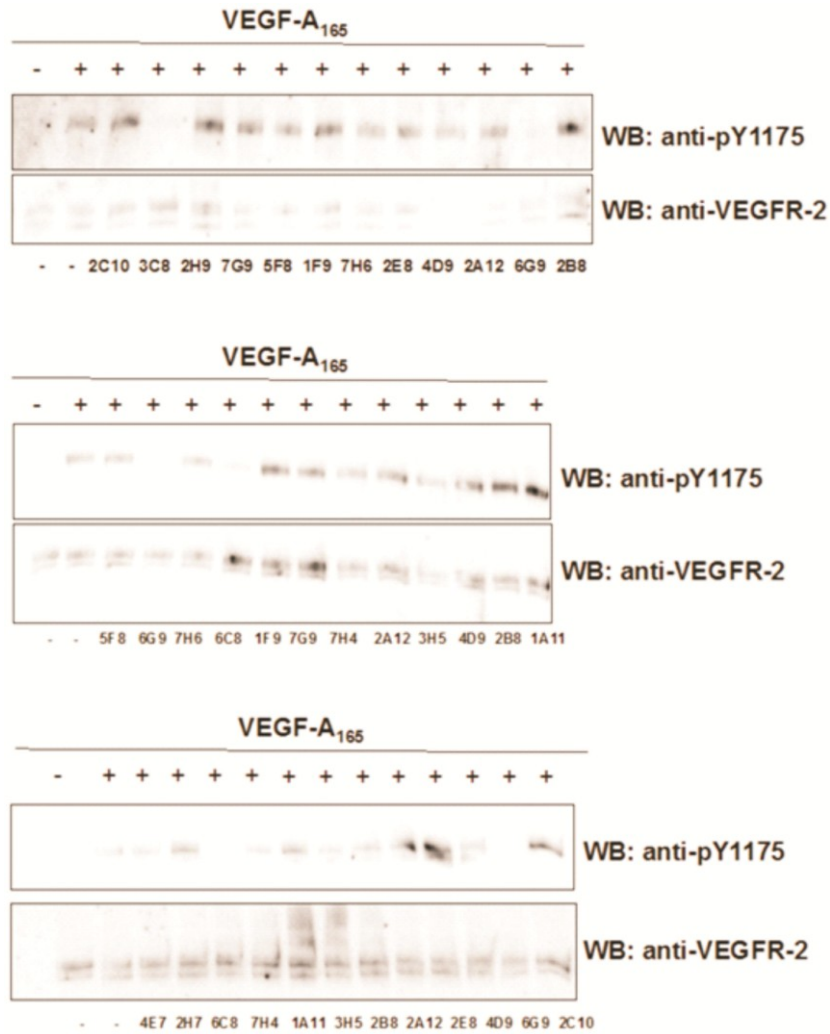
Fig. 7-16: DARPins3C8, 6G9, and 6C8 inhibit VEGFR-2 activation.
*PAE-VEGFR-2 cells were incubated with 100 nMDARPins for 30 min at 37°C
and stimulated with 1.5 nM VEGF-A165 for 10 min at 37°C. Cell lysates were
analysed by immunoblot with phospho-specific antibody pY1175 and
anti-VEGFR-2 antibody.*

Table 7-1: Primers used for cloning VEGFR-2 3/5 mutant.

Construct	Orientation	5 – 3 sequence
pcDNA5 FRT VEGFR-2 3/5	forward	5´GCA CAT TTG TCA GGG TCC ATG AAA AAC CAG ACC CGG CTC TCT ACC 3´
	reverse	5´GAT TAG AGA TTT CTC ACC AAT CTG GGG TGG CAC ATC TGT GAT ATA AAA GC 3´

Table 7-2: Primers used for cloning VEGFR-2 domain 7 mutants.
*The codons introducing the mutations are underlined.*

Construct	Orientation	5 – 3 sequence
pcDNA5 FRT VR2 R	forward	5´CCGGAACCTCACTATCCGCGCAGTGAGG AAGGAGGACGAAGG3´
pcDNA5 FRT VR2 D	forward	5´AGTGAGGAAGGAGGCCGAAGGCCTCTA CACCTGCC3´
pcDNA5 FRT VR2 xD7EF	forward	5´GGGAACCGGAACCTCACTATCGCCGCAG TGGCCTCAGCCGCCGAAGGCCTCTACACC TGCCAG3´
pcDNA5 FRT VR2 RR	forward	5´GGG AAC CGG AAC CTC ACT ATC <u>GCCGCA</u> GTG <u>GCC</u> AAG GAG GAC GAA GGC CTC TAC ACC TGC CAG3´
pcDNA5 FRT VR2 RRR	forward	5´GGG AAC CGG AAC CTC ACT ATC <u>GCCGCA</u> GTG <u>GCCTCA</u> GAG GAC GAA GGC CTC TAC ACC TGC CAG3´
pcDNA5 FRT VR2 ED	forward	5´GGG AAC CGG AAC CTC ACT ATC CGC AGA GTG AGG AAG <u>GCCGCC</u> GAA GGC CTC TAC ACC TGC CAG3´
pcDNA5 FRT VR2 EDE	forward	5´GGG AAC CGG AAC CTC ACT ATC CGC AGA GTG AGG AAG <u>GCCGCCGCC</u> GGC CTC TAC ACC TGC CAG3´
Reverse primer (for all above)	reverse	5´ACA GGG ATT GCT CCA ACG TAG 3´

124

Table 7-3: Primers used for cloning pLIB constructs.
The codons introducing the restriction sites or the mutations are underlined.

Construct	Orientation	5 – 3 sequence
pLIB VEGFR-2 wt	forward(SalI restriction site underlined)	5´GAT C<u>GT CGA C</u>AT GGA GAG CAA GGT GCT GCT GGC CG 3´
	reverse(NotI restriction site underlined)	5´TAG ACT CGA <u>GCG GCC GCT</u> CAC AGA TCC TCT TC 3´
pLIB VEGFR-23/5	forward/reverse as first entry	
pLIB VEGFR-2 K868M	forward/reverse as first entry	
pLIB VEGFR-2 R	forward/reverse as first entry	
pLIB VEGFR-2 D	forward/reverse as first entry	
pLIB VEGFR-2 RD	forward/reverse as first entry	
pLIB VEGFR-2 RR	forward	5´GGG AAC CGG AAC CTC ACT ATC <u>GCCGCA</u> GTG <u>GCC</u> AAG GAG GAC GAA GGC CTC TAC ACC TGC CAG 3´
pLIB VEGFR-2 RRR	forward	5´GGG AAC CGG AAC CTC ACT ATC <u>GCCGCA</u> GTG <u>GCCTCA</u> GAG GAC GAA GGC CTC TAC ACC TGC CAG 3´
pLIB VEGFR-2 ED	forward	5´GGG AAC CGG AAC CTC ACT ATC CGC AGA GTG AGG AAG <u>GCCGCC</u> GAA GGC CTC TAC ACC TGC CAG 3´
pLIB VEGFR-2 EDE	forward	5´GGG AAC CGG AAC CTC ACT ATC CGC AGA GTG AGG AAG <u>GCCGCCGCC</u> GGC CTC TAC ACC TGC CAG 3´
Reverse primer (for the four constructs: RR, RRR, ED, EDE)	reverse	5´ACA GGG ATT GCT CCA ACG TAG 3´

8   Conclusion

VEGFRs are the major regulators of angiogenic and lymphatic development. In addition, VEGFR signaling associated with pathological angiogenesis is involved in a number of pathological conditions such as in cancer and in various ischemic and inflammatory diseases (Carmeliet and Jain, 2000). Hence, structural studies of this receptor system are expected to further contribute to elucidate the molecular mechanism underlying receptor activation and to identify new target sites on the receptor for the development of new inhibitory drugs. During this project, I showed that binding of individual VEGFR-1 ligands gave rise to conformationally similar ligand/VEGFR-1 ECD complexes. The complexes are characterized by heterotypic ligand/receptor and homotypic receptor/receptor interactions in the membrane proximal Ig-homology domains, as reported for VEGFR-2 and type III RTKs (Ruch et al., 2007; Yang et al., 2010; Yuzawa et al., 2007; Yang et al., 2008). Furthermore, this is the first study addressing the thermodynamic contribution of individual Ig-homology domains of VEGFR-1 to ligand binding. My data showed that the presence of VEGFR-1 D4-7 increases ligand binding affinity due to enthalpic contributions. Surprisingly, I discovered that Ig-homology domain 1 blocks PlGF-1 binding to VEGFR-1 D1-3, but not to D1-7. However, the mechanism explaining this phenomenon remains unclear.

In a second project, we aimed at inhibiting VEGFR-2 signaling by targeting the homotypic receptor/receptor interactions that are formed upon ligand binding. We showed that a DARPin binding to Ig-homology domain 4 leads to decreased VEGFR-2 phosphorylation without preventing the formation of the VEGF-A/VEGFR-2 complex. This inhibitor also affected downstream signaling to PLCγ1 and inhibited sprout formation of endothelial cell spheroids. In this study we thus describe a new way to inhibit VEGFR-2 that may complement other treatments such as receptor inactivation with low Mr inhibitors binding to the kinase domain and may improve the efficiency of anti-angiogenic therapy.

8.1   Therapeutic potential of targeting VEGFR ECD

Several drugs targeting VEGF-mediated pathological angiogenesis have been developed so far including small molecule kinase inhibitors, a VEGF-trap, and antibodies against VEGF or VEGFR-2. Here we describe a new mechanism to inhibit VEGFR-2 signaling. The identified DARPin binds to the receptor without interfering with ligand binding and does not prevent receptor ligand complex formation that is needed for kinase activation. At the time of writing, similar approaches were published for VEGFR-2 and VEGFR-3 using antibodies (Kendrew et al., 2011; Tvorogov et al., 2010).

A number of studies on type III and V RTKs highlighted the importance of low affinity homotypic interactions in the ECD for receptor activation. In c-Kit, PDGFRs, and VEGFRs, receptor dimerization is not sufficient for kinase activation, in addition the kinase domains need to be positioned in a specific orientation for full activity. Thus, the described interactions serve as valuable targets and may lead to the development of inhibitors interfering with RTK signaling, even though such inhibitors may not fully prevent receptor phosphorylation.

The fact that ligand binding to the receptor is not affected by such inhibitors is a clear advantage over other therapeutic approaches. First of all, only signaling pathways driven by the targeted receptor would be blocked. Drugs that are used in therapy targeting VEGF itself block all VEGF mediated functions, in particular all functions mediated through VEGFR-1 and -2. Furthermore, kinase inhibitors display additional off-target effects by blocking additional cellular kinases (Ivy et al., 2009). Based on the discovery of soluble VEGFR-1 and VEGFR-2 variants in humans, additional mechanisms to regulate the VEGF concentration have been proposed (Kendall and Thomas, 1993; Ebos et al., 2004). These soluble receptors sequester freely diffusable VEGF thereby spatially regulating the VEGF concentration. In contrast to molecules that prevent ligand binding such as Ramucirumab (IMC-1121), the identified DARPin would not interfere with this additional level of VEGF regulation (Spratlin, 2011). Furthermore, ligand binding blocking agents are susceptible to increased ligand concentrations due to competition for the same binding site. At high ligand

concentrations such agents are less effective, as described for a VEGFR-3 ligand blocking antibody (Tvorogov et al., 2010). Tvorogov and colleagues therefore showed that combined application of the ligand binding blocking antibody and an antibody against Ig-homology domain 5 displayed the most prominent effect on endothelial and lymphatic cell sprouting. The identified DARPin against Ig-homology domain 4 of VEGFR-2 may complement existing anti-angiogenic therapies and enhance the efficiency of the treatment.

Although DARPin 6C8 blocked biological functions of VEGFR-2 such as endothelial cell sprouting, residual receptor phosphorylation was still observed. This means that distinct signaling pathways are still activated by membrane localized VEGFR-2. However, signaling pathways that require receptor internalization or coreceptor binding might be blocked by the presence of our allosteric inhibitors. Hence, these new allosteric inhibitors display biased antagonistic signaling, i.e. not all signaling pathways are affected by the inhibitor.

8.2 Outlook

The final aim of our study is to understand the molecular mechanism underlying VEGFR activation. In addition, the question remains how different ligands lead to distinct patterns of receptor tyrosine phosphorylation and activation of downstream signaling pathways. A crystal structure of any VEGFR ectodomain alone as well as in complex with one of the ligands may elucidate the molecular basis of binding specificity and receptor activation. Including VEGFR ECDs from other organisms in future crystallization screens may be required to get better diffracting crystals. In addition, inhibitors such as scFvs or DARPins can be raised against VEGFR-1 ECD and be added in crystallization screens to promote crystal growth. To date, all available crystal structures of VEGFs only reveal the structure of the folded core unit. However, the C-terminal tail plays an important role in coreceptor binding, which is known to further modulate signal output (Cébe-Suarez et al., 2006; Cebe-Suarez et al., 2008). Thus, structural data of a VEGF/VEGFR/Neuropilin complex would help to understand how coreceptors influence the overall topology of the VEGF/VEGFR complex. In

addition, low resolution structural data of the full length VEGFR may further contribute to dissect the molecular interactions involved in the process of receptor activation, from ligand binding to the ectodomain to proper positioning and activation of the intracellular kinase domain.

We showed that targeting the Ig-homology domain 4 of VEGFR-2 effectively inhibited receptor activation and endothelial cell sprouting *in vitro*. In order to characterize its therapeutic potential, data for mouse animal models are required. Therefore, cross-reactivity of DARPin 6C8 with mouse VEGFR-2 has to be tested. In case mouse VEGFR-2 can be targeted by our DARPins, the application of the inhibitors to treat mouse tumor models might be assessed. Hereby, the application of the DARPin alone or in combination with other VEGF or VEGFR-2 targeting agents can be characterized. *In vivo* data from mouse tumor models may then show whether a DARPin targeting Ig-homology domain 4 of VEGFR-2 is applicable in anti-cancer therapy.

Furthermore, the described DARPins can be used in crystallization experiments of VEGFR-2 ECD protein. The addition of DARPins to promote crystallization of difficult targets has been successfully used (Sennhauser and Grutter, 2008). In addition, a crystal structure of VEGFR-2 ECD in complex with DARPin 6C8 may explain the mode of inhibition.

9   Appendix

Table A-1:   Primers   used   for   cloning   the   VEGFR-1   and   VEGFR-2 expression plasmids

| Construct	Primer sequences	Primer name
pcDNA3-VEGFR-2 D7-GCN4	for: CCGCCTCTGTGGGTTTGCCTGAGCGTGTGGCACCCACGAT rev: GGAGCGAACGACCTACACCGAACTGAGATACCTACAGCG	ES04 847
pcDNA3-VEGFR-2 D7	for: ATGGAGAGCAAGGTGCTGC rev: GTGATGCTGGAAGTAGAGGTTCTCCAAGTTCGTCTTTTCCTGGGC	ES12 CR5
pcDNA3-VEGFR-2 D6	for: CGCCTCTGTGGGTTTGCCTAGGGGTCCTGAAATTACTTTGC rev: GGTGATGCTGGAAGTAGAGGTTCTCGGGTGCCACACGCTCTAGG	ES25 ES26
pcDNA3-VEGFR-2 D6-7	for: CGCCTCTGTGGGTTTGCCTAGGGGTCCTGAAATTACTTTGC rev: GTGATGCTGGAAGTAGAGGTTCTCCAAGTTCGTCTTTTCCTGGGC	ES25 CR5
pcDNA3-VEGFR-2 2xD4-GSL	for: GCTAGGTACCCCTTTTGTTGCTTTTGGAAGTGG rev: GCTATCCGGAACCGCCTCCACCAATCTGGGGTGGGACA TACACAAC	ES8F ES8R
pcDNA3-VEGFR-2 2xD7-GSL	for: GCTAGGTACCCCCACGATCACAGGAAACCTGG rev: GCTATCCGGAACCGCCTCCACCGGCACCTTCTATTATGAAAAATG CCTCC	ES7F ES7R

pcDNA3-VEGFR-2 D6-7-GSL	for: CCGCCTCTGTGGGTTTGCCTGGTACCATTACTTTGCAACCTGACATGCAGC
	rev: GATGGTGATGCTGGAAGTAGAGGTTCTCCGAATTCGTGGCACCTT
	     CTATTATGAAAAATGCCTCC
	GS-linker: CAGTCCTAGAGCGTGTGGCAGGTGGAGGCGGTTCAGGCGG
	Kpn2I-site: GTGTGGCAGGTGGAGGCGGTTCCGGAGGAGGTGGCTCTGG
	     CGGTGG
		ES1F
		
		ES1R
		
		ES2F
		ES3F

pcDNA3-VEGFR-2 D6-4-GSL	for: GCTAGGATCCCCTTTTGTTGCTTTTGGAAGTGG rev: GCTAGAATTCGTAATCTGGGGTGGGACATACACAAC	ES9F ES9R
pcDNA3-VEGFR-2 xxx-N704Q	for: GATCATGTGGTTTAAAGATCAAGAGACCCTTGTAGAAGACTCAGGC rev: GGAGCGAACGACCTACACCGAACTGAGATACCTACAGCG	ES23 847
pcDNA3-VEGFR-2 xxx-N721Q	for: GAAGGATGGGAACCGGCAACTCACTATCCGCAGAGTGAGG rev: GGAGCGAACGACCTACACCGAACTGAGATACCTACAGCG	ES24 847
pcDNA3-VEGFR-2 xxx-N675Q	for: CACGATCACAGGAAACCTGGAGCAACAGACGACAAGTATTGGGGAAAG rev: GTGATGCTGGAAGTAGAGGTTCTCCAAGTTCGTCTTTTCCTGGGC	ES37 CR5
pcDNA3-VEGFR-2 xxx-N631Q	for: ATGACATTTTGATCATGGAGCTTAAGCAAGCATCCTTGCAGGACCAAG rev: GTGATGCTGGAAGTAGAGGTTCTCCAAGTTCGTCTTTTCCTGGGC	ES36 CR5
pcDNA3-VEGFR-2	for: AAGAACTTGGATACTCTTTGGAAATTGCAAGCCACCATGTTCTCTC AAAGCACAAATGACATTTTGATCATG	ES35

xxx-N613/619Q	rev: GTGATGCTGGAAGTAGAGGTTCTCCAAGTTCGTCTTTTCCTGGGC	CR5
pcDNA3-VEGFR-2 xxx-N580Q	for: CACTGCAGACAGATCTACGTTTGAGCAACTCACATGGTACAAGCTTGGC rev: GTGATGCTGGAAGTAGAGGTTCTCCAAGTTCGTCTTTTCCTGGGC	ES34 CR5
pPICZαA-VEGFR-2 D7-GCN4	for: GCTGAATTCGAGCGTGTGGCACCCACG rev: GATGGTCGACGGATCCACGCGGAACCAGACCAACCAGTTTTTTCA GACGAGC	ES21 ES22

pColdI-VEGFR-2 D7	for: CAAAGTGCATCATCATCATCATCATCTGGTTCCGCGTGGATCCGA
	   GCGTGTGGCACCCACG
	rev: GATTCTGTGCTTTTAAGCAGAGATTACCTACAAGTTCGTCTTTTCCT
	   GGGC
		ES29
		
		ES30

pFLmb-VEGFR-1 D1-7-N32	for: CCAGAGCCGCATCTCCTGAACTGAGTTTAAAAGGCAC rev: TGTCTGCCCTCGATTCCTTGAACAGTGAGGTATGCTG	ES47 ES42
pFLmb-VEGFR-1 D1-6-N32	for: CCAGAGCCGCATCTCCTGAACTGAGTTTAAAAGGCAC rev: TGTCTGCCCTCGATTGCTTCCTGATCTCTGATTGTAATTTC	ES47 ES46
pFLmb-VEGFR-1 D1-5-N32	for: CCAGAGCCGCATCTCCTGAACTGAGTTTAAAAGGCAC rev: TGTCTGCCCTCGATATCTGTGATATAAAAGCTTATGTTTCTTC	ES47 ES45
pFLmb-VEGFR-1 D1-4-N32	for: CCAGAGCCGCATCTCCTGAACTGAGTTTAAAAGGCAC rev: TGTCTGCCCTCGATGGCAGTGAGGTTTTTAAACACATTTG	ES47 ES44
pFLmb-VEGFR-1 D1-3-N32	for: CCAGAGCCGCATCTCCTGAACTGAGTTTAAAAGGCAC rev: TGTCTGCCCTCGATTTTATCATATATATGCACTGAGGTGTTAAC	ES47 ES40
pFLmb-VEGFR-1 D1-7-N27	for: CCAGAGCCGCATCTTCAAAATTAAAAGATCCTGAACTGAG rev: TGTCTGCCCTCGATTCCTTGAACAGTGAGGTATGCTG	ES39 ES42
pFLmb-VEGFR-1 D1-6-N27	for: CCAGAGCCGCATCTTCAAAATTAAAAGATCCTGAACTGAG rev: TGTCTGCCCTCGATTGCTTCCTGATCTCTGATTGTAATTTC	ES39 ES46
pFLmb-VEGFR-1 D1-5-N27	for: CCAGAGCCGCATCTTCAAAATTAAAAGATCCTGAACTGAG rev: TGTCTGCCCTCGATATCTGTGATATAAAAGCTTATGTTTCTTC	ES39 ES45
pFLmb-VEGFR-1 D1-4-N27	for: CCAGAGCCGCATCTTCAAAATTAAAAGATCCTGAACTGAG rev: TGTCTGCCCTCGATGGCAGTGAGGTTTTTAAACACATTTG	ES39 ES44
pFLmb-VEGFR-1 D1-3-N27	for: CCAGAGCCGCATCTTCAAAATTAAAAGATCCTGAACTGAG rev: TGTCTGCCCTCGATTTTATCATATATATGCACTGAGGTGTTAAC	ES39 ES40
pFLmb-VEGFR-1 D2-7	for: CCAGAGCCGCATCTGGTAGACCTTTCGTAGAGATGTACAG rev: TGTCTGCCCTCGATTCCTTGAACAGTGAGGTATGCTG	ES43 ES42
pFLmb-VEGFR-1 D2-6	for: CCAGAGCCGCATCTGGTAGACCTTTCGTAGAGATGTACAG rev: TGTCTGCCCTCGATTGCTTCCTGATCTCTGATTGTAATTTC	ES43 ES46
pFLmb-VEGFR-1 D2-5	for: CCAGAGCCGCATCTGGTAGACCTTTCGTAGAGATGTACAG rev: TGTCTGCCCTCGATATCTGTGATATAAAAGCTTATGTTTCTTC	ES43 ES45
pFLmb-VEGFR-1	for: CCAGAGCCGCATCTGGTAGACCTTTCGTAGAGATGTACAG rev: TGTCTGCCCTCGATGGCAGTGAGGTTTTTAAACACATTTG	ES43 ES44

D2-4		
pFLmb- VEGFR-1 D2-3	for: CCAGAGCCGCATCTGGTAGACCTTTCGTAGAGATGTACAG rev: TGTCTGCCCTCGATTTTATCATATATATGCACTGAGGTGTTAAC	ES43 ES40
pFLmb- VEGFR-1 D4-7	for: CCAGAGCCGCATCTGTGCTTGAAACCGTAGCTGG rev: TGTCTGCCCTCGATTCCTTGAACAGTGAGGTATGCTG	ES41 ES42
pFLmb- VEGFR-1 D4-6	for: CCAGAGCCGCATCTGTGCTTGAAACCGTAGCTGG rev: TGTCTGCCCTCGATTGCTTCCTGATCTCTGATTGTAATTTC	ES41 ES46
pFLmb- VEGFR-1 D4-5	for: CCAGAGCCGCATCTGTGCTTGAAACCGTAGCTGG rev: TGTCTGCCCTCGATATCTGTGATATAAAAGCTTATGTTTCTTC	ES41 ES45
pFLmb- PlGF- 1_1fzv	for: CCAGAGCCGCATCTCTGCCTGCTGTGCCCCC rev: TGTCTGCCCTCGATCCTCCGGGGAACAGCATCG	ES67 ES68
pFLmb- PlGF- 1_1rv6	for: CCAGAGCCGCATCTGAGGTGGAAGTGGTACCCTTCC rev: TGTCTGCCCTCGATCATCTTCTCCCGCAGAGGC	ES63 ES64
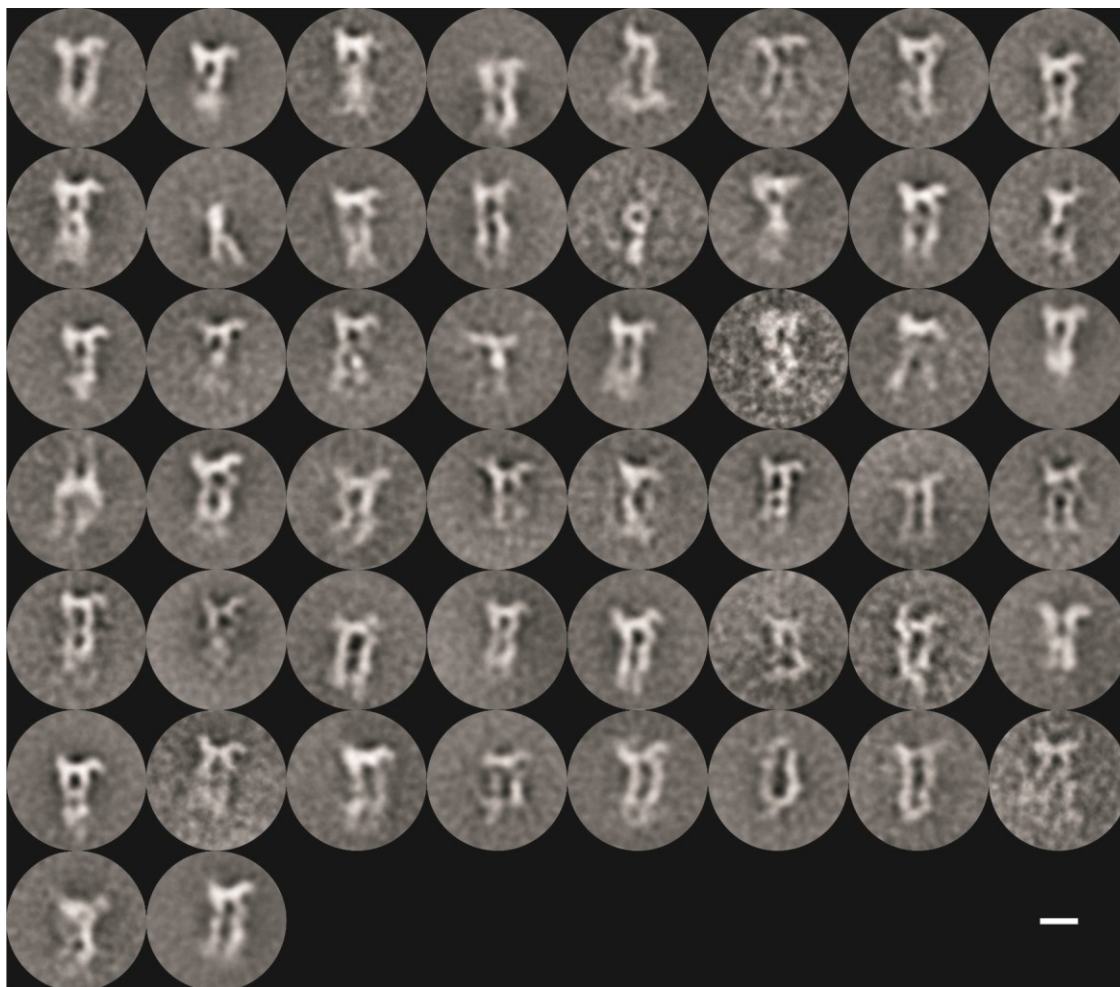
Fig. A-1: Electron Microscopy of the VEGFR-1 ECD/VEGF-A$_{121}$ complex
6260 particles were windowed in 70x70 pixel windows and classified in 50 groups. Scale bar, 15 nm.
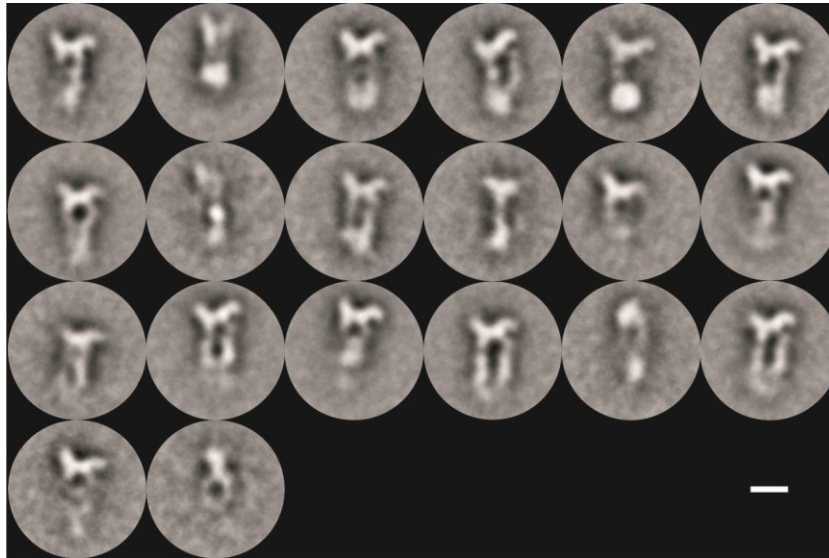
Fig. A-2: Electron Microscopy of the VEGFR-1 ECD/PlGF-1 complex
2203 particles were windowed in 70x70 pixel windows and classified in 20 groups. Scale bar, 15 nm.
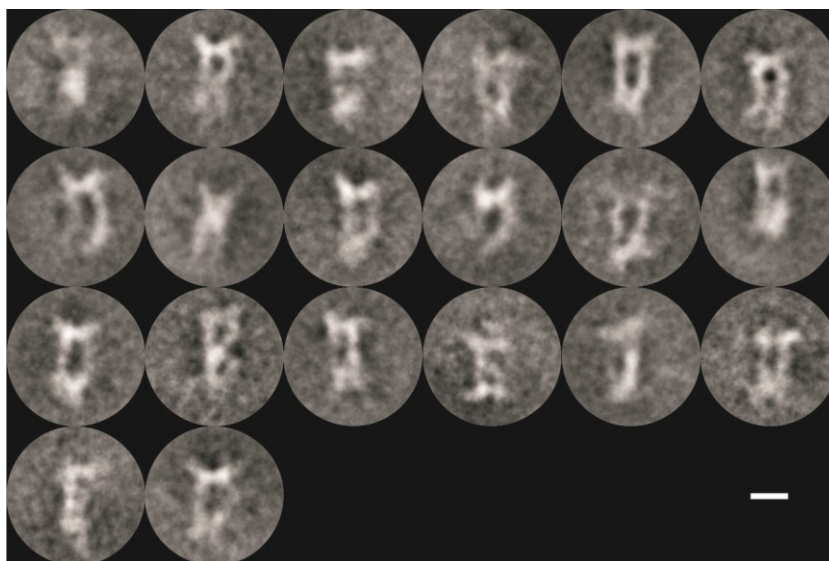
Fig. A-3: Electron Microscopy of the VEGFR-1 ECD/VEGF-B complex
1234 particles were windowed in 70x70 pixel windows and classified in 20 groups. Scale bar, 15 nm.
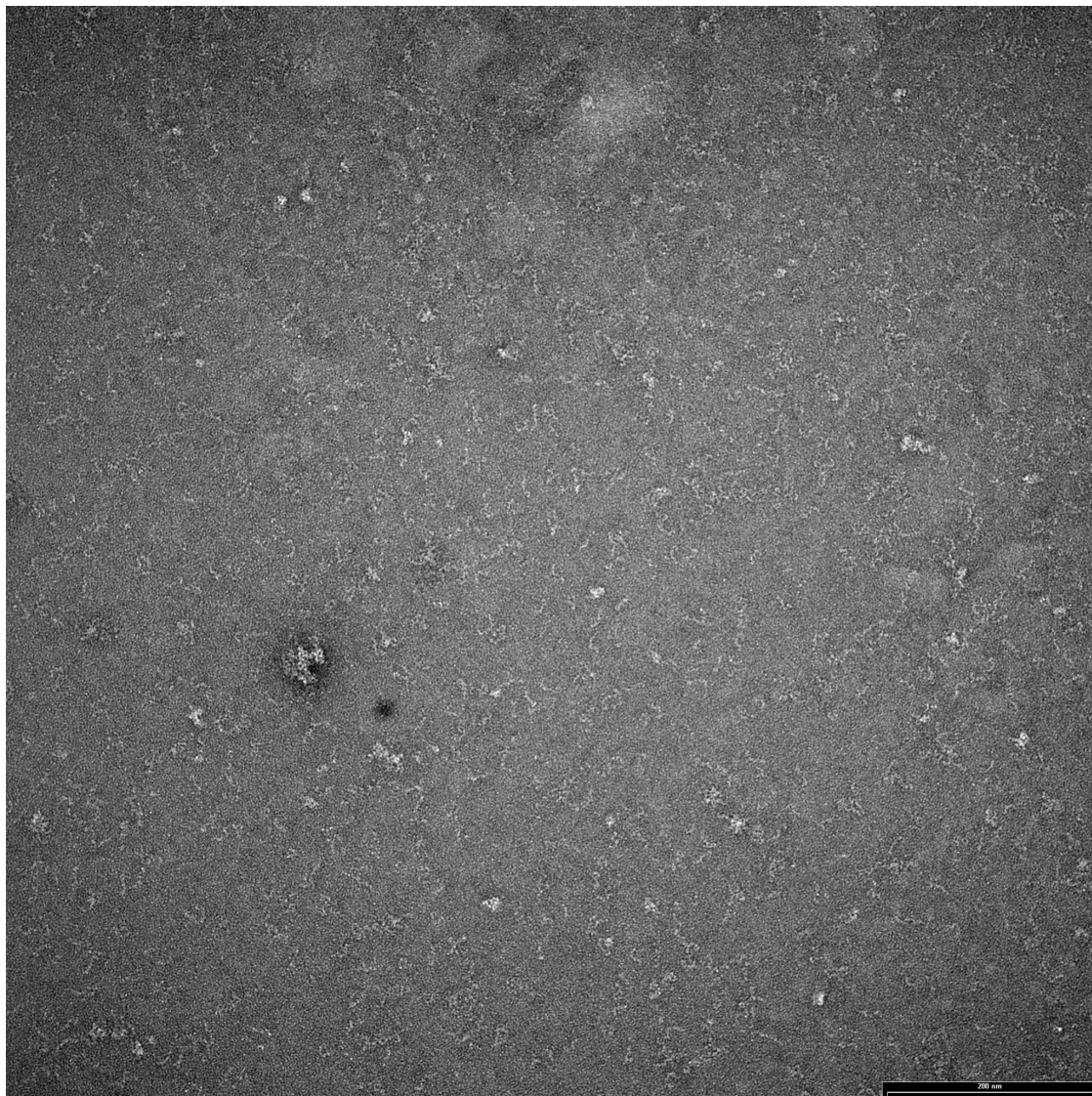
Fig. A-4: Raw EM image of VEGFR-1 D1-7
Scale bar, 200 nm.
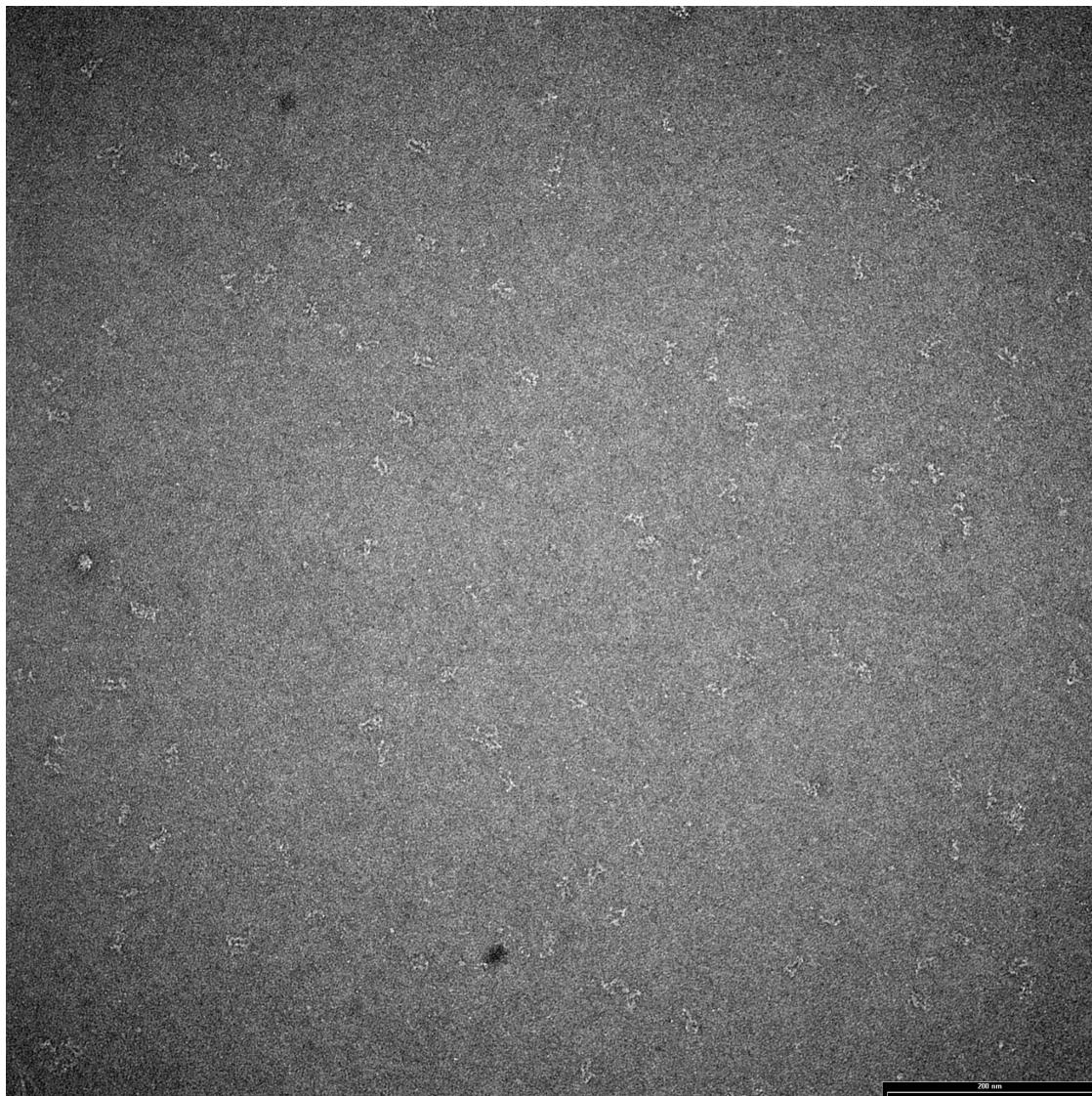
Fig. A 5: Raw EM image of VEGFR-1 D1-7/VEGF-A$_{121}$
Scale bar, 200 nm.

136
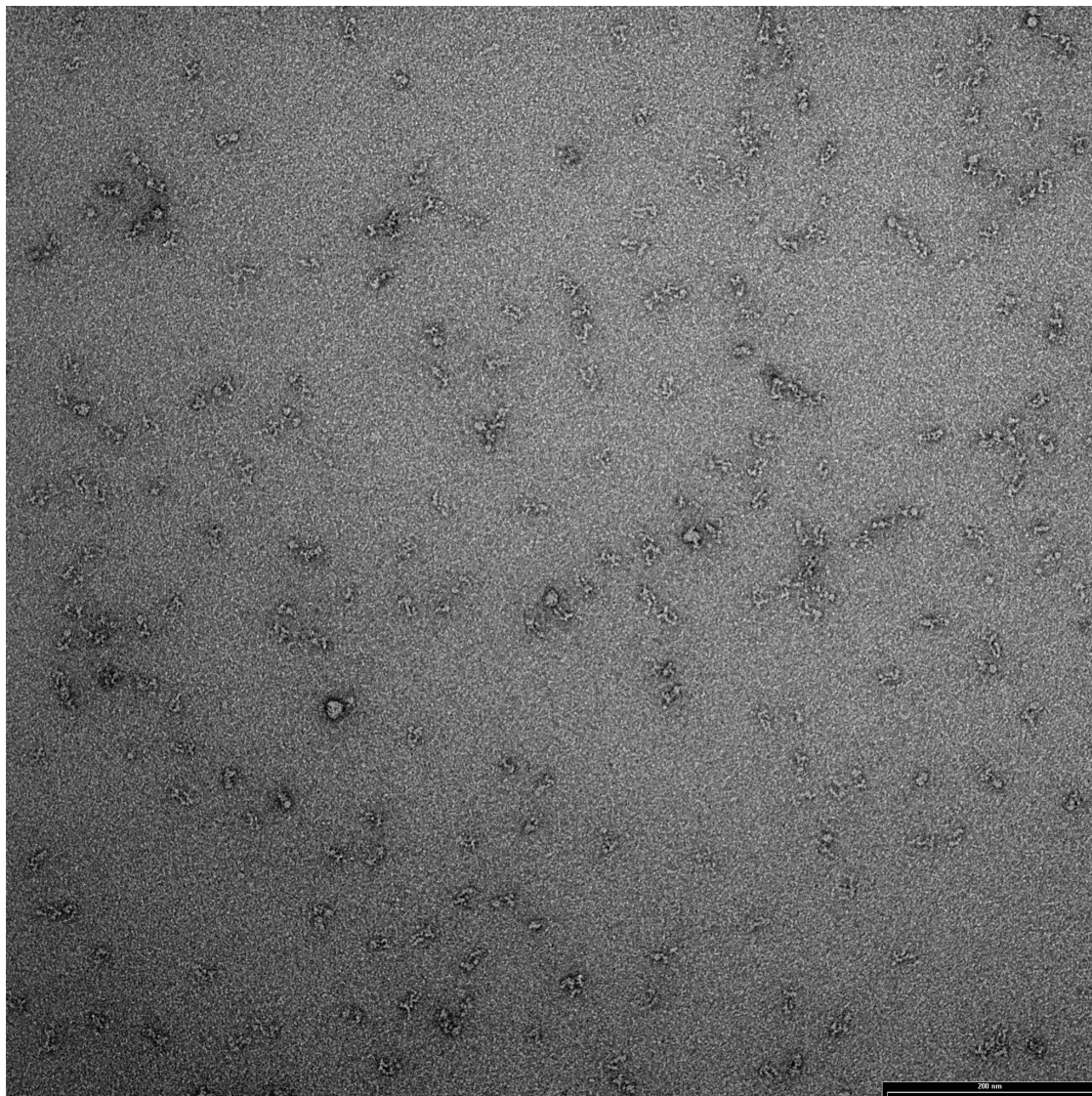
Fig. A 6: Raw EM image of VEGFR-1 D1-7/PlGF-1
Scale bar, 200 nm.
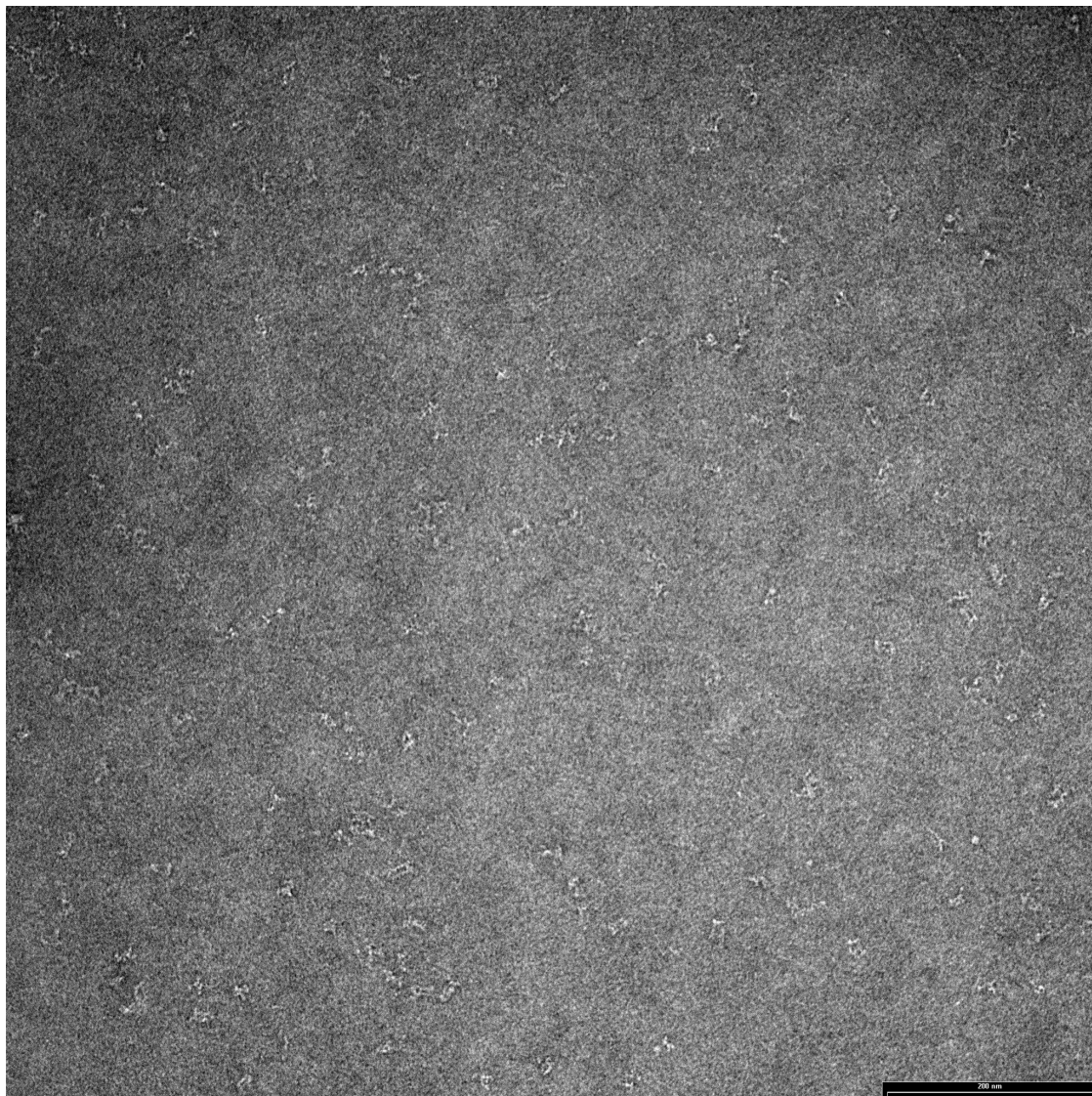
Fig. A 7: Raw EM image of VEGFR-1 D1-7/VEGF-B
Scale bar, 200 nm.

10   Acknowledgment

First of all, I would like to thank Prof. Dr. Kurt Ballmer-Hofer for giving me the opportunity to pursue a PhD in his research group. He always encouraged and supported me throughout this thesis. It was a pleasure to work with such an enthusiastic supervisor. My thanks go to my thesis committee, Dr. Nicolas Thomä and Prof. Dr. Therese Resink, for their time and their valuable input during all our meetings.

I thank the whole Molecular Cell Biology group for always providing a good atmosphere in the lab. My thanks go to all present and former members of the MCB lab: Anja, Kathi, Philipp, Thomas, Sandro, Alex, Maurice, Pascale, and Debbie. Special thanks go to Kaisa for introducing me to the small angles of X-ray diffraction, to Andrea for his advice on protein crystallography, and of course to Ulla. She is the "key regulator" of BMR that keeps the work and research running.

For his help and his advice in electron microscopy, I would like to thank Dr. Ken Goldie from the C-CINA in Basel.

Last but not least I would like to thank my family and Susann Kumpf.

11   References

Aase,K., Lymboussaki,A., Kaipainen,A., Olofsson,B., Alitalo,K., and Eriksson,U. (1999). Localization of VEGF-B in the mouse embryo suggests a paracrine role of the growth factor in the developing vasculature. Dev. Dyn. *215*, 12-25.

Aase,K., von,E.G., Li,X., Ponten,A., Thoren,P., Cao,R., Cao,Y., Olofsson,B., Gebre-Medhin,S., Pekny,M., Alitalo,K., Betsholtz,C., and Eriksson,U. (2001). Vascular endothelial growth factor-B-deficient mice display an atrial conduction defect. Circulation *104*, 358-364.

Albuquerque,R.J.C., Hayashi,T., Cho,W.G., Kleinman,M.E., Dridi,S., Takeda,A., Baffi,J.Z., Yamada,K., Kaneko,H., Green,M.G., Chappell,J., Wilting,J., Weich,H.A., Yamagami,S., Amano,S., Mizuki,N., Alexander,J.S., Peterson,M.L., Brekken,R.A., Hirashima,M., Capoor,S., Usui,T., Ambati,B.K., and Ambati,J. (2009). Alternatively spliced vascular endothelial growth factor receptor-2 is an essential endogenous inhibitor of lymphatic vessel growth. Nat Med *15*, 1023-1030.

Andre,T., Kotelevets,L., Vaillant,J.C., Coudray,A.M., Weber,L., Prevot,S., Parc,R., Gespach,C., and Chastre,E. (2000). Vegf, Vegf-B, Vegf-C and their receptors KDR, FLT-1 and FLT-4 during the neoplastic progression of human colonic mucosa. Int. J. Cancer *86*, 174-181.

Aricescu,A.R., Lu,W., and Jones,E.Y. (2006). A time- and cost-efficient system for high-level protein production in mammalian cells. Acta Crystallogr. D. Biol. Crystallogr. *62*, 1243-1250.

Autiero,M., Waltenberger,J., Communi,D., Kranz,A., Moons,L., Lambrechts,D., Kroll,J., Plaisance,S., De Mol,M., Bono,F., Kliche,S., Fellbrich,G., Ballmer-Hofer,K., Maglione,D., Mayr-Beyrle,U., Dewerchin,M., Dombrowski,S., Stanimirovic,D., Van Hummelen,P., Dehio,C., Hicklin,D.J., Persico,G., Herbert,J.M., Communi,D., Shibuya,M., Collen,D., Conway,E.M., and Carmeliet,P. (2003). Role of PlGF in the intra- and intermolecular cross talk between the VEGF receptors Flt1 and Flk1. Nat. Med. *9*, 936-943.

Badache,A. and Hynes,N.E. (2004). A new therapeutic antibody masks ErbB2 to its partners. Cancer cell *5*, 299-301.

Bais,C., Wu,X., Yao,J., Yang,S., Crawford,Y., McCutcheon,K., Tan,C., Kolumam,G., Vernes,J.M., Eastham-Anderson,J., Haughney,P., Kowanetz,M., Hagenbeek,T., Kasman,I., Reslan,H.B., Ross,J., Van,B.N., Carano,R.A., Meng,Y.J., Hongo,J.A., Stephan,J.P., Shibuya,M., and Ferrara,N. (2010). PlGF blockade does not inhibit angiogenesis during primary tumor growth. Cell *141*, 166-177.

Baish,J.W. and Jain,R.K. (2000). Fractals and cancer. Cancer Res. *60*, 3683-3688.

Baldwin,M.E., Halford,M.M., Roufail,S., Williams,R.A., Hibbs,M.L., Grail,D., Kubo,H., Stacker,S.A., and Achen,M.G. (2005). Vascular endothelial growth factor D is dispensable for development of the lymphatic system. Mol. Cell Biol. *25*, 2441-2449.

Barleon,B., Sozzani,S., Zhou,D., Weich,H.A., Mantovani,A., and Marme,D. (1996). Migration of human monocytes in response to vascular endothelial growth factor (VEGF) is mediated via the VEGF receptor flt-1. Blood *87*, 3336-3343.

Barleon,B., Totzke,F., Herzog,C., Blanke,S., Kremmer,E., Siemeister,G., Marmé,D., and Martiny-Baron,G. (1997). Mapping of the sites for ligand binding and receptor dimerization at the extracellular domain of the vascular endothelial growth factor receptor FLT-1. J. Biol. Chem. *272*, 10382-10388.

Bates,D.O., Cui,T.G., Doughty,J.M., Winkler,M., Sugiono,M., Shields,J.D., Peat,D., Gillatt,D.,

and Harper,S.J. (2002). VEGF(165)b, an Inhibitory Splice Variant of Vascular Endothelial Growth Factor, Is Down-Regulated in Renal Cell Carcinoma. Cancer Res. *62*, 4123-4131.

Bell,C.A., Tynan,J.A., Hart,K.C., Meyer,A.N., Robertson,S.C., and Donoghue,D.J. (2000). Rotational coupling of the transmembrane and kinase domains of the Neu receptor tyrosine kinase. Mol. Biol. Cell *11*, 3589-3599.

Bellomo,D., Headrick,J.P., Silins,G.U., Paterson,C.A., Thomas,P.S., Gartside,M., Mould,A., Cahill,M.M., Tonks,I.D., Grimmond,S.M., Townson,S., Wells,C., Little,M., Cummings,M.C., Hayward,N.K., and Kay,G.F. (2000). Mice lacking the vascular endothelial growth factor-B gene (Vegfb) have smaller hearts, dysfunctional coronary vasculature, and impaired recovery from cardiac ischemia. Circ. Res. *86*, E29-E35.

Berger,I., Fitzgerald,D.J., and Richmond,T.J. (2004). Baculovirus expression system for heterologous multiprotein complexes. Nat Biotechnol. *22*, 1583-1587.

Bergers,G. and Hanahan,D. (2008). Modes of resistance to anti-angiogenic therapy. Nat. Rev. Cancer *8*, 592-603.

Berman,H.M., Westbrook,J., Feng,Z., Gilliland,G., Bhat,T.N., Weissig,H., Shindyalov,I.N., and Bourne,P.E. (2000). The Protein Data Bank. Nucleic Acids Res. *28*, 235-242.

Binz,H.K., Amstutz,P., Kohl,A., Stumpp,M.T., Briand,C., Forrer,P., Grutter,M.G., and Pluckthun,A. (2004). High-affinity binders selected from designed ankyrin repeat protein libraries. Nat. Biotechnol. *22*, 575-582.

Bostrom,J., Yu,S.F., Kan,D., Appleton,B.A., Lee,C.V., Billeci,K., Man,W., Peale,F., Ross,S., Wiesmann,C., and Fuh,G. (2009). Variants of the antibody herceptin that interact with HER2 and VEGF at the antigen binding site. Science *323*, 1610-1614.

Carmeliet,P. (2000). Mechanisms of angiogenesis and arteriogenesis. Nat. Med. *6*, 389-395.

Carmeliet,P. and Collen,D. (2000). Molecular basis of angiogenesis. Role of VEGF and VE-cadherin. Ann. N. Y. Acad. Sci. *902*, 249-262.

Carmeliet,P., Dor,Y., Herbert,J.M., Fukumura,D., Brusselmans,K., Dewerchin,M., Neeman,M., Bono,F., Abramovitch,R., Maxwell,P., Koch,C.J., Ratcliffe,P., Moons,L., Jain,R.K., Collen,D., and Keshert,E. (1998). Role of HIF-1alpha in hypoxia-mediated apoptosis, cell proliferation and tumour angiogenesis. Nature *394*, 485-490.

Carmeliet,P., Ferreira,V., Breier,G., Pollefeyt,S., Kieckens,L., Gertsenstein,M., Fahrig,M., Vandenhoeck,A., Harpal,K., Eberhardt,C., Declercq,C., Pawling,J., Moons,L., Collen,D., Risau,W., and Nagy,A. (1996). Abnormal blood vessel development and lethality in embryos lacking a single VEGF allele. Nature *380*, 435-439.

Carmeliet,P. and Jain,R.K. (2000). Angiogenesis in cancer and other diseases. Nature *407*, 249-257.

Carmeliet,P., Lampugnani,M.G., Moons,L., Breviario,F., Compernolle,V., Bono,F., Balconi,G., Spagnuolo,R., Oosthuyse,B., Dewerchin,M., Zanetti,A., Angellilo,A., Mattot,V., Nuyens,D., Lutgens,E., Clotman,F., de Ruiter,M.C., Gittenberger-de,G.A., Poelmann,R., Lupu,F., Herbert,J.M., Collen,D., and Dejana,E. (1999a). Targeted deficiency or cytosolic truncation of the VE-cadherin gene in mice impairs VEGF-mediated endothelial survival and angiogenesis. Cell *98*, 147-157.

Carmeliet,P., Moons,L., Luttun,A., Vincenti,V., Compernolle,V., De Mol,M., Wu,Y., Bono,F., Devy,L., Beck,H., Scholz,D., Acker,T., DiPalma,T., Dewerchin,M., Noel,A., Stalmans,I., Barra,A., Blacher,S., Vandendriessche,T., Ponten,A., Eriksson,U., Plate,K.H., Foidart,J.M., Schaper,W., Charnock-Jones,D.S., Hicklin,D.J., Herbert,J.M., Collen,D., and Persico,M.G.

(2001). Synergism between vascular endothelial growth factor and placental growth factor contributes to angiogenesis and plasma extravasation in pathological conditions. Nat. Med. *7*, 575-583.

Carmeliet,P., Ng,Y.S., Nuyens,D., Theilmeier,G., Brusselmans,K., Cornelissen,I., Ehler,E., Kakkar,V.V., Stalmans,I., Mattot,V., Perriard,J.C., Dewerchin,M., Flameng,W., Nagy,A., Lupu,F., Moons,L., Collen,D., D'Amore,P.A., and Shima,D.T. (1999b). Impaired myocardial angiogenesis and ischemic cardiomyopathy in mice lacking the vascular endothelial growth factor isoforms VEGF164 and VEGF188. Nat. Med. *5*, 495-502.

Cebe-Suarez,S., Grunewald,F.S., Jaussi,R., Li,X., Claesson-Welsh,L., Spillmann,D., Mercer,A.A., Prota,A.E., and Ballmer-Hofer,K. (2008). Orf virus VEGF-E NZ2 promotes paracellular NRP-1/VEGFR-2 coreceptor assembly via the peptide RPPR. FASEB J. *22*, 3078-3086.

Cébe-Suarez,S., Pieren,M., Cariolato,L., Arn,S., Hoffmann,U., Bogucki,A., Manlius,C., Wood,J., and Ballmer-Hofer,K. (2006). A VEGF-A splice variant defective for heparan sulfate and neuropilin-1 binding shows attenuated signaling through VEGFR-2. Cell Mol. Life Sci. *63*, 2067-2077.

Chang,V.T., Crispin,M., Aricescu,A.R., Harvey,D.J., Nettleship,J.E., Fennelly,J.A., Yu,C., Boles,K.S., Evans,E.J., Stuart,D.I., Dwek,R.A., Jones,E.Y., Owens,R.J., and Davis,S.J. (2007). Glycoprotein structural genomics: solving the glycosylation problem. Structure *15*, 267-273.

Chang,Y.S., di,T.E., McDonald,D.M., Jones,R., Jain,R.K., and Munn,L.L. (2000). Mosaic blood vessels in tumors: frequency of cancer cells in contact with flowing blood. Proc. Natl. Acad. Sci. U. S. A *97*, 14608-14613.

Chen,L., Placone,J., Novicky,L., and Hristova,K. (2010). The extracellular domain of fibroblast growth factor receptor 3 inhibits ligand-independent dimerization. Sci. Signal *3*, ra86.

Chen,Y., Wiesmann,C., Fuh,G., Li,B., Christinger,H.W., McKay,P., de Vos,A.M., and Lowman,H.B. (1999). Selection and analysis of an optimized anti-VEGF antibody: crystal structure of an affinity-matured Fab in complex with antigen. J. Mol. Biol. *293*, 865-881.

Christinger,H.W., Fuh,G., de Vos,A.M., and Wiesmann,C. (2004). The crystal structure of placental growth factor in complex with domain 2 of vascular endothelial growth factor receptor-1. J. Biol. Chem. *279*, 10382-10388.

Chung,I., Akita,R., Vandlen,R., Toomre,D., Schlessinger,J., and Mellman,I. (2010). Spatial control of EGF receptor activation by reversible dimerization on living cells. Nature *advance online publication*.

Clauss,M., Weich,H., Breier,G., Knies,U., Rockl,W., Waltenberger,J., and Risau,W. (1996). The vascular endothelial growth factor receptor Flt-1 mediates biological activities. Implications for a functional role of placenta growth factor in monocyte activation and chemotaxis. J. Biol. Chem. *271*, 17629-17634.

Conway,J.F., Trus,B.L., Booy,F.P., Newcomb,W.W., Brown,J.C., and Steven,A.C. (1996). Visualization of Three-Dimensional Density Maps Reconstructed from Cryoelectron Micrographs of Viral Capsids. Journal of Structural Biology *116*, 200-208.

Cunningham,S.A., Arrate,M.P., Brock,T.A., and Waxham,M.N. (1997). Interactions of FLT-1 and KDR with phospholipase C gamma: identification of the phosphotyrosine binding sites. Biochem. Biophys. Res. Commun. *240*, 635-639.

Cunningham,S.A., Waxham,M.N., Arrate,P.M., and Brock,T.A. (1995). Interaction of the Flt-1 tyrosine kinase receptor with the p85 subunit of phosphatidylinositol 3-kinase. Mapping of a novel site involved in binding. J. Biol. Chem. *270*, 20254-20257.

Davis,T.R., Trotter,K.M., Granados,R.R., and Wood,H.A. (1992). Baculovirus expression of alkaline phosphatase as a reporter gene for evaluation of production, glycosylation and secretion. Biotechnology (N. Y.) *10*, 1148-1150.

Davis-Smyth,T., Chen,H., Park,J., Presta,L.G., and Ferrara,N. (1996). The second immunoglobulin-like domain of the VEGF tyrosine kinase receptor Flt-1 determines ligand binding and may initiate a signal transduction cascade. EMBO J. *15*, 4919-4927.

Davis-Smyth,T., Presta,L.G., and Ferrara,N. (1998). Mapping the Charged Residues in the Second Immunoglobulin-like Domain of the Vascular Endothelial Growth Factor/Placenta Growth Factor Receptor Flt-1 Required for Binding and Structural Stability. J. Biol. Chem. *273*, 3216-3222.

Dell'Era Dosch,D. and Ballmer-Hofer,K. (2010). Transmembrane domain-mediated orientation of receptor monomers in active VEGFR-2 dimers. FASEB J. *24*, 32-38.

Dias,S., Hattori,K., Zhu,Z., Heissig,B., Choy,M., Lane,W., Wu,Y., Chadburn,A., Hyjek,E., Gill,M., Hicklin,D.J., Witte,L., Moore,M.A., and Rafii,S. (2000). Autocrine stimulation of VEGFR-2 activates human leukemic cell growth and migration. J. Clin. Invest *106*, 511-521.

Dimmeler,S., Fleming,I., Fisslthaler,B., Hermann,C., Busse,R., and Zeiher,A.M. (1999). Activation of nitric oxide synthase in endothelial cells by Akt-dependent phosphorylation. Nature *399*, 601-605.

Dixelius,J., Makinen,T., Wirzenius,M., Karkkainen,M.J., Wernstedt,C., Alitalo,K., and Claesson-Welsh,L. (2003). Ligand-induced vascular endothelial growth factor receptor-3 (VEGFR-3) heterodimerization with VEGFR-2 in primary lymphatic endothelial cells regulates tyrosine phosphorylation sites. J. Biol. Chem. *278*, 40973-40979.

Dong,A., Xu,X., and Edwards,A.M. (2007). In situ proteolysis for protein crystallization and structure determination. Nat Meth *4*, 1019-1021.

Dukkipati,A., Park,H.H., Waghray,D., Fischer,S., and Garcia,K.C. (2008). BacMam system for high-level expression of recombinant soluble and membrane glycoproteins for structural studies. Protein Expr. Purif. *62*, 160-170.

Dumont,D.J., Gradwohl,G., Fong,G.H., Puri,M.C., Gertsenstein,M., Auerbach,A., and Breitman,M.L. (1994). Dominant-negative and targeted null mutations in the endothelial receptor tyrosine kinase, tek, reveal a critical role in vasculogenesis of the embryo. Genes Dev. *8*, 1897-1909.

Dumont,D.J., Jussila,L., Taipale,J., Lymboussaki,A., Mustonen,T., Pajusola,K., Breitman,M., and Alitalo,K. (1998). Cardiovascular failure in mouse embryos deficient in VEGF receptor-3. Science *282*, 946-949.

Ebos,J.M., Bocci,G., Man,S., Thorpe,P.E., Hicklin,D.J., Zhou,D., Jia,X., and Kerbel,R.S. (2004). A naturally occurring soluble form of vascular endothelial growth factor receptor 2 detected in mouse and human plasma. Mol Cancer Res *2*, 315-326.

Fellouse,F.A., Esaki,K., Birtalan,S., Raptis,D., Cancasci,V.J., Koide,A., Jhurani,P., Vasser,M., Wiesmann,C., Kossiakoff,A.A., Koide,S., and Sidhu,S.S. (2007). High-throughput generation of synthetic antibodies from highly functional minimalist phage-displayed libraries. J. Mol. Biol. *373*, 924-940.

Fellouse,F.A., Wiesmann,C., and Sidhu,S.S. (2004). Synthetic antibodies from a four-amino-acid code: a dominant role for tyrosine in antigen recognition. Proc. Natl. Acad. Sci. U. S. A *101*, 12467-12472.

Ferrara,N., Carver Moore,K., Chen,H., Dowd,M., Lu,L., O Shea,K.S., Powell,B.L., Hillan,K.J.,

and Moore,M.W. (1996). Heterozygous embryonic lethality induced by targeted inactivation of the VEGF gene. Nature *380*, 439-442.

Ferrara,N., Damico,L., Shams,N., Lowman,H., and Kim,R. (2006). Development of ranibizumab, an anti-vascular endothelial growth factor antigen binding fragment, as therapy for neovascular age-related macular degeneration. Retina *26*, 859-870.

Ferrara,N. and Davis-Smyth,T. (1997). The biology of vascular endothelial growth factor. Endocr. Rev. *18*, 4-25.

Ferrara,N. and Henzel,W.J. (1989). Pituitary follicular cells secrete a novel heparin-binding growth factor specific for vascular endothelial cells. Biochem. Biophys. Res. Commun. *161*, 851-858.

Ferrara,N., Hillan,K.J., Gerber,H.P., and Novotny,W. (2004). Discovery and development of bevacizumab, an anti-VEGF antibody for treating cancer. Nat. Rev. Drug Discov. *3*, 391-400.

Ferrara,N. and Kerbel,R.S. (2005). Angiogenesis as a therapeutic target. Nature *438*, 967-974.

Fischer,C., Jonckx,B., Mazzone,M., Zacchigna,S., Loges,S., Pattarini,L., Chorianopoulos,E., Liesenborghs,L., Koch,M., De,M.M., Autiero,M., Wyns,S., Plaisance,S., Moons,L., van,R.N., Giacca,M., Stassen,J.M., Dewerchin,M., Collen,D., and Carmeliet,P. (2007). Anti-PlGF inhibits growth of VEGF(R)-inhibitor-resistant tumors without affecting healthy vessels. Cell *131*, 463-475.

Fischer,C., Mazzone,M., Jonckx,B., and Carmeliet,P. (2008). FLT1 and its ligands VEGFB and PlGF: drug targets for anti-angiogenic therapy? Nat Rev Cancer *8*, 942-956.

Folkman,J. (1995). Angiogenesis in cancer, vascular, rheumatoid and other disease. Nat. Med. *1*, 27-31.

Fong,G.H., Rossant,J., Gertsenstein,M., and Breitman,M.L. (1995). Role of the Flt-1 receptor tyrosine kinase in regulating the assembly of vascular endothelium. Nature *376*, 66-70.

Fong,G.H., Zhang,L., Bryce,D.M., and Peng,J. (1999). Increased hemangioblast commitment, not vascular disorganization, is the primary defect in flt-1 knock-out mice. Development *126*, 3015-3025.

Frank,J., Radermacher,M., Penczek,P., Zhu,J., Li,Y., Ladjadj,M., and Leith,A. (1996). SPIDER and WEB: Processing and Visualization of Images in 3D Electron Microscopy and Related Fields. Journal of Structural Biology *116*, 190-199.

Franklin,M.C., Carey,K.D., Vajdos,F.F., Leahy,D.J., de Vos,A.M., and Sliwkowski,M.X. (2004). Insights into ErbB signaling from the structure of the ErbB2-pertuzumab complex. Cancer cell *5*, 317-328.

Freeman,M.R., Schneck,F.X., Gagnon,M.L., Corless,C., Soker,S., Niknejad,K., Peoples,G.E., and Klagsbrun,M. (1995). Peripheral blood T lymphocytes and lymphocytes infiltrating human cancers express vascular endothelial growth factor: a potential role for T cells in angiogenesis. Cancer Res. *55*, 4140-4145.

Fuh,G., Wu,P., Liang,W.C., Ultsch,M., Lee,C.V., Moffat,B., and Wiesmann,C. (2006). Structure-function studies of two synthetic anti-vascular endothelial growth factor Fabs and comparison with the Avastin Fab. J. Biol. Chem. *281*, 6625-6631.

Fujio,Y. and Walsh,K. (1999). Akt mediates cytoprotection of endothelial cells by vascular endothelial growth factor in an anchorage-dependent manner. J. Biol. Chem. *274*, 16349-16354.

Fulton,D., Gratton,J.P., McCabe,T.J., Fontana,J., Fujio,Y., Walsh,K., Franke,T.F., Papapetropoulos,A., and Sessa,W.C. (1999). Regulation of endothelium-derived nitric oxide production by the protein kinase Akt. Nature *399*, 597-601.

Gasteiger,E., Gattiker,A., Hoogland,C., Ivanyi,I., Appel,R.D., and Bairoch,A. (2003). ExPASy: The proteomics server for in-depth protein knowledge and analysis. Nucleic Acids Res. *31*, 3784-3788.

Geiser,M., Cébe,R., Drewello,D., and Schmitz,R. (2001). Integration of PCR fragments at any specific site within cloning vectors without the use of restriction enzymes and DNA ligase. Biotechniques *31*, 88-90, 92.

Gerety,S.S., Wang,H.U., Chen,Z.F., and Anderson,D.J. (1999). Symmetrical mutant phenotypes of the receptor EphB4 and its specific transmembrane ligand ephrin-B2 in cardiovascular development. Mol. Cell *4*, 403-414.

Gille,H., Kowalski,J., Yu,L., Chen,H., Pisabarro,M.T., Davis,S.T., and Ferrara,N. (2000). A repressor sequence in the juxtamembrane domain of Flt-1 (VEGFR-1) constitutively inhibits vascular endothelial growth factor-dependent phosphatidylinositol 3'-kinase activation and endothelial cell migration. EMBO J. *19*, 4064-4073.

Gragoudas,E.S., Adamis,A.P., Cunningham,E.T., Jr., Feinsod,M., and Guyer,D.R. (2004). Pegaptanib for neovascular age-related macular degeneration. N. Engl. J. Med. *351*, 2805-2816.

Grueninger-Leitch,F., D'Arcy,A., D'Arcy,B., and Chene,C. (1996). Deglycosylation of proteins for crystallization using recombinant fusion protein glycosidases. Protein Sci. *5*, 2617-2622.

Grünewald,F.S., Prota,A.E., Giese,A., and Ballmer-Hofer,K. (2010). Structure-function analysis of VEGF receptor activation and the role of coreceptors in angiogenic signaling. Biochimica et Biophysica Acta (BBA) - Proteins & Proteomics *1804*, 567-580.

Hagberg,C.E., Falkevall,A., Wang,X., Larsson,E., Huusko,J., Nilsson,I., van Meeteren,L.A., Samen,E., Lu,L., Vanwildemeersch,M., Klar,J., Genove,G., Pietras,K., Stone-Elander,S., Claesson-Welsh,L., Yla-Herttuala,S., Lindahl,P., and Eriksson,U. (2010). Vascular endothelial growth factor B controls endothelial fatty acid uptake. Nature *464*, 917-921.

Harpaz,Y. and Chothia,C. (1994). Many of the immunoglobulin superfamily domains in cell adhesion molecules and surface receptors belong to a new structural set which is close to that containing variable domains. J. Mol. Biol. *238*, 528-539.

Hashizume,H., Baluk,P., Morikawa,S., McLean,J.W., Thurston,G., Roberge,S., Jain,R.K., and McDonald,D.M. (2000). Openings between defective endothelial cells explain tumor vessel leakiness. Am. J. Pathol. *156*, 1363-1380.

Hattori,K., Heissig,B., Wu,Y., Dias,S., Tejada,R., Ferris,B., Hicklin,D.J., Zhu,Z., Bohlen,P., Witte,L., Hendrikx,J., Hackett,N.R., Crystal,R.G., Moore,M.A., Werb,Z., Lyden,D., and Rafii,S. (2002). Placental growth factor reconstitutes hematopoiesis by recruiting VEGFR1(+) stem cells from bone-marrow microenvironment. Nat. Med. *8*, 841-849.

Hellstrom,M., Gerhardt,H., Kalen,M., Li,X., Eriksson,U., Wolburg,H., and Betsholtz,C. (2001). Lack of pericytes leads to endothelial hyperplasia and abnormal vascular morphogenesis. J. Cell Biol. *153*, 543-553.

Hellstrom,M., Kalen,M., Lindahl,P., Abramsson,A., and Betsholtz,C. (1999). Role of PDGF-B and PDGFR-beta in recruitment of vascular smooth muscle cells and pericytes during embryonic blood vessel formation in the mouse. Development *126*, 3047-3055.

Hellstrom,M., Phng,L.K., Hofmann,J.J., Wallgard,E., Coultas,L., Lindblom,P., Alva,J.,

Nilsson,A.K., Karlsson,L., Gaiano,N., Yoon,K., Rossant,J., Iruela-Arispe,M.L., Kalen,M., Gerhardt,H., and Betsholtz,C. (2007). Dll4 signalling through Notch1 regulates formation of tip cells during angiogenesis. Nature *445*, 776-780.

Hiratsuka,S., Minowa,O., Kuno,J., Noda,T., and Shibuya,M. (1998). Flt-1 lacking the tyrosine kinase domain is sufficient for normal development and angiogenesis in mice. Proc. Natl. Acad. Sci. U. S. A. *95*, 9349-9354.

Hiratsuka,S., Nakao,K., Nakamura,K., Katsuki,M., Maru,Y., and Shibuya,M. (2005). Membrane fixation of vascular endothelial growth factor receptor 1 ligand-binding domain is important for vasculogenesis and angiogenesis in mice. Mol. Cell Biol. *25*, 346-354.

Holash,J., Davis,S., Papadopoulos,N., Croll,S.D., Ho,L., Russell,M., Boland,P., Leidich,R., Hylton,D., Burova,E., Ioffe,E., Huang,T., Radziejewski,C., Bailey,K., Fandl,J.P., Daly,T., Wiegand,S.J., Yancopoulos,G.D., and Rudge,J.S. (2002). VEGF-Trap: a VEGF blocker with potent antitumor effects. Proc. Natl. Acad. Sci. U. S. A *99*, 11393-11398.

Holash,J., Wiegand,S.J., and Yancopoulos,G.D. (1999). New model of tumor angiogenesis: dynamic balance between vessel regression and growth mediated by angiopoietins and VEGF. Oncogene *18*, 5356-5362.

Holmqvist,K., Cross,M., Riley,D., and Welsh,M. (2003). The Shb adaptor protein causes Src-dependent cell spreading and activation of focal adhesion kinase in murine brain endothelial cells. Cell Signal. *15*, 171-179.

Holmqvist,K., Cross,M.J., Rolny,C., Hagerkvist,R., Rahimi,N., Matsumoto,T., Claesson-Welsh,L., and Welsh,M. (2004). The adaptor protein shb binds to tyrosine 1175 in vascular endothelial growth factor (VEGF) receptor-2 and regulates VEGF-dependent cellular migration. J. Biol. Chem. *279*, 22267-22275.

Houck,K.A., Ferrara,N., Winer,J., Cachianes,G., Li,B., and Leung,D.W. (1991). The vascular endothelial growth factor family: identification of a fourth molecular species and characterization of alternative splicing of RNA. Mol. Endocrinol. *5*, 1806-1814.

Huang,T.C., Toraya,H., Blanton,T.N., and Wu,Y. (1993). X-ray powder diffraction analysis of silver behenate, a possible low-angle diffraction standard. J. Appl. Cryst. *26*, 180-184.

Hye-Ryong Shim,A., Liu,H., Focia,P.J., Chen,X., Lin,P.C., and He,X. (2010). Structures of a platelet-derived growth factor/propeptide complex and a platelet-derived growth factor/receptor complex. Proceedings of the National Academy of Sciences *107*, 11307-11312.

Ito,N., Huang,K., and Claesson-Welsh,L. (2001). Signal transduction by VEGF receptor-1 wild type and mutant proteins. Cellular Signalling *13*, 849-854.

Ivy,S.P., Wick,J.Y., and Kaufman,B.M. (2009). An overview of small-molecule inhibitors of VEGFR signaling. Nat. Rev. Clin. Oncol. *6*, 569-579.

Iyer,S., Darley,P.I., and Acharya,K.R. (2010). Structural insights into the binding of VEGF-B by VEGFR-1D2: Recognition and specificity. J. Biol. Chem.

Iyer,S., Leonidas,D.D., Swaminathan,G.J., Maglione,D., Battisti,M., Tucci,M., Persico,M.G., and Acharya,K.R. (2001). The Crystal Structure of Human Placenta Growth Factor-1 (PlGF-1), an Angiogenic Protein, at 2.0 A Resolution. J. Biol. Chem. *276*, 12153-12161.

Iyer,S., Scotney,P.D., Nash,A.D., and Ravi Acharya,K. (2006). Crystal Structure of Human Vascular Endothelial Growth Factor-B: Identification of Amino Acids Important for Receptor Binding. Journal of Molecular Biology *359*, 76-85.

Jacques,D.A. and Trewhella,J. (2010). Small-angle scattering for structural biology--expanding the frontier while avoiding the pitfalls. Protein Sci. *19*, 642-657.

Jain,R.K. (2003). Molecular regulation of vessel maturation. Nat. Med. *9*, 685-693.

Kaipainen,A., Korhonen,J., Mustonen,T., van,H., V, Fang,G.H., Dumont,D., Breitman,M., and Alitalo,K. (1995). Expression of the fms-like tyrosine kinase 4 gene becomes restricted to lymphatic endothelium during development. Proc. Natl. Acad. Sci. U. S. A *92*, 3566-3570.

Karkkainen,M.J., Haiko,P., Sainio,K., Partanen,J., Taipale,J., Petrova,T.V., Jeltsch,M., Jackson,D.G., Talikka,M., Rauvala,H., Betsholtz,C., and Alitalo,K. (2004). Vascular endothelial growth factor C is required for sprouting of the first lymphatic vessels from embryonic veins. Nat. Immunol. *5*, 74-80.

Kendall,R.L., Rutledge,R.Z., Mao,X., Tebben,A.J., Hungate,R.W., and Thomas,K.A. (1999). Vascular endothelial growth factor receptor KDR tyrosine kinase activity is increased by autophosphorylation of two activation loop tyrosine residues. J. Biol. Chem. *274*, 6453-6460.

Kendall,R.L. and Thomas,K.A. (1993). Inhibition of vascular endothelial cell growth factor activity by an endogenously encoded soluble receptor. Proc. Natl. Acad. Sci. U. S. A *90*, 10705-10709.

Kendrew,J., Eberlein,C., Hedberg,B., McDaid,K., Smith,N.R., Weir,H.M., Wedge,S.R., Blakey,D.C., Foltz,I.N., Zhou,J., Kang,J.S., and Barry,S.T. (2011). An antibody targetted to VEGFR-2 Ig domains 4-7 inhibits VEGFR-2 activation and VEGFR-2 dependent angiogenesis without affecting ligand binding. Mol. Cancer Ther.

Keyt,B.A., Berleau,L.T., Nguyen,H.V., Chen,H., Heinsohn,H., Vandlen,R., and Ferrara,N. (1996a). The carboxyl-terminal domain (111-165) of vascular endothelial growth factor is critical for its mitogenic potency. J. Biol. Chem. *271*, 7788-7795.

Keyt,B.A., Nguyen,H.V., Berleau,L.T., Duarte,C.M., Park,J., Chen,H., and Ferrara,N. (1996b). Identification of vascular endothelial growth factor determinants for binding KDR and FLT-1 receptors. Generation of receptor-selective VEGF variants by site-directed mutagenesis. J. Biol. Chem. *271*, 5638-5646.

Konarev,P.V., Volkov,V.V., Sokolova,A.V., Koch,M.H.J., and Svergun,D.I. (2003). PRIMUS: a Windows PC-based system for small-angle scattering data analysis. J. Appl. Cryst. *36*, 1277-1282.

Krah,K., Mironov,V., Risau,W., and Flamme,I. (1994). Induction of vasculogenesis in quail blastodisc-derived embryoid bodies. Dev. Biol. *164*, 123-132.

Lagercrantz,J., Larsson,C., Grimmond,S., Fredriksson,M., Weber,G., and Piehl,F. (1996). Expression of the VEGF-related factor gene in pre- and postnatal mouse. Biochem. Biophys. Res. Commun. *220*, 147-152.

Lamalice,L., Houle,F., and Huot,J. (2006). Phosphorylation of Tyr1214 within VEGFR-2 triggers the recruitment of Nck and activation of Fyn leading to SAPK2/p38 activation and endothelial cell migration in response to VEGF. J. Biol. Chem. *281*, 34009-34020.

Lawson,N.D., Scheer,N., Pham,V.N., Kim,C.H., Chitnis,A.B., Campos-Ortega,J.A., and Weinstein,B.M. (2001). Notch signaling is required for arterial-venous differentiation during embryonic vascular development. Development *128*, 3675-3683.

Lemmon,M.A. and Ferguson,K.M. (2007). A new twist in the transmembrane signaling tool-kit. Cell *130*, 213-215.

Lemmon,M.A. and Schlessinger,J. (2010). Cell signaling by receptor tyrosine kinases. Cell *141*, 1117-1134.

Leonard,P., Scotney,P.D., Jabeen,T., Iyer,S., Fabri,L.J., Nash,A.D., and Acharya,K.R. (2008). Crystal structure of vascular endothelial growth factor-B in complex with a neutralising antibody Fab fragment. J. Mol. Biol. *384*, 1203-1217.

Leppanen,V.M., Jeltsch,M., Anisimov,A., Tvorogov,D., Aho,K., Kalkkinen,N., Toivanen,P., Yla-Herttuala,S., Ballmer-Hofer,K., and Alitalo,K. (2010a). Structural determinants of vascular endothelial growth factor-D - receptor binding and specificity. Blood.

Leppanen,V.M., Prota,A.E., Jeltsch,M., Anisimov,A., Kalkkinen,N., Strandin,T., Lankinen,H., Goldman,A., Ballmer-Hofer,K., and Alitalo,K. (2010b). Structural determinants of growth factor binding and specificity by VEGF receptor 2. Proceedings of the National Academy of Sciences *107*, 2425-2430.

Leveen,P., Pekny,M., Gebre-Medhin,S., Swolin,B., Larsson,E., and Betsholtz,C. (1994). Mice deficient for PDGF B show renal, cardiovascular, and hematological abnormalities. Genes Dev. *8*, 1875-1887.

Lindahl,P., Johansson,B.R., Leveen,P., and Betsholtz,C. (1997). Pericyte loss and microaneurysm formation in PDGF-B-deficient mice. Science *277*, 242-245.

Luttun,A., Tjwa,M., Moons,L., Wu,Y., ngelillo-Scherrer,A., Liao,F., Nagy,J.A., Hooper,A., Priller,J., De,K.B., Compernolle,V., Daci,E., Bohlen,P., Dewerchin,M., Herbert,J.M., Fava,R., Matthys,P., Carmeliet,G., Collen,D., Dvorak,H.F., Hicklin,D.J., and Carmeliet,P. (2002). Revascularization of ischemic tissues by PlGF treatment, and inhibition of tumor angiogenesis, arthritis and atherosclerosis by anti-Flt1. Nat. Med. *8*, 831-840.

Mack,G.S. (2009). Mixed news for Avastin. Nat. Biotechnol. *27*, 494.

Maes,C., Carmeliet,P., Moermans,K., Stockmans,I., Smets,N., Collen,D., Bouillon,R., and Carmeliet,G. (2002). Impaired angiogenesis and endochondral bone formation in mice lacking the vascular endothelial growth factor isoforms VEGF164 and VEGF188. Mech. Dev. *111*, 61-73.

Maglione,D., Guerriero,V., Viglietto,G., Ferraro,M.G., Aprelikova,O., Alitalo,K., Del,V.S., Lei,K.J., Chou,J.Y., and Persico,M.G. (1993). Two alternative mRNAs coding for the angiogenic factor, placenta growth factor (PlGF), are transcribed from a single gene of chromosome 14. Oncogene *8*, 925-931.

Maglione,D., Guerriero,V., Viglietto,G., Ii-Bovi,P., and Persico,M.G. (1991). Isolation of a human placenta cDNA coding for a protein related to the vascular permeability factor. Proceedings of the National Academy of Sciences of the United States of America *88*, 9267-9271.

Maisonpierre,P.C., Suri,C., Jones,P.F., Bartunkova,S., Wiegand,S.J., Radziejewski,C., Compton,D., McClain,J., Aldrich,T.H., Papadopoulos,N., Daly,T.J., Davis,S., Sato,T.N., and Yancopoulos,G.D. (1997). Angiopoietin-2, a natural antagonist for Tie2 that disrupts in vivo angiogenesis. Science *277*, 55-60.

Makinen,T., Olofsson,B., Karpanen,T., Hellman,U., Soker,S., Klagsbrun,M., Eriksson,U., and Alitalo,K. (1999). Differential binding of vascular endothelial growth factor B splice and proteolytic isoforms to neuropilin-1. J. Biol. Chem. *274*, 21217-21222.

Matsumoto,T., Bohman,S., Dixelius,J., Berge,T., Dimberg,A., Magnusson,P., Wang,L., Wikner,C., Qi,J.H., Wernstedt,C., Wu,J., Bruheim,S., Mugishima,H., Mukhopadhyay,D., Spurkland,A., and Claesson-Welsh,L. (2005). VEGF receptor-2 Y951 signaling and a role for the adapter molecule TSAd in tumor angiogenesis. EMBO J. *24*, 2342-2353.

Matsumoto,T. and Claesson-Welsh,L. (2001). VEGF receptor signal transduction. Sci. STKE. *2001*, re21.

Maynard,S.E., Min,J.Y., Merchan,J., Lim,K.H., Li,J., Mondal,S., Libermann,T.A., Morgan,J.P., Sellke,F.W., Stillman,I.E., Epstein,F.H., Sukhatme,V.P., and Karumanchi,S.A. (2003). Excess placental soluble fms-like tyrosine kinase 1 (sFlt1) may contribute to endothelial dysfunction, hypertension, and proteinuria in preeclampsia. J. Clin. Invest *111*, 649-658.

McTigue,M.A., Wickersham,J.A., Pinko,C., Showalter,R.E., Parast,C., V, Tempczyk,R.A., Gehring,M.R., Mroczkowski,B., Kan,C.C., Villafranca,J.E., and Appelt,K. (1999). Crystal structure of the kinase domain of human vascular endothelial growth factor receptor 2: a key enzyme in angiogenesis. Structure *7*, 319-330.

Mertens,H.D.T. and Svergun,D.I. (2010). Structural characterization of proteins and complexes using small-angle X-ray solution scattering. Journal of Structural Biology *172*, 128-141.

Meyer,R.D., Mohammadi,M., and Rahimi,N. (2006). A single amino acid substitution in the activation loop defines the decoy characteristic of VEGFR-1/FLT-1. J. Biol. Chem. *281*, 867-875.

Millauer,B., Wizigmann-Voos,S., Schnurch,H., Martinez,R., Moller,N.P., Risau,W., and Ullrich,A. (1993). High affinity VEGF binding and developmental expression suggest Flk-1 as a major regulator of vasculogenesis and angiogenesis. Cell *72*, 835-846.

Morikawa,S., Baluk,P., Kaidoh,T., Haskell,A., Jain,R.K., and McDonald,D.M. (2002). Abnormalities in pericytes on blood vessels and endothelial sprouts in tumors. Am. J. Pathol. *160*, 985-1000.

Muller,Y.A., Chen,Y., Christinger,H.W., Li,B., Cunningham,B.C., Lowman,H.B., and de Vos,A.M. (1998). VEGF and the Fab fragment of a humanized neutralizing antibody: crystal structure of the complex at 2.4 A resolution and mutational analysis of the interface. Structure. *6*, 1153-1167.

Muller,Y.A., Christinger,H.W., Keyt,B.A., and de-Vos,A.M. (1997a). The crystal structure of vascular endothelial growth factor (VEGF) refined to 1.93 A resolution: multiple copy flexibility and receptor binding. Structure *5*, 1325-1338.

Muller,Y.A., Heiring,C., Misselwitz,R., Welfle,K., and Welfle,H. (2002). The cystine knot promotes folding and not thermodynamic stability in vascular endothelial growth factor. J. Biol. Chem. *277*, 43410-43416.

Muller,Y.A., Li,B., Christinger,H.W., Wells,J.A., Cunningham,B.C., and de Vos,A.M. (1997b). Vascular endothelial growth factor: Crystal structure and functional mapping of the kinase domain receptor bindingΓÇësite. Proceedings of the National Academy of Sciences of the United States of America *94*, 7192-7197.

Nagy,P., Claus,J., Jovin,T.M., and rndt-Jovin,D.J. (2010). Distribution of resting and ligand-bound ErbB1 and ErbB2 receptor tyrosine kinases in living cells using number and brightness analysis. Proc. Natl. Acad. Sci. U. S. A *107*, 16524-16529.

Niki,T., Iba,S., Tokunou,M., Yamada,T., Matsuno,Y., and Hirohashi,S. (2000). Expression of vascular endothelial growth factors A, B, C, and D and their relationships to lymph node status in lung adenocarcinoma. Clin. Cancer Res. *6*, 2431-2439.

Nilsson,I., Bahram,F., Li,X., Gualandi,L., Koch,S., Jarvius,M., Soderberg,O., Anisimov,A., Kholova,I., Pytowski,B., Baldwin,M., Yla-Herttuala,S., Alitalo,K., Kreuger,J., and Claesson-Welsh,L. (2010). VEGF receptor 2/-3 heterodimers detected in situ by proximity ligation on angiogenic sprouts. EMBO J *advance online publication*.

Oefner,C., D'Arcy,A., Winkler,F.K., Eggimann,B., and Hosang,M. (1992). Crystal structure of human platelet-derived growth factor BB. EMBO J. *11*, 3921-3926.

Ohi,M., Li,Y., Cheng,Y., and Walz,T. (2004). Negative Staining and Image Classification - Powerful Tools in Modern Electron Microscopy. Biol Proced. Online. *6*, 23-34.

Olofsson,B., Pajusola,K., Kaipainen,A., von,E.G., Joukov,V., Saksela,O., Orpana,A., Pettersson,R.F., Alitalo,K., and Eriksson,U. (1996a). Vascular endothelial growth factor B, a novel growth factor for endothelial cells. Proc. Natl. Acad. Sci. U. S. A *93*, 2576-2581.

Olofsson,B., Pajusola,K., von,E.G., Chilov,D., Alitalo,K., and Eriksson,U. (1996b). Genomic organization of the mouse and human genes for vascular endothelial growth factor B (VEGF-B) and characterization of a second splice isoform. J. Biol. Chem. *271*, 19310-19317.

Olsson,A.K., Dimberg,A., Kreuger,J., and Claesson-Welsh,L. (2006). VEGF receptor signalling - in control of vascular function. Nat. Rev. Mol. Cell Biol. *7*, 359-371.

Pajusola,K., Aprelikova,O., Korhonen,J., Kaipainen,A., Pertovaara,L., Alitalo,R., and Alitalo,K. (1992). FLT4 receptor tyrosine kinase contains seven immunoglobulin-like loops and is expressed in multiple human tissues and cell lines. Cancer Res. *52*, 5738-5743.

Park,J.E., Chen,H.H., Winer,J., Houck,K.A., and Ferrara,N. (1994). Placenta growth factor. Potentiation of vascular endothelial growth factor bioactivity, in vitro and in vivo, and high affinity binding to Flt-1 but not to Flk-1/KDR. J. Biol. Chem. *269*, 25646-25654.

Park,J.E., Keller,G.A., and Ferrara,N. (1993). The vascular endothelial growth factor (VEGF) isoforms: differential deposition into the subepithelial extracellular matrix and bioactivity of extracellular matrix-bound VEGF. Mol. Biol. Cell *4*, 1317-1326.

Pepper,M.S. (1997). Transforming growth factor-beta: vasculogenesis, angiogenesis, and vessel wall integrity. Cytokine Growth Factor Rev. *8*, 21-43.

Persico,M.G., Vincenti,V., and DiPalma,T. (1999). Structure, expression and receptor-binding properties of placenta growth factor (PlGF). Curr. Top. Microbiol. Immunol. *237*, 31-40.

Petoukhov,M.V., Konarev,P.V., Kikhney,A.G., and Svergun,D.I. (2007). ATSAS 2.1 - towards automated and web-supported small-angle scattering data analysis. J. Appl. Cryst. *40*, s223-s228.

Pieren,M., Prota,A., Ruch,C., Kostrewa,D., Wagner,A., Biedermann,K., Winkler,F., and Ballmer-Hofer,K. (2006). Crystal structure of the Orf virus NZ2 variant of VEGF-E: Implications for receptor specificity. J. Biol. Chem. *281*, 19578-19587.

Plate,K.H., Breier,G., Weich,H.A., Mennel,H.D., and Risau,W. (1994). Vascular endothelial growth factor and glioma angiogenesis: coordinate induction of VEGF receptors, distribution of VEGF protein and possible in vivo regulatory mechanisms. Int. J. Cancer *59*, 520-529.

Plouet,J., Moro,F., Bertagnolli,S., Coldeboeuf,N., Mazarguil,H., Clamens,S., and Bayard,F. (1997). Extracellular cleavage of the vascular endothelial growth factor 189-amino acid form by urokinase is required for its mitogenic effect. J. Biol. Chem. *272*, 13390-13396.

Reeves,P.J., Callewaert,N., Contreras,R., and Khorana,H.G. (2002). Structure and function in rhodopsin: high-level expression of rhodopsin with restricted and homogeneous N-glycosylation by a tetracycline-inducible N-acetylglucosaminyltransferase I-negative HEK293S stable mammalian cell line. Proc. Natl. Acad. Sci. U. S. A *99*, 13419-13424.

Risau,W. (1997). Mechanisms of angiogenesis. Nature *386*, 671-674.

Risau,W. and Flamme,I. (1995). Vasculogenesis. Annu. Rev. Cell Dev. Biol. *11*, 73-91.

Ruch,C., Skiniotis,G., Steinmetz,M.O., Walz,T., and Ballmer-Hofer,K. (2007). Structure of a VEGF-VEGF receptor complex determined by electron microscopy. Nat. Struct. Mol. Biol. *14*, 249-250.

Sakurai,Y., Ohgimoto,K., Kataoka,Y., Yoshida,N., and Shibuya,M. (2005). Essential role of Flk-1 (VEGF receptor 2) tyrosine residue 1173 in vasculogenesis in mice. Proc. Natl. Acad. Sci. U. S. A *102*, 1076-1081.

Salven,P., Lymboussaki,A., Heikkila,P., Jaaskela-Saari,H., Enholm,B., Aase,K., von,E.G., Eriksson,U., Alitalo,K., and Joensuu,H. (1998). Vascular endothelial growth factors VEGF-B and VEGF-C are expressed in human tumors. Am. J. Pathol. *153*, 103-108.

Sato,T.N., Tozawa,Y., Deutsch,U., Wolburg-Buchholz,K., Fujiwara,Y., Gendron-Maguire,M., Gridley,T., Wolburg,H., Risau,W., and Qin,Y. (1995). Distinct roles of the receptor tyrosine kinases Tie-1 and Tie-2 in blood vessel formation. Nature *376*, 70-74.

Sawamiphak,S., Seidel,S., Essmann,C.L., Wilkinson,G.A., Pitulescu,M.E., Acker,T., and cker-Palmer,A. (2010). Ephrin-B2 regulates VEGFR2 function in developmental and tumour angiogenesis. Nature *advance online publication*.

Sawano,A., Iwai,S., Sakurai,Y., Ito,M., Shitara,K., Nakahata,T., and Shibuya,M. (2001). Flt-1, vascular endothelial growth factor receptor 1, is a novel cell surface marker for the lineage of monocyte-macrophages in humans. Blood *97*, 785-791.

Sawano,A., Takahashi,T., Yamaguchi,S., and Shibuya,M. (1997). The Phosphorylated 1169-Tyrosine Containing Region of Flt-1 Kinase (VEGFR-1) Is a Major Binding Site for PLC[gamma]. Biochem. Biophys. Res. Commun. *238*, 487-491.

Schlunegger,M.P. and Grutter,M.G. (1992). An unusual feature revealed by the crystal structure at 2.2 A resolution of human transforming growth factor-beta 2. Nature *358*, 430-434.

Seetharam,L., Gotoh,N., Maru,Y., Neufeld,G., Yamaguchi,S., and Shibuya,M. (1995). A unique signal transduction from FLT tyrosine kinase, a receptor for vascular endothelial growth factor VEGF. Oncogene *10*, 135-147.

Sennhauser,G. and Grutter,M.G. (2008). Chaperone-Assisted Crystallography with DARPins. Structure *16*, 1443-1453.

Shalaby,F., Rossant,J., Yamaguchi,T.P., Gertsenstein,M., Wu,X.F., Breitman,M.L., and Schuh,A.C. (1995). Failure of blood-island formation and vasculogenesis in Flk-1- deficient mice. Nature *376*, 62-66.

Shibuya,M. (2003). Vascular endothelial growth factor receptor-2: Its unique signaling and specific ligand, VEGF-E. Cancer Sci. *94*, 751-756.

Shibuya,M., Yamaguchi,S., Yamane,A., Ikeda,T., Tojo,A., Matsushime,H., and Sato,M. (1990). Nucleotide sequence and expression of a novel human receptor-type tyrosine kinase gene (flt) closely related to the fms family. Oncogene *5*, 519-524.

Shinkai,A., Ito,M., Anazawa,H., Yamaguchi,S., Shitara,K., and Shibuya,M. (1998). Mapping of the Sites Involved in Ligand Association and Dissociation at the Extracellular Domain of the Kinase Insert Domain-containing Receptor for Vascular Endothelial Growth Factor. J. Biol. Chem. *273*, 31283-31288.

Siekmann,A.F. and Lawson,N.D. (2007). Notch signalling limits angiogenic cell behaviour in developing zebrafish arteries. Nature *445*, 781-784.

Spratlin,J. (2011). Ramucirumab (IMC-1121B): Monoclonal antibody inhibition of vascular endothelial growth factor receptor-2. Curr. Oncol. Rep. *13*, 97-102.

Stalmans,I., Ng,Y.S., Rohan,R., Fruttiger,M., Bouche,A., Yuce,A., Fujisawa,H., Hermans,B., Shani,M., Jansen,S., Hicklin,D., Anderson,D.J., Gardiner,T., Hammes,H.P., Moons,L., Dewerchin,M., Collen,D., Carmeliet,P., and D'Amore,P.A. (2002). Arteriolar and venular patterning in retinas of mice selectively expressing VEGF isoforms. J. Clin. Invest *109*, 327-336.

Starovasnik,M.A., Christinger,H.W., Wiesmann,C., Champe,M.A., de Vos,A.M., and Skelton,N.J. (1999). Solution structure of the VEGF-binding domain of Flt-1: comparison of its free and bound states. J. Mol. Biol. *293*, 531-544.

Stuttfeld,E. and Ballmer-Hofer,K. (2009). Structure and function of VEGF receptors. IUBMB. Life *61*, 915-922.

Suri,C., Jones,P.F., Patan,S., Bartunkova,S., Maisonpierre,P.C., Davis,S., Sato,T.N., and Yancopoulos,G.D. (1996). Requisite role of angiopoietin-1, a ligand for the TIE2 receptor, during embryonic angiogenesis. Cell *87*, 1171-1180.

Suto,K., Yamazaki,Y., Morita,T., and Mizuno,H. (2005). Crystal structures of novel vascular endothelial growth factors (VEGF) from snake venoms: insight into selective VEGF binding to kinase insert domain-containing receptor but not to fms-like tyrosine kinase-1. J. Biol. Chem. *280*, 2126-2131.

Takahashi,H. and Shibuya,M. (2005). The vascular endothelial growth factor (VEGF)/VEGF receptor system and its role under physiological and pathological conditions. Clin. Sci. (Lond) *109*, 227-241.

Takahashi,T., Yamaguchi,S., Chida,K., and Shibuya,M. (2001). A single autophosphorylation site on KDR/Flk-1 is essential for VEGF-A-dependent activation of PLC-gamma and DNA synthesis in vascular endothelial cells. EMBO J. *20*, 2768-2778.

Tallquist,M.D., Soriano,P., and Klinghoffer,R.A. (1999). Growth factor signaling pathways in vascular development. Oncogene *18*, 7917-7932.

Tammela,T., Zarkada,G., Wallgard,E., Murtomaki,A., Suchting,S., Wirzenius,M., Waltari,M., Hellstrom,M., Schomber,T., Peltonen,R., Freitas,C., Duarte,A., Isoniemi,H., Laakkonen,P., Christofori,G., Yla-Herttuala,S., Shibuya,M., Pytowski,B., Eichmann,A., Betsholtz,C., and Alitalo,K. (2008). Blocking VEGFR-3 suppresses angiogenic sprouting and vascular network formation. Nature.

Tanaka,K., Yamaguchi,S., Sawano,A., and Shibuya,M. (1997). Characterization of the extracellular domain in vascular endothelial growth factor receptor-1 (Flt-1 tyrosine kinase). Jpn. J. Cancer Res *88*, 867-876.

Tang,N., Wang,L., Esko,J., Giordano,F.J., Huang,Y., Gerber,H.P., Ferrara,N., and Johnson,R.S. (2004). Loss of HIF-1alpha in endothelial cells disrupts a hypoxia-driven VEGF autocrine loop necessary for tumorigenesis. Cancer cell *6*, 485-495.

Tao,Q., Backer,M.V., Backer,J.M., and Terman,B.I. (2001). Kinase insert domain receptor (kdr) extracellular immunoglobulin-like domains 4-7 contain structural features that block receptor dimerization and vascular endothelial growth factor-induced signaling. J. Biol. Chem. *276*, 21916-21923.

Terman,B.I., Carrion,M.E., Kovacs,E., Rasmussen,B.A., Eddy,R.L., and Shows,T.B. (1991). Identification of a new endothelial cell growth factor receptor tyrosine kinase. Oncogene *6*, 1677-1683.

Tischer,E., Mitchell,R., Hartman,T., Silva,M., Gospodarowicz,D., Fiddes,J.C., and Abraham,J.A.

(1991). The human gene for vascular endothelial growth factor. Multiple protein forms are encoded through alternative exon splicing. J. Biol. Chem. *266*, 11947-11954.

Tvorogov,D., Anisimov,A., Zheng,W., Leppanen,V.M., Tammela,T., Laurinavicius,S., Holnthoner,W., Helotera,H., Holopainen,T., Jeltsch,M., Kalkkinen,N., Lankinen,H., Ojala,P.M., and Alitalo,K. (2010). Effective suppression of vascular network formation by combination of antibodies blocking VEGFR ligand binding and receptor dimerization. Cancer cell *18*, 630-640.

Van,d., V, Stalmans,I., Heindryckx,F., Oura,H., Tijeras-Raballand,A., Schmidt,T., Loges,S., Albrecht,I., Jonckx,B., Vinckier,S., Van,S.C., Tugues,S., Rolny,C., De,M.M., Dettori,D., Hainaud,P., Coenegrachts,L., Contreres,J.O., Van,B.T., Cuervo,H., Xiao,W.H., Le,H.C., Buysschaert,I., Kharabi,M.B., Geerts,A., Schomber,T., Bonnin,P., Lambert,V., Haustraete,J., Zacchigna,S., Rakic,J.M., Jimenez,W., Noel,A., Giacca,M., Colle,I., Foidart,J.M., Tobelem,G., Morales-Ruiz,M., Vilar,J., Maxwell,P., Vinores,S.A., Carmeliet,G., Dewerchin,M., Claesson-Welsh,L., Dupuy,E., Van,V.H., Christofori,G., Mazzone,M., Detmar,M., Collen,D., and Carmeliet,P. (2010). Further pharmacological and genetic evidence for the efficacy of PlGF inhibition in cancer and eye disease. Cell *141*, 178-190.

Vaughn,J.L., Goodwin,R.H., Tompkins,G.J., and McCawley,P. (1977). The establishment of two cell lines from the insect Spodoptera frugiperda (Lepidoptera; Noctuidae). In Vitro *13*, 213-217.

Verstraete,K., Vandriessche,G., Januar,M., Elegheert,J., Shkumatov,A.V., Desfosses,A., Van,C.K., Svergun,D.I., Gutsche,I., Vergauwen,B., and Savvides,S.N. (2011). Structural insights into the extracellular assembly of the hematopoietic Flt3 signaling complex. Blood.

Vervecken,W., Kaigorodov,V., Callewaert,N., Geysens,S., De,V.K., and Contreras,R. (2004). In vivo synthesis of mammalian-like, hybrid-type N-glycans in Pichia pastoris. Appl. Environ. Microbiol. *70*, 2639-2646.

Vincenti,V., Cassano,C., Rocchi,M., and Persico,G. (1996). Assignment of the vascular endothelial growth factor gene to human chromosome 6p21.3. Circulation *93*, 1493-1495.

Waltenberger,J., Claesson-Welsh,L., Siegbahn,A., Shibuya,M., and Heldin,C.H. (1994). Different signal transduction properties of KDR and Flt1, two receptors for vascular endothelial growth factor. J. Biol. Chem. *269*, 26988-26995.

Walter,T.S., Meier,C., Assenberg,R., Au,K.F., Ren,J., Verma,A., Nettleship,J., Owens,R.J., Stuart,D., and Grimes,J.M. (2006). Lysine Methylation as a Routine Rescue Strategy for Protein Crystallization. Structure *14*, 1617-1622.

Wang,H.U., Chen,Z.F., and Anderson,D.J. (1998). Molecular distinction and angiogenic interaction between embryonic arteries and veins revealed by ephrin-B2 and its receptor Eph-B4. Cell *93*, 741-753.

Wang,Y., Nakayama,M., Pitulescu,M.E., Schmidt,T.S., Bochenek,M.L., Sakakibara,A., Adams,S., Davy,A., Deutsch,U., Luthi,U., Barberis,A., Benjamin,L.E., Makinen,T., Nobes,C.D., and Adams,R.H. (2010). Ephrin-B2 controls VEGF-induced angiogenesis and lymphangiogenesis. Nature *advance online publication*.

Warner,A.J., Lopez-Dee,J., Knight,E.L., Feramisco,J.R., and Prigent,S.A. (2000). The Shc-related adaptor protein, Sck, forms a complex with the vascular-endothelial-growth-factor receptor KDR in transfected cells. Biochem. J. *347*, 501-509.

Wickham,T.J., Davis,T., Granados,R.R., Shuler,M.L., and Wood,H.A. (1992). Screening of insect cell lines for the production of recombinant proteins and infectious virus in the baculovirus expression system. Biotechnol. Prog. *8*, 391-396.

Wiesmann,C., Christinger,H.W., Cochran,A.G., Cunningham,B.C., Fairbrother,W.J., Keenan,C.J., Meng,G., and de Vos,A.M. (1998). Crystal structure of the complex between

VEGF and a receptor-blocking peptide. Biochemistry *37*, 17765-17772.

Wiesmann,C., Fuh,G., Christinger,H.W., Eigenbrot,C., Wells,J.A., and de,V.A. (1997). Crystal structure at 1.7 A resolution of VEGF in complex with domain 2 of the Flt-1 receptor. Cell *91*, 695-704.

Willis,M.C., Collins,B.D., Zhang,T., Green,L.S., Sebesta,D.P., Bell,C., Kellogg,E., Gill,S.C., Magallanez,A., Knauer,S., Bendele,R.A., Gill,P.S., and Janjic,N. (1998). Liposome-anchored vascular endothelial growth factor aptamers. Bioconjug. Chem. *9*, 573-582.

Wriggers,W. and Birmanns,S. (2001). Using Situs for Flexible and Rigid-Body Fitting of Multiresolution Single-Molecule Data. Journal of Structural Biology *133*, 193-202.

Wu,L.W., Mayo,L.D., Dunbar,J.D., Kessler,K.M., Ozes,O.N., Warren,R.S., and Donner,D.B. (2000). VRAP is an adaptor protein that binds KDR, a receptor for vascular endothelial cell growth factor. J. Biol. Chem. *275*, 6059-6062.

Wu,Y., Hooper,A.T., Zhong,Z., Witte,L., Bohlen,P., Rafii,S., and Hicklin,D.J. (2006). The vascular endothelial growth factor receptor (VEGFR-1) supports growth and survival of human breast carcinoma. Int. J. Cancer *119*, 1519-1529.

Yamaguchi,T.P., Dumont,D.J., Conlon,R.A., Breitman,M.L., and Rossant,J. (1993). flk-1, an flt-related receptor tyrosine kinase is an early marker for endothelial cell precursors. Development *118*, 489-498.

Yamashita,J., Itoh,H., Hirashima,M., Ogawa,M., Nishikawa,S., Yurugi,T., Naito,M., Nakao,K., and Nishikawa,S. (2000). Flk1-positive cells derived from embryonic stem cells serve as vascular progenitors. Nature *408*, 92-96.

Yamazaki,Y., Matsunaga,Y., Tokunaga,Y., Obayashi,S., Saito,M., and Morita,T. (2009). Snake venom vascular endothelial growth factors (VEGF-Fs) exclusively vary their structures and functions among species. J Biol Chem.

Yancopoulos,G.D., Davis,S., Gale,N.W., Rudge,J.S., Wiegand,S.J., and Holash,J. (2000). Vascular-specific growth factors and blood vessel formation. Nature *407*, 242-248.

Yang,W., Ahn,H., Hinrichs,M., Torry,R.J., and Torry,D.S. (2003). Evidence of a novel isoform of placenta growth factor (PlGF-4) expressed in human trophoblast and endothelial cells. J. Reprod. Immunol. *60*, 53-60.

Yang,Y., Xie,P., Opatowsky,Y., and Schlessinger,J. (2010). Direct contacts between extracellular membrane-proximal domains are required for VEGF receptor activation and cell signaling. Proceedings of the National Academy of Sciences.

Yang,Y., Yuzawa,S., and Schlessinger,J. (2008). Contacts between membrane proximal regions of the PDGF receptor ectodomain are required for receptor activation but not for receptor dimerization. Proceedings of the National Academy of Sciences *105*, 7681-7686.

Yuzawa,S., Opatowsky,Y., Zhang,Z., Mandiyan,V., Lax,I., and Schlessinger,J. (2007). Structural Basis for Activation of the Receptor Tyrosine Kinase KIT by Stem Cell Factor. Cell *130*, 323-334.

Zahnd,C., Amstutz,P., and Pluckthun,A. (2007). Ribosome display: selecting and evolving proteins in vitro that specifically bind to a target. Nat. Methods *4*, 269-279.

Zelzer,E., McLean,W., Ng,Y.S., Fukai,N., Reginato,A.M., Lovejoy,S., D'Amore,P.A., and Olsen,B.R. (2002). Skeletal defects in VEGF(120/120) mice reveal multiple roles for VEGF in skeletogenesis. Development *129*, 1893-1904.